A PARTITIONING SCHEME FOR MOLECULAR ELECTRONIC CHARGE DISTRIBUTIONS

A PARTITIONING SCHEME FOR MOLECULAR ELECTRONIC CHARGE DISTRIBUTIONS

By

GORDON RICHARD RUNTZ, B.Sc.

A Thesis

Submitted to the Faculty of Graduate Studies

in Partial Fulfilment of the Requirements

for the Degree

Doctor of Philosophy

McMaster University

August 1973

DOCTOR OF PHILOSOPHY (1973)
(Chemistry)

McMASTER UNIVERSITY
Hamilton, Ontario

TITLE: A Partitioning Scheme for Molecular Electronic Charge Distributions

AUTHOR: Gordon Richard Runtz, B.Sc. (University of Saskatchewan, Regina Campus).

SUPERVISOR: Professor R. F. W. Bader

NUMBER OF PAGES: viii, 161

SCOPE AND CONTENTS:

A method of spatially partitioning a chemical system into fragments, and describing the properties of that system directly in terms of the gross properties of its constituent fragments, is outlined and discussed. The partitioning surfaces are fully and uniquely defined by the topographical features of the three-dimensional electronic charge density -- an observable property of the system. For this reason, the method is of high generality, and may be readily applied to any chemical system, irrespective of its complexity or the form of the wavefunction which describes it. The usefulness of the method is illustrated in a study of (1) several Lewis acid-base complexes of BH_3 and BF_3, and (2) hydrogen bond formation in the reaction: $FH + F^- \rightarrow FHF^-$.

ACKNOWLEDGEMENTS

I would like to express my sincere thanks to Dr. R. F. W. Bader for his help, guidance, and remarkable tolerance of the author's numerous extra-curricular activities throughout the course of this work.

I would further like to thank the people of Canada for their generous support through the National Research Council of Canada and McMaster University.

Also, many thanks to Jan, for an excellent job in typing the manuscript.

Finally, to my many friends who have done so well in prolonging my stay at McMaster, I say a warm thank you.

This work is dedicated to my parents.

TABLE OF CONTENTS

LIST OF FIGURES

LIST OF TABLES

INTRODUCTION

The physical laws and the mathematical prescription for obtaining a rigorous quantum-mechanical description of chemical systems were put forth nearly a half century ago. Unfortunately, the exact application of these laws leads to equations which are presently intractable, and which will probably remain so for some time to come. Consequently, emphasis has been placed on developing a framework within which approximate solutions to these equations may be obtained. A variety of approximate methods of solution are presently available, ranging from the simpler semi-empirical valence electron techniques to the more rigorous "ab initio" methods. Semi-empirical techniques have been applied extensively to a wide variety of chemical systems including, more recently, polymers.[100] "Ab initio" techniques, on the other hand, are notoriously time-consuming, and their application to all but the simplest chemical systems has been generally impractical. Recent years, however, have seen a dramatic increase in the number of these calculations undertaken. With the present state of advancing computer technology, good "ab initio" calculations on systems containing up to 30-40 electrons are now feasable. Only practical and fiscal obstacles presently prohibit calculations for larger systems.

The quantum-mechanical wavefunctions obtained from these calculations contain a vast amount of detailed information. One of the major concerns of theoretical chemistry today has been to find a method of relating this information to the present-day chemical language.

Chemical intuition has spawned a localized picture of the molecular electronic charge distribution. Most chemists think of molecules in terms of core and valence electrons, bonded and lone electron pairs. Quantum mechanics, on the other hand, gives a completely delocalized picture of the charge distribution, a picture in which it is no longer possible to distinguish between individual electrons, or types of electrons. Several attempts have been made to bridge this gap, and a number of schemes for partitioning the charge distribution have been proposed to this end. Most of these schemes are based on some special property of the approximate wavefunction and, hence, lack generality, as well as rigorous physical meaning. The few spatial partitioning schemes which have been proposed (that is, schemes for physically partitioning the three-dimensional space occupied by a molecule), although free from the above criticism, generally suffer from a certain degree of arbitrariness or intractability.

There is little doubt that a well-defined and general method for partitioning the molecular space would prove extremely useful for characterizing the main features of molecular charge distributions -- irrespective of whether or not it provided a direct link with the present-day chemical language. The full description of a charge distribution afforded by quantum mechanics is probably unnecessarily detailed for most purposes. It would be convenient if the main features of the distribution could be summarized in terms of a smaller number of parameters and if these parameters could be used to give a meaningful quantitative comparison of various systems. In this respect, a method of spatially partitioning a chemical system into fragments, and

characterizing the system in terms of the average properties of these fragments, is particularly appealing.

The concept of a molecular fragment may be more than a useful theoretical construct. There is a considerable body of experimental evidence which suggests that molecules are, to a good approximation, constructed from largely self-contained fragments -- fragments which generally undergo surprisingly minor changes upon transfer from one system to another. It is the constancy of functional group properties, particularly with respect to chemical reactions, which has made possible the systemization of a large portion of chemistry. Electronic and vibrational transitions can often be assigned to specific molecular fragments, and it is the near-constancy of these transition frequencies from system to system which has made it possible to use spectroscopy as an analytical tool. A number of additivity schemes for fragment properties -- particularly bond additivity schemes for dipole moments, polarizabilities, and energies -- have proved to be quite useful. These, and other similar observations, lend considerable support to the concept of "fragments in molecules", and suggest that there may be some "best", if not fundamental method of partitioning the molecular space, and hence quantitatively defining these fragments.

In this thesis, a method for spatially partitioning the electronic charge distribution is proposed -- a method which may well be both "best" and fundamental for reasons to be discussed. The partitioning surfaces are fully and uniquely defined by the topographical features of the three-dimensional electronic charge distribution -- an observable property of the system. The method is applied to a study of a series of boron compounds, and several linear configurations of the bifluoride

ion. The wavefunctions employed in this study are of the "ab initio" type. They were computed within the self-consistent-field framework and are believed to be quite close to the Hartree-Fock limit with respect to most properties.

Chapter 1 contains a discussion of Hartree-Fock wavefunctions, particularly with respect to the position they occupy in the general framework of approximate calculations, and the reliability of properties computed from them. In Chapter 2 the partitioning scheme is outlined and discussed. Chapter 3 contains a discussion and summary of the Hartree-Fock calculations. In Chapter 4, the partitioning method is applied to a study of (1) the Lewis acids, BH_3 and BF_3; (2) four of their complexes: BH_3-H^-, BH_3-F^-, BH_3-CO, and BF_3-H^-; (3) hydrogen bond formation in the reaction, $FH(g) + F^-(g) \rightarrow FHF^-(g)$. A concluding summary of the work is given in Chapter 5.

The details of the partitioning surface calculations and numerical integrations over molecular fragments have been omitted from the main body of the thesis, and are given in Appendix I. Appendix II contains a general derivation of the molecular virial theorem. (A discussion of this theorem, and its possible implications for molecular fragments appears in Chapter 2.) Finally, Appendix III contains a listing of the linear combinations of terminal d-type functions which form a basis for the irreducible representations of the C_{3v} and D_{3h} symmetry groups. These combinations were generated using projection operator techniques and used to simplify the Hartree-Fock calculation on BF_3.

CHAPTER 1

THE CALCULATION OF MOLECULAR WAVEFUNCTIONS

A. General Framework

The eigenfunctions, and subsequently any observable property of a molecular system in any of its available stationary states may, in principle, be determined by solution of the time-independent Schrödinger equation,

$$H_R \Psi_R = E_R \Psi_R \qquad [1.1]$$

where H_R is the full relativistic Hamiltonian for the system, Ψ_R is an eigenfunction describing a stationary state of the system, and E_R is the energy of that state. Exact solutions for Equation [1.1] have never been found, even for the simplest of chemical systems. Nevertheless, considerable progress has been made in the way of approximate solutions.

The general starting point for all approximate molecular calculations is the non-relativistic Schrödinger equation,

$$H_{NR} \Psi_{NR} = E_{NR} \Psi_{NR} \qquad [1.2]$$

The non-relativistic Hamiltonian, H_{NR}, differs from its relativistic counterpart, H_R, in that it includes only those particle interactions which are purely electrostatic in origin. All terms corresponding to more general electromagnetic interactions and relativistic effects are omitted. These relativistic corrections are generally quite small for systems built from first-row atoms, and are usually treated using perturbation theory techniques.[1] For an N-particle system,

the non-relativistic Hamiltonian may be written (in atomic units) as

$$H_{NR} = -\tfrac{1}{2}\sum_{k=\ell}^{N}(\nabla_k^2/m_k) + \sum_{k>\ell=1}^{N}(Z_k Z_\ell / r_{k\ell}) \qquad [1.3]$$

The first term in [1.3] is the quantum-mechanical kinetic energy operator for the system; ∇_k^2 is the Laplacian operator for the k^{th} particle and m_k is the mass of that particle. The second term is the potential energy operator for the electrostatic interactions between the particles; Z_k and Z_ℓ are the charges on the k^{th} and ℓ^{th} particles, respectively, and $r_{k\ell}$ is the distance between them.

In 1927, Born and Oppenheimer[2] showed that in most cases Ψ_{NR} can, to a good approximation, be written as a single product of an electronic and a nuclear wavefunction. Equation [1.2] can then be separated into an electronic eigenvalue equation,

$$H_e\Psi_e = E_e\Psi_e \qquad [1.4]$$

and a nuclear eigenvalue equation,

$$H_n\Psi_n = E_n\Psi_n \qquad [1.5]$$

Electronic eigenfunctions, Ψ_e, can then be determined for any given nuclear configuration, $\{\underset{\sim}{R}\}$. The corresponding electronic energies, E_e, appear in the form of a potential function, $E_e(\{\underset{\sim}{R}\})$, in Equation [1.5]. The electronic and nuclear Hamiltonians are then given by

$$H_e = -\tfrac{1}{2}\sum_i \nabla_i^2 - \sum_\alpha\sum_i (Z_\alpha/r_{\alpha i}) + \sum_{i>j}(1/r_{ij}) \qquad [1.6]$$

and

$$H_n = -\tfrac{1}{2}\sum_\alpha (\nabla_\alpha^2/m_\alpha) + \sum_{\alpha>\beta}(Z_\alpha Z_\beta/r_{\alpha\beta}) + E_e(\{\underset{\sim}{R}\}) \qquad [1.7]$$

where the subscripts α and β refer to nuclei, and i and j refer to electrons.

Equation [1.4] forms the basis for the calculation of approximate molecular electronic wavefunctions. Closed-form analytical solutions are available only for simple one-electron systems. Solutions for the many-electron case are presently obtained by expressing the electronic wavefunction in terms of products of one-electron functions, ψ_i, called molecular spin-orbitals (MSO's).

Any one-electron wavefunction, $\Psi_e(\underline{x})$, may be expanded in terms of a complete set of functions, $\{\psi_i(\underline{x})\}$.

$$\Psi_e(\underline{x}) = \sum_i c_i \psi_i(\underline{x}) \qquad [1.8]$$

In the above, $\underline{x}$ denotes the complete set of space and spin variables for the electron, and c_i denotes an expansion coefficient. It is generally assumed that if the set $\{\psi_i\}$ is indeed complete, then the set of all possible N-membered products, $\{\psi_i(\underline{x}_1)\psi_j(\underline{x}_2) \ldots \psi_p(\underline{x}_N)\}$, is also complete, and any N-electron wavefunction may be written as a linear combination of these products.

$$\Psi_e(\underline{x}_1\underline{x}_2 \ldots \underline{x}_N) = \sum c_{ij\ldots p}\, \psi_i(\underline{x}_1)\psi_j(\underline{x}_2) \ldots \psi_p(\underline{x}_N) \qquad [1.9]$$

The $\{\psi_i\}$ may be chosen as an orthonormal set with no loss in generality. The set of product functions will then be orthogonal and the expansion coefficients in Equation [1.9] will be given by

$$c_{ij\ldots p} = \langle \psi_i(\underline{x}_1)\psi_j(\underline{x}_2) \ldots \psi_p(\underline{x}_N) | \Psi_e(\underline{x}_1, \underline{x}_2, \ldots \underline{x}_N) \rangle \qquad [1.10]$$

From this expression it is easily seen that coefficients of all spin-orbital products involving the same selection of spin-orbitals (differing only in their order), can differ only in their sign. This follows since the labelling of the variables in [1.10] is arbitrary, but Ψ_e must be

antisymmetric with respect to electron exchange. The right-hand side of [1.9] can then be written as a linear combination of antisymmetrized products, or Slater determinants.[3] Using κ to denote a particular set of N spin-orbitals in some standard order, we may write

$$\Psi_e(\underline{x}_1, \underline{x}_2, \cdots \underline{x}_N) = \sum c_\kappa \Phi_\kappa(\underline{x}_1, \underline{x}_2, \cdots \underline{x}_N) \qquad [1.11]$$

where

$$\Phi_\kappa(\underline{x}_1, \underline{x}_2, \cdots \underline{x}_N) = \begin{vmatrix} \psi_I(\underline{x}_1)\psi_J(\underline{x}_1) & \cdots & \psi_P(\underline{x}_1) \\ \psi_I(\underline{x}_2)\psi_J(\underline{x}_2) & \cdots & \psi_P(\underline{x}_2) \\ \psi_I(\underline{x}_N)\psi_J(\underline{x}_N) & \cdots & \psi_P(\underline{x}_N) \end{vmatrix} \qquad [1.12]$$

A complete set of MSO's would generally be infinite and the determinant in [1.12] would be of infinite order. In practice, one uses a finite number of MSO's, and finite expansions of the form given in Equation [1.11] yield the best approximations to solutions of [1.4] calculated to date.

Sometimes it is possible to obtain a very good approximation to Ψ_e using only a single term of the expansion in [1.11]. Wavefunctions of this type are generally known as single-determinantal wavefunctions. The "best" wavefunctions of this form are known as Hartree-Fock wavefunctions, and it is to a discussion of their calculation that we now turn.

B. The Hartree-Fock Method

The equations for calculating the "best" approximate wave-

functions of single-determinantal form [1.12] were derived independently by Fock[5] and Slater.[6] Their work extended the earlier work of Hartree[4] for single product wavefunctions (i.e., wavefunctions constructed from a single term in [1.9]).

In the absence of spin-orbit coupling, each MSO, $\psi_i(\underline{x})$, may be factored into a spatial function, $\phi_i(\underline{r})$, generally known as a molecular orbital (MO), and a spin function, $\eta_i(s)$. The spin function for a given electron may take one of two possible forms, which will be denoted here as α and β. A single-determinantal wavefunction for an N-electron system may be written [1.13]

$$\Phi_K(\underline{x}_1, \underline{x}_2, \ldots \underline{x}_N) = (N!)^{-\frac{1}{2}} |\phi_1(\underline{r}_1)\eta_1(s_1)\ \phi_2(\underline{r}_2)\eta_2(s_2)\ \ldots\ \phi_N(\underline{r}_N)\eta_N(s_N)|$$

where $(N!)^{-\frac{1}{2}}$ has been included as a normalization factor (assuming that the ϕ_i and η_i form orthonormal sets), and the shorthand convention of writing down only the diagonal elements of the determinant [1.12] has been employed. A further restriction is usually placed on Φ_K when it is assumed that each MO may occur twice, coupled once with each of the two possible spin functions. Wavefunctions of this form are generally known as <u>restricted</u> Hartree-Fock (RHF) wavefunctions; those of the more general form [1.13], where each electron is assigned to its own MO, are termed <u>unrestricted</u>. All wavefunctions reported here are of the RHF type.

In general, single-determinantal RHF wavefunctions are reasonably good approximations to the correct non-relativistic solutions only for <u>closed-shell</u> systems. Most molecules in their electronic ground states belong in this category; and hence, these wavefunctions have rather wide applicability. A closed-shell ground state is probably best defined as one for which there exists only <u>one</u> single-determinantal

wavefunction (i.e., one term in [1.11]) for which the energy reaches its absolute minimum.[10] This has several implications. First, the system must contain an even number of electrons, and each MO in Φ_K must be doubly occupied. Hence, for a system of N-electrons occupying n = N/2 MO's,

$$\Phi_K(\underset{\sim}{x}_1, \underset{\sim}{x}_2, \ldots \underset{\sim}{x}_N) = (N!)^{-\frac{1}{2}} |\phi_1(1)\alpha(1)\ \phi_1(2)\beta(2)\ \phi_2(3)\alpha(3)\ \ldots\ \phi_n(N)\beta(N)| \qquad [1.14]$$

Further, Φ_K must belong to the identity representation of the symmetry group for the system. That is, Φ_K must be invariant with respect to any symmetry operation of the point group for the system (see Roothaan[10] for the proof). Since all molecules in this work are of the closed-shell type, we now confine ourselves to the Hartree-Fock method for this particular case.

The electronic energy of a closed-shell system described by [1.14] is given by

$$E_e = 2\sum_{i=1}^{n} H_{ii} + \sum_{i,j=1}^{n} (2J_{ij} - K_{ij}) \qquad [1.15]$$

where

$$H_{ii} = \langle \phi_i(1) | -\tfrac{1}{2}\nabla_1^2 - \sum_{\alpha} \frac{Z_\alpha}{r_{\alpha 1}} | \phi_i(1) \rangle \qquad [1.16]$$

$$J_{ij} = \langle \phi_i(1)\phi_j(2) | \frac{1}{r_{12}} | \phi_i(1)\phi_j(2) \rangle \qquad [1.17]$$

$$K_{ij} = \langle \phi_i(1)\phi_j(2) | \frac{1}{r_{12}} | \phi_j(1)\phi_i(2) \rangle \qquad [1.18]$$

The integrals [1.17] and [1.18] are known as coulomb and exchange integrals, respectively. The Hartree-Fock equations for the "best"

ϕ_i are obtained by applying the variational principle[7-9] to [1.15]. One searches for the conditions under which E_e is stationary with respect to variations in the ϕ_i, subject to the condition that the ϕ_i remain orthonormal -- a condition which results in no loss in generality since the ϕ_i are defined only to within a unitary transformation among themselves, and hence can always be chosen as orthonormal. The orthonormality conditions are imposed using the method of Lagrangian multipliers.

One then searches for stationary values of the functional

$$Q = E_e - \tfrac{1}{2} \sum_{ij}^{n} \epsilon_{ij}(\langle\phi_i|\phi_j\rangle - \delta_{ij}) \qquad [1.19]$$

where the Lagrangian multipliers have been chosen to be $\frac{1}{2}\epsilon_{ij}$, and δ_{ij} is the usual Krönecker delta. The conditions for $\delta Q = 0$ are that each ϕ_i satisfy an equation

$$F|\phi_i(1)\rangle = \sum_{j=1}^{n} \epsilon_{ij}|\phi_j(1)\rangle \qquad [1.20]$$

where the Fock operator, F, is defined as

$$F = H + \sum_{j=1}^{n} (2J_j - K_j) \qquad [1.21]$$

and the operators H, J_j and K_j are defined by

$$H|\phi_i(1)\rangle = (-\tfrac{1}{2}\nabla_1^2 - \sum_{\alpha} \frac{Z_\alpha}{r_{\alpha 1}})|\phi_i(1)\rangle \qquad [1.22]$$

$$J_j|\phi_i(1)\rangle = \langle\phi_j(2)|\frac{1}{r_{12}}|\phi_j(2)\rangle|\phi_i(1)\rangle \qquad [1.23]$$

and

$$K_j|\phi_i(1)\rangle = \langle\phi_j(2)|\frac{1}{r_{12}}|\phi_i(2)\rangle|\phi_j(1)\rangle \qquad [1.24]$$

It is always possible to find a unitary transformation of the orbitals

which brings [1.20] into diagonal form, leaving F and the total wavefunction invariant.[10] Each ϕ_i will then satisfy a pseudo-eigenvalue equation,

$$F|\phi_i(1)\rangle = \varepsilon_i|\phi_i(1)\rangle \qquad [1.25]$$

where the operator F actually depends on its eigenfunctions, ϕ_i, through the J and K operators. Equation [1.25] may be solved via an iterative procedure known as the self-consistent-field (SCF) method. One guesses at an initial set of ϕ_i, determines the operator F, and solves for a new set of ϕ_i. This process is continued until the assumed and calculated ϕ_i agree to within some prescribed accuracy.

Completely general solutions to [1.25] must normally be found using numerical techniques, and are not practical, except perhaps for systems of spherical symmetry (i.e., atoms). In 1951, Roothaan[10] proposed a method for obtaining analytical solutions to [1.25], a method which opened the way for Hartree-Fock calculations on molecular systems. Specifically, Roothaan showed that MO's expanded as linear combinations of atomic orbitals (LCAO-MO's) could readily be incorporated into the Hartree-Fock framework, greatly alleviating the computational difficulties. If one expands the ϕ_i in terms of an m-membered complete set, $\{\chi_t\}$,

$$\phi_i = \sum_{t=1}^{m} c_{it}\chi_t \qquad [1.26]$$

each equation [1.25] becomes a set of equations for the expansion coefficients,

$$\sum_{t=1}^{m}(F_{qt} - \varepsilon_i S_{qt})c_{it} = 0 \qquad \begin{matrix} q = 1,2, \ldots m \\ i = 1,2, \ldots n \end{matrix} \qquad [1.27],$$

where

$$F_{qt} = T_{qt} + V_{qt} + \sum_{i=1}^{n}\sum_{r=1}^{m}\sum_{s=1}^{m} c_{ir}^{*}c_{is}[2J_{qrst} - J_{qrts}] \qquad [1.28]$$

and

$$T_{qt} = \langle \chi_q(1) | -\tfrac{1}{2}\nabla_1^2 | \chi_t(1) \rangle \qquad [1.29]$$

$$V_{qt} = \langle \chi_q(1) | -\sum_{\alpha} \frac{Z_\alpha}{r_{\alpha 1}} | \chi_t(1) \rangle \qquad [1.30]$$

$$J_{qrst} = \langle \chi_q(1)\chi_r(2) | \frac{1}{r_{12}} | \chi_s(1)\chi_t(2) \rangle \qquad [1.31]$$

$$S_{qt} = \langle \chi_q(1) | \chi_t(1) \rangle \qquad [1.32]$$

A complete set of basis functions, $\{\chi_r\}$, would normally be infinite in number. In practice, of course, one uses a finite set. With an m-membered set, one can solve for m of the ϕ_i, and hence the size of the basis set must always be such that $m \geq n$. Equations [1.27] for an m-membered basis set can be written as an m x m matrix equation. The F matrix is calculated by occupying only n of the ϕ_i. For the ground state of a system, one would normally occupy the ϕ_i with the n lowest orbital eigenvalues, ϵ_i. The remaining unoccupied ϕ_i are called <u>virtual</u> orbitals.

Solutions are again obtained via an iterative procedure. The method is basically as follows:

(1) A set of basis functions, $\{\chi_r\}$, is chosen.

(2) The integrals [1.29]-[1.32] are evaluated.

(3) The F matrix [1.28] is calculated from an initial assumed set of expansion coefficients.

(4) The matrix equation [1.27] is then solved by diagonalization of the F matrix which is first transformed to the basis of the eigenvectors of the S matrix.

(5) The new solutions are compared with the input solutions.

If they agree to within some prescribed limits (generally taken as convergence of the electronic energy to a certain number of significant figures) then the procedure is terminated. If not, the new coefficients are used as input, and the procedure is repeated until convergence is achieved.

Since a finite basis set is used in the expansion [1.26], the calculated ϕ_i are now only approximations to the actual Hartree-Fock ϕ_i. The problem of choosing a good basis set when setting up a calculation is then of prime importance if one wishes to obtain a wavefunction which is close to Hartree-Fock accuracy.

Two types of basis sets are in common use today. The first, and earliest set employed, is the Slater-type basis set with functions of the form

$$\chi_p = N_p\, r_\alpha^{(n-1)} Y_{\ell m}(\theta_\alpha,\phi_\alpha) e^{-\beta_p r_\alpha} \qquad n>\ell\geq|m|\geq 0 \quad \text{(integers)} \qquad [1.33]$$

where N_p is a normalization factor, $Y_{\ell m}(\theta_\alpha,\phi_\alpha)$ is a spherical harmonic, β_p is an orbital exponent, and the function is defined in terms of a spherical coordinate system, (r,θ,ϕ), centred at α (usually a nuclear coordinate). The second type of basis, originally suggested by Boys,[11] is the Gaussian-type set with functions of the form

$$\chi_p = N_p\, x_\alpha^{\ell} y_\alpha^{m} z_\alpha^{n} e^{-\beta_p r_\alpha^2} \qquad n,\ell,m\geq 0 \quad \text{(integers)} \qquad [1.34]$$

where the definitions are as in [1.33], and x, y, and z denote Cartesian coordinates. These functions have an advantage over Slater functions in that the integrals [1.29]-[1.32] required in the calculation are much

simpler to evaluate, especially the time-consuming, multi-centre, two-electron integrals, [1.31]. This is partially offset since approximately twice as many Gaussian functions are required to give a wavefunction of the same calibre as one calculated with a Slater basis set.

All wavefunctions reported in this work were computed using Gaussian basis sets. A complete description of these sets will be given in Chapter 3.

C. Characteristics of Hartree-Fock Wavefunctions

In any analysis based on an approximate wavefunction, it is particularly important to have a good idea of the quality of the wavefunction, and hence, the reliability of properties computed from it. Hartree-Fock wavefunctions stand fairly well documented in this respect. (Throughout this section, "Hartree-Fock" refers to the "best" general solutions of [1.25], not the LCAO-MO approximations to them. The latter are discussed towards the end.)

Brillouin[12] was the first to show that, within the non-relativistic framework, the Hartree-Fock energy is correct to second-order. Shortly after, Moller and Plesset[13] employed a perturbation treatment to show that the first-order corrections to both the energy and the three-dimensional electronic charge density are zero. Their treatment was extended by Cohen and Dalgarno[14] to include all one-electron properties.

Hartree-Fock wavefunctions have also been shown to satisfy the Hellmann-Feynman and quantum-mechanical virial theorems. The generalized Hellmann-Feynman theorem[15,16] states that for any eigenfunction, ψ, of

some Hamiltonian, H,

$$\frac{\partial E}{\partial \lambda} = \langle \psi | \frac{\partial H}{\partial \lambda} | \psi \rangle \qquad [1.35]$$

where E is the energy eigenvalue associated with ψ, and λ is any parameter appearing in H. Stanton[17] has shown that [1.35] is also valid for Hartree-Fock approximations to ψ. One of the main uses of the theorem is that it allows one to calculate intramolecular forces on nuclei by simple electrostatics. Thus, if one chooses λ to be a nuclear coordinate, say x_α, then it can be shown that

$$\frac{\partial E_e}{\partial x_\alpha} = (-F_{x_\alpha}^{el}) = -Z_\alpha \iiint \rho(x,y,z) \frac{x-x_\alpha}{r_\alpha^3} dxdydz \qquad [1.36]$$

where $\rho(x,y,z)$ is the electronic charge density at the point (x,y,z), r_α is distance from that point to the nucleus, and $F_{x_\alpha}^{el}$ is the x component of the electronic force on nucleus α. This specific form of the Hellmann-Feynman theorem is generally known as the electrostatic theorem.

The quantum-mechanical virial theorem can be derived in a number of ways. The "scaling" derivation, originally due to Fock[18] and since extended by a number of authors (most of the references are given by Löwdin[19]), shows the validity of the theorem for both true solutions to Schrödinger's equation and properly-scaled approximate solutions (a category which includes Hartree-Fock wavefunctions). An alternate derivation has been given by Slater[20] who first proved the validity of the theorem for molecular electronic wavefunctions. More recently, it has been derived by way of what is generally called the <u>hypervirial</u> theorem.[21-23]

For an electronic wavefunction, ψ_e, the virial theorem takes the form

$$2\langle\psi_e|\hat{T}_e|\psi_e\rangle = \langle\psi_e|\sum_{i=1}^{3n} q_i \frac{\partial \hat{V}_e}{\partial q_i}|\psi_e\rangle \qquad [1.37]$$

where $\hat{T}_e$ and $\hat{V}_e$ are the electronic kinetic and potential energy operators for the system, respectively, and the summation and integrations are taken over the 3n electronic Cartesian coordinates, q_i. With the aid of Euler's theorem for homogeneous functions, and the Hellmann-Feynman theorem, Equation [1.37] may be expanded to read (see Appendix II)

$$-2\bar{T}_e = \bar{V}_e - \sum_\alpha \vec{R}_\alpha \cdot \vec{F}_\alpha^{el} \qquad [1.38]$$

In the above, $\bar{T}_e$ and $\bar{V}_e$ denote the average values of the electronic kinetic and potential energies, respectively. $\vec{R}_\alpha$ denotes the position vector of the α^{th} nucleus, and $\vec{F}_\alpha^{el}$ denotes the electronic force on it (as calculated from the electrostatic theorem, [1.36]). The summation is over all nuclei in the system. Alternately, [1.38] may be written in terms of the electronic energy, $\bar{E}_e$, as

$$-\bar{T}_e = \bar{E}_e - \sum_\alpha \vec{R}_\alpha \cdot \vec{F}_\alpha^{el} \qquad [1.39]$$

For an atom, the last term in [1.39] is identically zero ($\vec{F}_\alpha^{el} = 0$). For a molecule in its equilibrium geometry, it reduces the nuclear repulsion potential, $\bar{V}_n$, and the theorem assumes the limiting form

$$-\bar{T}_e = \bar{E} \qquad [1.40]$$

where $\bar{E}$ is the total energy ($\bar{E}_e + \bar{V}_n$) of the system. The virial theorem, particularly with respect to its possible implications for molecular fragments, will be discussed in more detail in Chapter 2.

To say a wavefunction gives most properties correct to second order is rather vague. In recent years, a limited number of wavefunctions of better than Hartree-Fock quality have been obtained, and somewhat more quantitative estimates of accuracy have been possible. On the basis of the data now available, it appears that the Hartree-Fock energy is within about 1% of the correct non-relativistic value. The electronic charge density appears to be correct to within 2-5%, and most other properties (the one-electron properties in particular) appear correct to within 2-10% of their non-relativistic values.[30] In some respects this is encouraging, as it indicates that these wavefunctions are at least capable of giving a good semi-quantitative description of molecular systems. However, much of the interesting chemical information is concerned with differences between systems, and changes which occur during chemical reactions. These changes are generally quite small, and are of about the same magnitude as the errors quoted for Hartree-Fock wavefunctions. In this respect, the errors take on a much greater importance, and the possibility of using these wavefunctions to study chemical change may appear rather remote. However, such is not necessarily the case.

Whenever a series of wavefunctions is used to study chemical changes, it is not so important that these wavefunctions be absolutely accurate with respect to all properties, but <u>that they be of the same relative accuracy with respect to the particular properties under study</u>. If this is the case, the absolute errors in the wavefunctions will cancel during the differencing operation, and changes in these properties will be faithfully reproduced.

Consider specifically the energy of a system. The energy of a Hartree-Fock wavefunction lies above the true experimental energy by the sum of the relativistic and correlation energies. The relativistic energy is generally defined as the difference between the experimental and non-relativistic energies, which may, in principle, be determined by solution of Equations [1.1] and [1.2], respectively. The correlation energy is most commonly defined[24] as the difference between the non-relativistic and Hartree-Fock energies.† The difference is a reflection of the fact that the Hartree-Fock equations describe a situation in which each electron moves in the field of the nuclei plus the average field of the other electrons. Hence, the instantaneous correlations between the motions of the electrons are not properly described. Both the relativistic energy ($\bar{E}_{rel} = \bar{E}_{exp} - \bar{E}_{nonrel}$) and the correlation energy ($\bar{E}_{corr} = \bar{E}_{nonrel} - \bar{E}_{HF}$) are negative (stabilizing) quantities.

It is to be expected then, that Hartree-Fock wavefunctions will faithfully reproduce energy changes when both the relativistic and

---

† Actually, Hartree-Fock wavefunctions are already partially correlated for electrons of the same spin by virtue of their antisymmetry. As Clementi[25] has pointed out, because of this *precorrelation*, it might be better from a conceptual point of view to define the correlation energy as the difference between the non-relativistic and Hartree[4] energies. Hartree wavefunctions are the "best" wavefunctions of single product form (i.e., are constructed from a single term in [1.9]) and hence, treat all electrons identically. However, Hartree wavefunctions are now very rare, and the definition in terms of the Hartree-Fock energy has mainly a practical value.

correlation energies are conserved. The relativistic energies for atoms are roughly proportional to the fourth power of their nuclear charges. For atoms in the first-row of the periodic table these energies are considerably less than the correlation energies. Specifically, from He to Ne the relativistic energy varies from -.00007 to -.13 au,[27] whereas the correlation energy varies from -.042 to -.40 au.[25] Since the main contributions to the relativistic energy come from the "core" regions,[27] one can expect that molecular relativistic energies will be approximately equal to the sums of the relativistic energies of the constituent atoms. The major changes in correlation energy occur upon "pairing" of electrons.[25,26] For these reasons, one can expect that relativistic energies will be conserved to a far greater degree than correlation energies (at least for molecules built from first-row atoms), and that the conservation of correlation energy will depend, to a large extent, on the conservation of number of electron pairs. This has been substantiated by Snyder,[28] who showed that Hartree-Fock wavefunctions can predict heats of reaction (gas-phase) between closed-shell systems to a reasonable degree of accuracy (i.e., to within $\sim$ 6 kcal/mole per bond formed). For molecules constructed from atoms with higher nuclear charges, the relativistic energy takes on a far greater importance, and methods of estimating its behaviour may well be required.

An interesting question arises with respect to the components of the total energy. When the relativistic and correlation energies are conserved between systems, does this necessarily imply the same for their kinetic and potential energy components? (The components of the potential energy -- viz. the electron-nuclear, electron-electron

and nuclear-nuclear terms -- will henceforth be denoted as $\overline{V}'$, $\overline{V}''$, and $\overline{V}_n$, respectively.) From the virial theorem [1.40], it is obvious that the kinetic energy component ($\overline{T}_{corr}$) of the correlation energy is conserved to the same extent the correlation energy itself is conserved, providing the systems are all at their equilibrium geometries. This follows since a true non-relativistic solution to [1.4] and the Hartree-Fock approximation to it both satisfy the virial theorem. The situation as regards the electronic potential energy components ($\overline{V}'_{corr}$ and $\overline{V}''_{corr}$) is not quite as clear. Certainly, one would expect $\overline{V}''_{corr}$ always to be negative (stabilizing) since correlation tends to keep the electrons farther apart. Therefore, at least partial conservation of this component can be expected. The sign of $\overline{V}'_{corr}$, however, is uncertain, and it is not clear as to whether or not there is even a general rule here. Of course, if $\overline{E}_{corr}$, $\overline{T}_{corr}$, and $\overline{V}''_{corr}$ are conserved, then $\overline{V}'_{corr}$ is conserved by difference.

The components of the relativistic energy are many, and little is known about the effects of relativistic corrections on $\overline{T}$, $\overline{V}'$, and $\overline{V}''$. As long as the total relativistic energy is small, it is probably safe to assume that $\overline{T}_{rel}$, $\overline{V}'_{rel}$, and $\overline{V}''_{rel}$ are also small, and conservation is not as important as it is for the correlation energy components.

Most wavefunctions calculated within the Hartree-Fock approximation (including those reported here) are not true Hartree-Fock wavefunctions, but rather, LCAO-MO approximations to them. Hence, the preceding discussion does require some qualification.

The energy of an LCAO-MO wavefunction lies above the true

Hartree-Fock energy by what might be called the *LCAO-MO energy gap*. The magnitude of this gap depends upon the size and nature of the basis set employed. As the flexibility of a given basis set is increased, the size of the gap decreases and the LCAO-MO wavefunction is said to approach the Hartree-Fock limit. In order that these wavefunctions faithfully reproduce energy changes between systems, it is necessary not only that the relativistic and correlation energies be conserved, but also that the magnitude of the LCAO-MO energy gap be conserved.

So far, the discussion has been limited to the energy. Some extension to other properties is now necessary. It is well-known that the total energy is a fairly insensitive measure of the overall "quality" of a wavefunction. The refinement of a wavefunction, although it may bring about only a small change in energy, may bring about a substantial change in some other property. This is particularly true of LCAO-MO wavefunctions. Any wavefunction constructed from a finite basis set has limited flexibility, and the exact nature of the limitations depends upon the particular basis set employed. The sensitivity of the charge distribution to the choice of basis set was pointed out sometime ago by Kern and Karplus,[29] and has been studied more recently by Cade[30] and Lipscomb.[31] Some properties tend to emphasize particular regions of charge distribution. When a description of a particular region in a molecule is poor, then so too will be the prediction of properties sensitive to that description. A property of particular relevance to this work is the electronic force on a nucleus. These forces are particularly sensitive to the charge distribution in the nuclear regions. The charge density in these regions is extremely high and even relatively small errors in the distribution here can, and

do cause large errors in the forces. Further, most basis sets are designed for greater flexibility in the "valence" regions, and a good description of the "core" is sacrificed.

Thus, it can be quite dangerous to study changes in molecular properties by comparing wavefunctions which employ different basis sets. Maximum conservation of errors in a series of wavefunctions is most likely if those wavefunctions employ closely-related, if not identical basis sets. Further, the basis sets must be capable of giving an equally good description of all the systems. For example, it is known that a basis set which gives a good description of a neutral atom, may give an inferior description of its negative ion.[32] The reason for this is that the electrons in the negative ion tend to spread out more than they do in the neutral atom. Basis sets which have been optimized for the atom often do not contain enough diffuse functions to allow for this. Thus, it is often necessary to augment a given basis set, even a fairly extensive one, with additional functions.

LCAO-MO wavefunctions do not rigorously satisfy the Hellmann-Feynman theorem, and in particular, the electrostatic theorem. Even if they did satisfy the theorem, this would not necessarily imply reliability of forces computed from [1.36] for the reasons previously discussed.

Most LCAO-MO wavefunctions do not satisfy the virial theorem rigorously. Any approximate wavefunction can be made to satisfy the theorem if it is properly "scaled". That is, if all coordinates in the wavefunction are multiplied by some scale factor, n, and if n is chosen

such that it minimizes the energy, then that wavefunction will satisfy the virial theorem.[19] For an LCAO-MO wavefunction this is tantamount to further optimization of the energy with respect to the exponents in the basis functions. Most basis sets contain functions whose exponents have been energy-optimized for atoms. During the calculation of a molecular wavefunction, these exponents are usually held fixed, and the energy is optimized only with respect to the linear expansion coefficients in [1.26]. In practice, these partially optimized wavefunctions usually come fairly close to satisfying the virial theorem. For the wavefunctions reported in Chapter 3, the two sides of [1.38] generally differ by less than 1%.

CHAPTER 2

PARTITIONING OF ELECTRONIC CHARGE DISTRIBUTIONS

A. Previous Methods

There has never been a completely satisfactory method for partitioning electronic charge distributions. Of course, exactly what constitutes a satisfactory method depends upon the use to which it is to be put. If a partitioning scheme is to be used to classify the gross features of a charge distribution, then it should be well-defined for any system, regardless of its complexity. If the scheme is to provide a framework for comparing a series of charge distributions, then it should clearly reflect the basic differences in these distributions. An important prerequisite of any partitioning scheme is that it be independent of the particular form a wavefunction might happen to take. In this respect, it would seem particularly desirable that the scheme be based on an observable property of the system.[51]

The most popular method of characterizing and comparing charge distributions has been the population analysis of Mulliken.[33] When an approximate wavefunction is constructed from a series of orbital products, and when the orbitals are of LCAO form (Equation [1.26]), the total number of electrons in the system, n_T, can generally be written

$$n_T = \sum_k \lambda_k \left[\sum_{i,j} c_{ki} c_{kj} S_{ij} \right] \qquad [2.1]$$

where the subscript k refers to orbitals, and the subscripts i and j refer to basis functions. S_{ij} denotes the overlap integral between

the I^{th} and J^{th} basis functions, $\langle\chi_I|\chi_J\rangle$; the c's are the expansion coefficients for the orbitals; λ_k denotes the weighting factor (usually the occupation number) of the k^{th} orbital. The bracketed term in [2.1] contains both monocentric and bicentric terms -- that is, terms in which χ_I and χ_J belong to the same or different centres, respectively. Mulliken's original proposal was that the population of a given "atom" in a molecule be defined as the sum of all monocentric terms in [2.1] centred at that atom, plus one-half the sum of all bicentric terms involving basis functions centred at that atom. Thus, the population of some atom, A, would be given by

$$n(A) = \sum_k \lambda_k \left[\sum_{a,a'} c_{ka} c_{ka'} S_{aa'} + \sum_{a,b} c_{ka} c_{kb} S_{ab} \right] \qquad [2.2]$$

where a and a' denote basis functions centred at A, and b denotes those centred elsewhere. The method was originally criticized for its equal partitioning of the bicentric terms between the centres involved, and a number of alternate criteria for apportioning these terms were proposed.[34] Mulliken himself has pointed out[35] that even the assignment of the monocentric terms can be misleading. The charge density associated with a basis function on a given centre is always assigned to that centre, even though that density may be largely localized in another region of the molecule. Further, it has become apparent that the method can yield quite different results when applied to wavefunctions which employ different basis sets, even if these sets are of approximately the same quality from an energy criterion.[29] The basic deficiency of the method is simply that it requires that the wavefunction be of LCAO form, and further, that the basis functions be centred at

nuclear positions. There is no reason why a wavefunction should necessarily have these properties.

Another popular method of partitioning the charge distribution is based on the orbital concept. When a wavefunction is constructed from orbital products, the electronic charge density at any point $\underset{\sim}{r}$, $\rho(\underset{\sim}{r})$, can generally be written as the sum of the orbital densities at that point. That is,

$$\rho(\underset{\sim}{r}) = \sum_k \lambda_k \rho_k(\underset{\sim}{r}) \qquad [2.3]$$

where λ_k is the occupation number of the k^{th} orbital, and $\rho_k(\underset{\sim}{r})$ is the orbital density. It is then possible to analyze and compare charge distributions orbital by orbital. The problem here is that there is no unique set of orbitals for a given wavefunction. For example, the MO's in a Hartree-Fock wavefunction are defined only to within a unitary transformation among themselves -- a transformation which leaves the total wavefunction invariant (to within a phase factor), and the physical description unchanged.[10] Probably the most objective criterion for choosing a set of MO's for Hartree-Fock wavefunctions is that of Edmiston and Ruedenberg.[36] These authors proposed using those MO's which minimize the sum of the exchange integrals in the expression for the energy (i.e., minimize $\sum_{i\neq j} \langle\phi_i(1)\phi_j(2)|\frac{1}{r_{12}}|\phi_i(2)\phi_j(1)\rangle$). These MO's also minimize the off-diagonal coulomb sum, $\sum_{i\neq j} \langle\phi_i(1)\phi_j(2)|\frac{1}{r_{12}}|\phi_i(1)\phi_j(2)\rangle$, and hence are termed localized molecular orbitals (LMO's). LMO's have generally been found to correspond to core orbitals, bond orbitals, and lone pair orbitals,[37] although a complete spatial separation has never been possible. Thus, they seem to provide some link between quantum-

mechanical wavefunctions and the usual chemical language. Recently they have found considerable use in studying the transferability of "bonds" between various systems.[38] Again, the basic shortcoming of the method is its dependence on wavefunction form. There is no reason, apart from present mathematical convenience, why a wavefunction should necessarily be constructed from orbital products -- let alone be of single antisymmetrized product form.

A better method of fragmenting a charge distribution would be to physically partition the three-dimensional space. Such a method would at least be independent of wavefunction structure. Politzer and Harris[39] have suggested spatially partitioning molecules into atomic (mono-nuclear) fragments. Their partitioning scheme is arbitrarily defined in terms of a hypothetical charge distribution constructed by superimposing the densities of unperturbed atoms, placed at their corresponding positions in the molecule. The surfaces proposed are those for which the atomic fragments in this hypothetical situation have the same electron populations as the free atoms. Of course, any number of surfaces meet this criterion. To date, these authors have applied the scheme only to linear molecules, and considered only planar surfaces perpendicular to the internuclear axes. Extension of this method to non-linear systems is impossible.

A better spatial partitioning scheme, at least in the sense that it is completely general, and defined for any system, is the "loge" method of Daudel.[40] A loge is simply a portion of the physical space of an atom or molecule. Suppose the space is to be divided into ν volumes or loges, $V_\lambda(\lambda = 1,\nu)$. The probability of finding simultaneously

n_1 electrons in V_1, n_2 in V_2, ..., and n_ν in V_ν is given by

$$P(\{n_\lambda \in V_\lambda\}) = \int_{V_1} \{d\underset{\sim}{r}\}_{n_1} \int_{V_2} \{d\underset{\sim}{r}\}_{n_2} \cdots \int_{V_\nu} \{d\underset{\sim}{r}\}_{n_\nu} \Gamma^{(N)}(\underset{\sim}{r}_1, \underset{\sim}{r}_2, \ldots, \underset{\sim}{r}_N) \qquad [2.4]$$

where $\Gamma^{(N)}(\underset{\sim}{r}_1, \underset{\sim}{r}_2, \ldots, \underset{\sim}{r}_N)$ is the diagonal element of the spinless N^{th} order density matrix[41,42] for the N-electron system. There are $(N+\nu-1)!/N!(\nu-1)! = \ell(N,\nu)$ ways of distributing N electrons among ν loges, each with an associated probability, P_l. Daudel's hypothesis is that the "best" decomposition of the space is that which minimizes the "missing information function", I, defined as

$$I(\{n_\lambda \in V_\lambda\}) = -\sum_{l=1}^{\ell(N,\nu)} P_l \log_2 P_l \qquad [2.5]$$

where the sum is over all possible ways of distributing N electrons over ν loges. Even if one accepts Daudel's premise, one is still faced with substantial difficulties. There is presently no way of deciding, apart from a process of trial and error, what the best value of ν is for a given system, let alone finding the best surfaces for a given value of ν. The trial surfaces have at present been restricted to planes and nucleus-centred spheres.

The partitioning scheme proposed in this thesis is a spatial scheme. The partitioning surfaces are defined completely in terms of an observable property of the system -- the three-dimensional electronic charge distribution. The method may be applied directly to any chemical system, whether it be a single molecule or a collection of molecules, regardless of its complexity or symmetry. The work is an extension and generalization of the recently published method of Bader and co-workers.[43,44,45]

B. A Proposed Partitioning Scheme

It is proposed here that an electronic charge distribution, $\rho(\underset{\sim}{r})$, may be best partitioned by those closed surfaces through which the flux of $\vec{\nabla}\rho(\underset{\sim}{r})$ is everywhere zero. That is, if $S(\underset{\sim}{r})$ denotes a partitioning surface, then

$$\partial\rho(\underset{\sim}{r})/\partial\vec{n}(\underset{\sim}{r})=0 \quad \text{for all } \underset{\sim}{r} \in S(\underset{\sim}{r}) \qquad [2.6]$$

where $\rho(\underset{\sim}{r})$ is the charge density at the point $\underset{\sim}{r}$, and $\vec{n}(\underset{\sim}{r})$ is a vector normal to S at that point. Alternately, one may write [2.6] directly in terms of the gradient vectors, $\vec{\nabla}\rho(\underset{\sim}{r})$, as

$$\vec{\nabla}\rho(\underset{\sim}{r})\cdot\vec{n}(\underset{\sim}{r}) = 0 \qquad \text{for all } \underset{\sim}{r} \in S(\underset{\sim}{r}) \qquad [2.7]$$

There are an infinite number of surfaces of zero flux in a given system, but only a finite number of these are both closed and everywhere defined. Every point in a charge distribution lies on some surface(s) of zero flux, providing the gradient vector, $\vec{\nabla}\rho(\underset{\sim}{r})$, is defined at that point. That is, the dot product in [2.7] can always be made to vanish for a point, $\underset{\sim}{r}_k$, providing $\vec{n}(\underset{\sim}{r}_k)$ is chosen perpendicular to $\vec{\nabla}\rho(\underset{\sim}{r}_k)$. Thus, the surface (or surfaces) of zero flux which pass through a given point must always lie tangential to the gradient vector at that point. When $\vec{\nabla}\rho(\underset{\sim}{r}) = 0$ (i.e., when $\underset{\sim}{r}_k$ is a stationary point in the charge distribution) there are no restrictions on the orientation of these surfaces. The only points in the charge distribution for which $\vec{\nabla}\rho(\underset{\sim}{r})$ is not defined are the nuclear coordinates, since $\rho(\underset{\sim}{r})$ must satisfy a cusp condition here.[46-49] Thus, any surface of zero flux which contains a nucleus, exhibits a discontinuity at that nucleus, and therefore does not qualify as a proper partitioning surface. As will

shortly become apparent, almost all surfaces of zero flux pass through nuclei. The few which do not always contain stationary points. These stationary points play in important role in the determination of the partitioning surfaces.

Stationary points in a molecular charge distribution are generally saddle points (i.e., points where $\rho(\underset{\sim}{r})$ is a maximum with respect to certain directions, and a minimum with respect to others). Saddle points normally occur on or near the internuclear axes which connect pairs of so-called "bonded" nuclei. When the internuclear axis is coincident with a rotational symmetry axis of the molecule, the saddle point will be coincident with the point of minimum density between the nuclei. Otherwise, it will normally lie a short distance from it. For example, consider the molecule BH_3CO. This molecule is of C_{3v} symmetry, and the single rotational axis passes through the B, C and O nuclei. There are five saddle points in the charge distribution. Two lie on the rotational axis and are coincident with the density minima in the B-C and C-O internuclear axes. The other three lie in the σ_v symmetry planes containing the B-H internuclear axes, and are close to, but not coincident with the density minima on these axes. As will be shown later, a partitioning surface passes through each of the five saddle points. Each surface cuts the internuclear axis associated with its saddle point approximately at right angles. The molecule is thus partitioned into six fragments -- (B), (C), (O), and three equivalent (H) fragments. The partitioning surfaces all extend to infinity, and are closed there. (There is a closed surface of everywhere zero flux an infinite distance from any isolated system, since $\vec{\nabla}\rho(r)$ is everywhere zero there. Any partitioning surface which extends to infinity is closed there by virtue of its intersection with

this surface.)

Stationary points in charge distributions which are true minima or maxima are somewhat less common than saddle points. One example of a true density minimum would be at or near the ring centre of some cylical compound. For example, the benzene molecule has thirteen stationary points, all of which lie in the σ_h symmetry plane. Six of these are saddle points near the midpoints of the C-C axis connecting adjacent carbon nuclei; six are saddle points in the C-H axes (coincident with the density minima in these axes); one is the relative minimum at the centre of the molecule. As will be shown later, a partitioning surface passes through each of the twelve saddle points. The stationary point at the ring centre is common to six of these.

It is questionable whether one would ever observe a stationary point which was a true density maximum in a charge distribution. Of course, nuclei are density maxima, but these do not qualify as stationary points because of the cusps. As far as the author is aware, the only example of a true stationary maximum is at the bond midpoint of the Li_2 molecule.[50] The molecule has an extremely long equilibrium bond length ($\sim$ 5.0 au in the ground state) and apparently has a double minimum along the bond axis. Whether this is a feature of the true charge distribution, or simply a shortcoming of the approximate wavefunction, is not clear.

Surfaces of zero flux in general, and the partitioning surfaces in particular can generally be described in terms of the gradient paths which permeate a charge distribution. The path of steepest ascent

from a point $\underset{\sim}{r}_k$ (as traced by the vectors, $\vec{\nabla}\rho(\underset{\sim}{r})$), and the path of steepest descent from $\underset{\sim}{r}_k$ (as traced by the vectors, $-\vec{\nabla}\rho(\underset{\sim}{r})$), together define the gradient path through that point. The particular property of these paths which is of interest here, is that they always lie on surfaces of zero flux. This follows since the flux normal to a gradient path is zero for all points on it. A path can traverse more than one surface of zero flux when it lies along the intersection of those surfaces.

Every gradient path through a charge distribution must originate and terminate at (1) a stationary point (i.e., where $\vec{\nabla}\rho(\underset{\sim}{r}) = 0$), or (2) a nuclear coordinate (where $\rho(\underset{\sim}{r})$ cusps and $\vec{\nabla}\rho(\underset{\sim}{r})$ is undefined). (The point of minimum $\rho(\underset{\sim}{r})$ on a given path will now be referred to as the origin of that path; the point of maximum $\rho(\underset{\sim}{r})$ will be referred to as the terminus.) Almost all gradient paths through a charge distribution either originate or terminate at nuclear positions, and therefore do not traverse partitioning surfaces. (Recall that nuclei cannot lie on partitioning surfaces because of the discontinuity in $\vec{\nabla}\rho(\underset{\sim}{r})$.) The gradient paths which do lie on these surfaces, are those which both originate and terminate at stationary points in the charge distribution.

This can be best illustrated by an example. Fig. 2-1 shows a contour map of the charge distribution in one of the σ_v symmetry planes of the BH_3F^- molecule (C_{3v} symmetry). A number of gradient paths in this plane have been traced, starting from points exterior to the outermost density contour shown ($\rho(\underset{\sim}{r}) = .002$ au). (The paths actually originate at infinity, where $\vec{\nabla}\rho(\underset{\sim}{r})$ is everywhere zero.) All

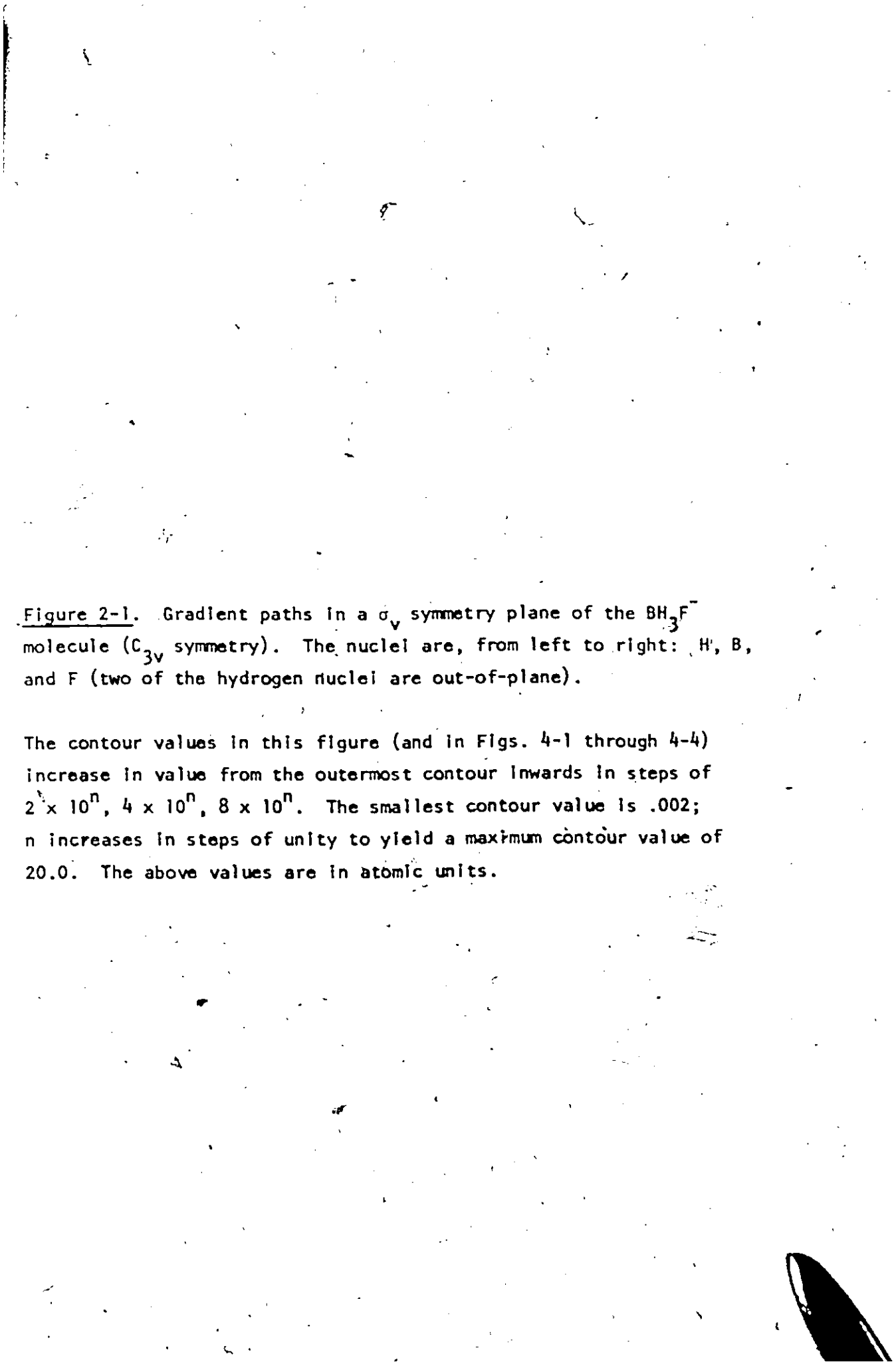

Figure 2-1. Gradient paths in a σ_v symmetry plane of the BH_3F^- molecule (C_{3v} symmetry). The nuclei are, from left to right: H, B, and F (two of the hydrogen nuclei are out-of-plane).

The contour values in this figure (and in Figs. 4-1 through 4-4) increase in value from the outermost contour inwards in steps of 2×10^n, 4×10^n, 8×10^n. The smallest contour value is .002; n increases in steps of unity to yield a maximum contour value of 20.0. The above values are in atomic units.

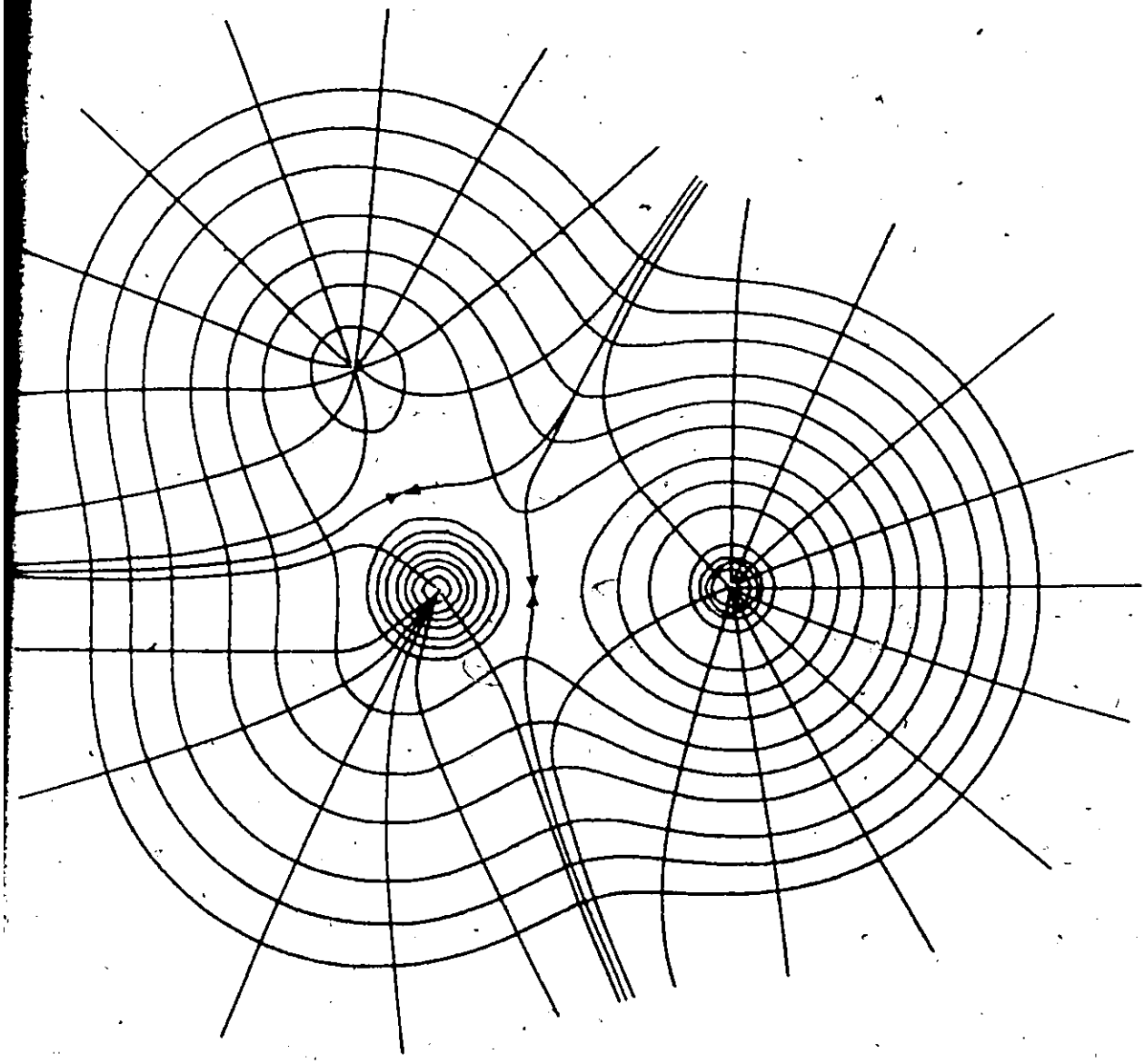

but four of these paths terminate at nuclei. Two of the four terminate at the saddle point on the B-F internuclear axis; the other two terminate at the saddle point near the B-H axis. Together, these four gradient paths define the intersections of the partitioning surfaces in this molecule with the σ_v symmetry plane.

That two, and only two gradient paths in a symmetry plane terminate at each saddle point in that plane follows directly from the topography of the charge distribution. Fig. 2-2 illustrates some representative density contours in the region of a saddle point. Several gradient paths in the vicinity are shown. An important property of gradient paths in a symmetry plane is that they must run perpendicular to the density contours. For this reason, only two of the paths in Fig. 2-2 actually terminate at the saddle point. These are the two which lie in the regions of lower density above and below the saddle point in the diagram. All other paths, no matter how close they may lie to these two, must eventually turn away from the saddle point. Whether or not the two paths actually lie on a proper partitioning surface depends on whether or not they originate at stationary points. In an isolated molecule (eg., BH_3F^- in Fig. 2-1) they would normally originate at infinity, and therefore would qualify in this respect.

Note that two other gradient paths in Fig. 2-2 also include the saddle point. These paths lie in the regions of higher density to the left and right of the saddle point, and actually originate at that point. They too will lie on partitioning surfaces, providing they also terminate at stationary points. Normally, in an isolated molecule, these paths would terminate at nuclei, and therefore would not be

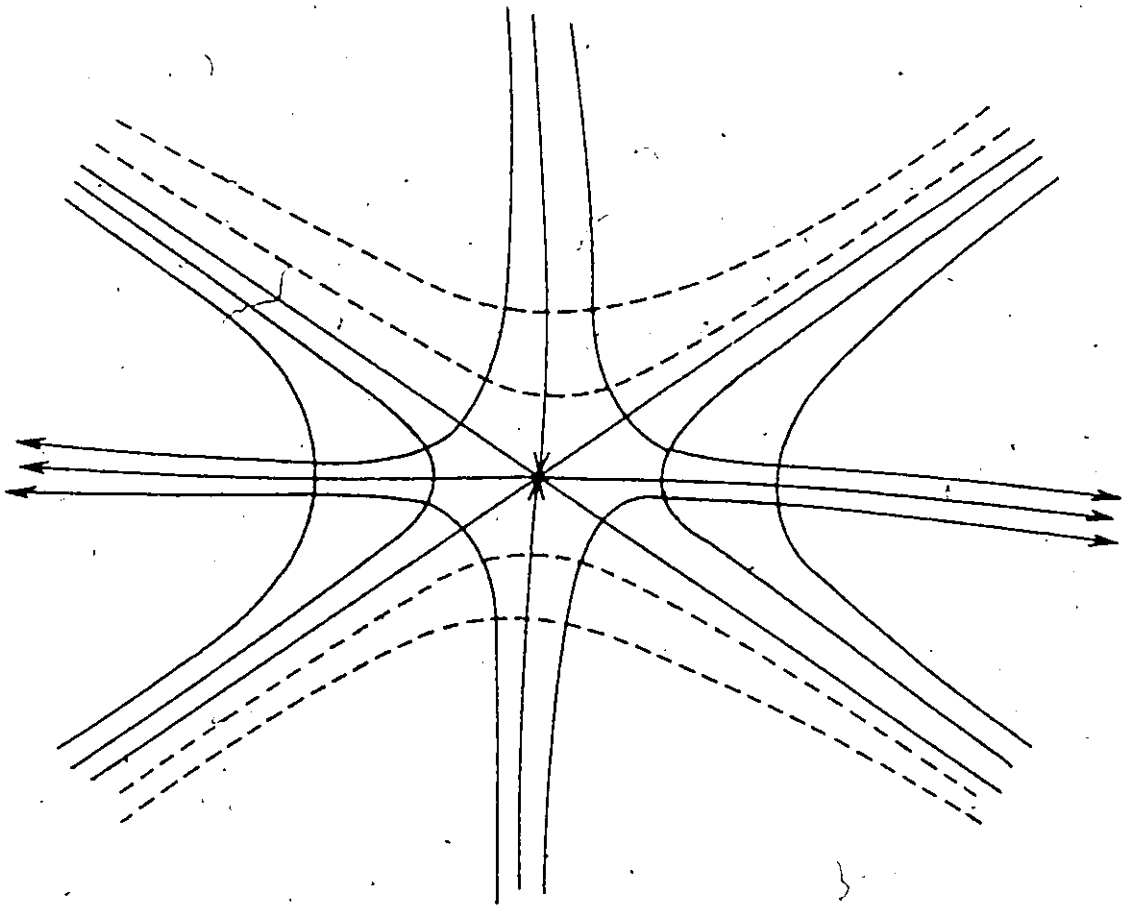

Figure 2-2. Gradient paths in the region of a saddle point, drawn in a plane of symmetry. The saddle point is coincident with the contour crossover at the centre. Solid contours denote increasing density as one moves away from the saddle point. Broken contours denote decreasing density. Gradient paths are denoted with arrowheads which point in the direction of steepest ascent through the charge distribution.

ligible. However, there are exceptions (for example, see Fig. 2-4).

The above discussion has been confined to symmetry planes for pictorial purposes. Only in a plane of symmetry is a two-dimensional representation of a gradient path possible. (A gradient vector in a symmetry plane has a zero component perpendicular to that plane.) In general, one must think in terms of three-dimensional charge distributions and gradient paths. The three-dimensional pictorial analogues of Figs. 2-1 and 2-2 may be mentally constructed if one visualizes density "shells" instead of contours. (A density contour is actually the intersection of a three-dimensional shell of constant density with a plane.) A saddle point occurs where two closed shells of the same density meet. Gradient paths in three dimensions can be readily visualized, as they must run normal to all density shells. The two-dimensional arguments presented above can readily be extended to the three-dimensional picture. Only the visualization is somewhat more difficult.

In most cases, one can define the partitioning surfaces directly in terms of the gradient paths. *Closed surfaces of everywhere zero flux* are operationally equivalent to *surfaces defined by the collection of all gradient paths which originate and terminate at stationary points in the charge distribution.* The difference is that the first definition includes the closed surface of zero flux at infinity, whereas the latter does not. (Since $\vec{\nabla}\rho(\underline{r})$ is everywhere zero at infinity, no gradient paths traverse the surface there.) The surface at infinity must be included if the closure condition in the original definition is to be satisfied. Strictly speaking, this closure condition is

necessary if the fragments are to be well-defined. Most of the gradient paths which traverse the partitioning surfaces in isolated molecules originate at infinity. These surfaces are closed only by virtue of their intersection with the surface at infinity. Thus, the original definition, although possibly not as visually appealing as the second, is the most complete of the two. The second definition is more useful from an operational viewpoint. At present, it appears that the only way of deciding whether or not a given point lies on a partitioning surface, is to determine whether or not the gradient path which passes through it originates and terminates at stationary points. This seems to be the only property specific to points on these surfaces.

A detailed discussion of the method of surface calculation used is given in Appendix I-B. Here we give only a brief summary.

(1) Stationary points in the charge distribution were determined. (Only saddle points were encountered in the molecules studied here.)

(2) The partitioning surface passing through a given saddle point was found by calculating several of the gradient paths terminating at that point. This was done by following paths of steepest descent through the charge distribution, starting at points a short distance from the saddle point (10^{-6} au), in a direction approximately perpendicular to the path of steepest ascent from it. The paths were calculated incrementally, using approximately 1000-1500 points per path over a span of about 10 au.

(3) Additional surface points were found by interpolation between these paths.

Of course, the gradient paths and surfaces calculated in the above manner are only approximations to the correct ones. However, convergence studies indicate that they are good approximations. Fragment properties (electronic populations, energies, and forces) calculated using these surfaces are generally correct to within ± 0.0001 au.

Before concluding this section, a few brief examples might serve to clarify the above discussion. First, atoms cannot be partitioned under the above scheme. Atomic charge distributions contain no stationary points. Therefore, all gradient paths terminate at the nucleus. There are, of course, an infinite number of zero flux surfaces (closed at infinity), but they all exhibit a discontinuity at the nucleus.

In Fig. 2-3, several molecules and the general characteristics of their partitioning surfaces are illustrated. Solid lines denote internuclear axes in the plane drawn; dotted lines represent the intersection of the partitioning surfaces with this plane; stationary points are denoted with an "x".

The partitioning surface in a homonuclear diatomic molecule is coincident with the σ_h symmetry plane which bisects that molecule. This plane extends to infinity in all directions and is closed by intersection with the zero flux surface there. There is one stationary point in the charge distribution -- a saddle point coincident with the density minimum at the bond midpoint. All gradient paths which originate in the σ_h plane (at infinity), terminate at this saddle point. Those which originate at points to the left of this plane, terminate at the nucleus on the left; those which originate at points to the right,

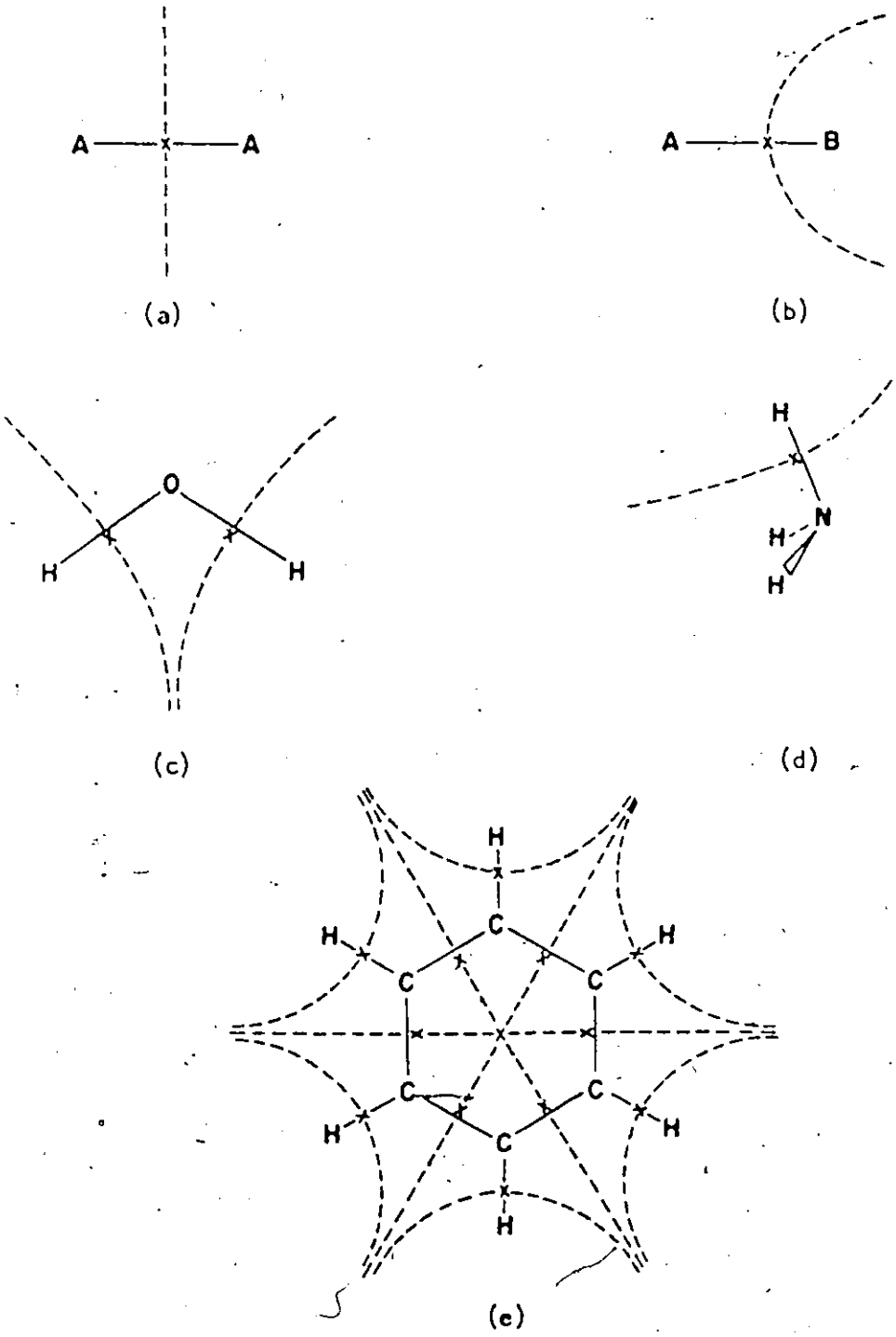

Figure 2-3. Some representative partitioning surfaces: (a) a homonuclear diatomic; (b) a heteronuclear diatomic; (c) water (C_{2v}); (d) ammonia (C_{3v}); (e) benzene (D_{6h}). Stationary points in the plane are denoted with an "x".

terminate at the nucleus on the right. It is worthwhile pointing out here, that all symmetry planes are surfaces of zero flux. These planes, in conjunction with surfaces which intersect with them and close them, can qualify as partitioning surfaces providing they are free from nuclear discontinuities. All linear molecules, for example, have an infinite number of σ_v symmetry planes which extend to, and are closed at infinity. However, all these planes contain the nuclei, and thus do not qualify as partitioning surfaces.

The partitioning surface through a heteronuclear diatomic molecule is a curved surface which passes through the point of minimum density on the internuclear axis, and intersects that axis at right angles. Again, the surface extends to infinity and is closed there. The saddle point in these molecules is always coincident with the density minimum on the internuclear axis. The gradient paths which traverse the partitioning surface originate at infinity and terminate at the saddle point. These paths are identical in all σ_v planes. Therefore, the full three-dimensional surface may be obtained by rotating a single path through 360° about the internuclear axis.

The H_2O molecule is of C_{2v} symmetry and contains two equivalent saddle points, one near each of the O-H internuclear axes. These saddle points lie <u>near</u> the density minima on these axes. The partitioning surfaces which pass through them are, again closed at infinity. Note that in the σ_v symmetry plane, two of the gradient paths on the surfaces run asymptotic to the C_2 rotational axis, as they extend to infinity. The partitioning surfaces are, of course, symmetric across both σ_v planes. Therefore, only one-half of one partitioning surface need be

evaluated; the rest may be obtained by reflection.

The NH_3 molecule is of C_{3v} symmetry and contains three equivalent stationary points -- all saddle points near the N-H axes in the σ_v symmetry planes. Only one is shown. The surfaces which define the (H) fragments are all equivalent. Only one surface intersects with the σ_v plane drawn. One gradient path in each σ_v plane runs asymptotic to the C_3 axis as it extends to infinity.

Finally, consider the benzene molecule. The thirteen stationary points previously discussed are indicated in the diagram. The surfaces which define the (H) fragments pass through the saddle points on the C-H axes and are of local C_{2v} symmetry. These surfaces, in conjunction with the three σ_v symmetry planes which bisect the C-C bonds, define the (C) fragments. The two sets of surfaces join and are closed at infinity. The gradient paths which traverse the curved surfaces originate at infinity, and terminate at the saddle points in C-H bonds. There are two sets of gradient paths which traverse the symmetry planes. Some of the paths originate at infinity and terminate at the saddle points near the C-C axes. The others originate at the stationary point at the centre of the molecule, and also terminate at the C-C saddle points.

In all the examples given so far, molecules have been partitioned into mono-nuclear fragments. It is not always possible to do this. For example, there are no partitioning surfaces passing through the charge distributions in FH^+ ($X\ ^2\Sigma^+$) and NeH^+ ($X\ ^1\Sigma^+$).[45] These charge distributions are so strongly dominated by the heavier nuclei that no saddle points appear. This is not a shortcoming of the partitioning method; it simply means that the hydrogen nuclei in these

molecules do not have sufficient influence over the charge distribution to define their own fragments. They act only as small perturbations within the system.

C. Properties of the Surfaces and Fragments

The partitioning surfaces discussed in the preceeding section, and the fragments they define, are unambiguously determined by the spatial topography of the electronic charge distribution. For this reason, the partitioning method is completely general and may be applied to any chemical system, regardless of its symmetry or complexity. When a single molecule is considered, the partitioning surfaces define the regions of space associated with the various nuclei in the molecule. When an ensemble of molecules, atoms, or ions is considered, the surfaces also partition the various members of the ensemble from each other. Thus, it is possible to associate a specific region of space with each constituent in a solid, liquid, or gas.

Further, the definition is a dynamic one. When the charge distribution undergoes a continuous change (e.g., as in a molecular vibration, or during the course of a chemical reaction), so too do the partitioning surfaces, the fragments they define, and the properties of these fragments (see below). It is interesting to note that the number of stationary points in a charge distribution, and sometimes even the number of partitioning surfaces, is not necessarily conserved during changes in nuclear configuration. Consider, for example, a portion of the potential surface for the $H_2 + H \rightarrow H_3$ reaction.

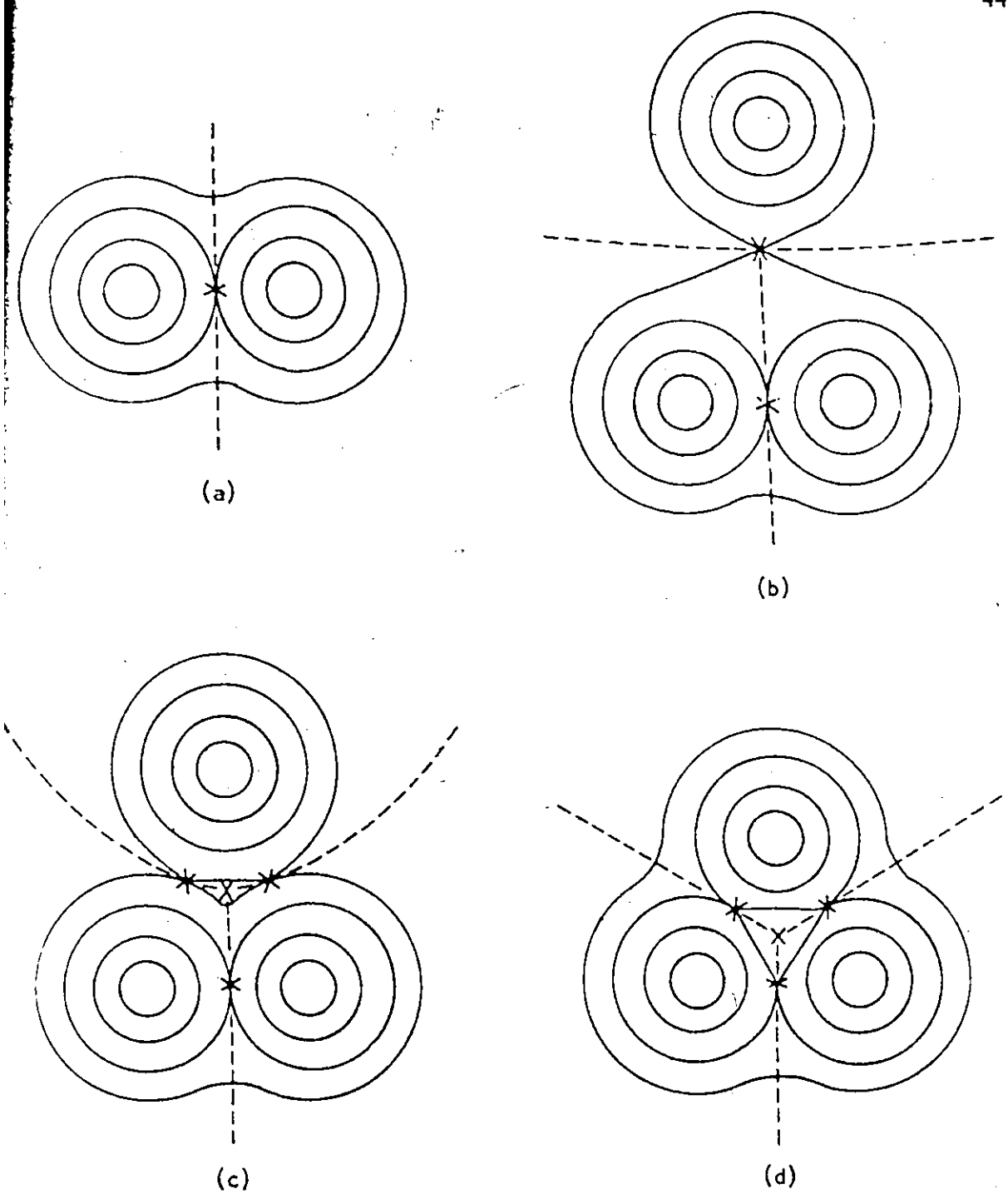

Figure 2-4. A sketch of partitioning surfaces and stationary points at several points on the potential surface for the reaction: $H_2 + H \rightarrow H_3$. Stationary points are marked with an "x"; partitioning surfaces are denoted by dotted lines.

Fig. 2-4 illustrates the behaviour of the partitioning surfaces and stationary points as the H atom approaches H_2 along a C_2 symmetry axis of that molecule. (a) The stationary point in the H_2 molecule is, of course, a saddle point coincident with the density minimum at the bond midpoint. The partitioning surface is coincident with the σ_h symmetry plane which bisects the molecule. (b) The approach of H is marked by the appearance of a new saddle point on the C_2 axis, and a new partitioning surface. The original partitioning surface in H_2 now terminates at this surface. The original saddle point still lies in the original σ_h plane, although it is no longer constrained (by symmetry) to remain on the H_2 internuclear axis. (c) As H approaches more closely, the density in the region of the new saddle point increases, and it eventually splits into three -- two saddle points, one on each side of the C_2 axis, and a true density minimum on that axis. Note that the number of partitioning surfaces does not change. As the reaction proceeds, the density minimum continues to move down the C_2 axis with the H, and the two new saddle points gradually move away from each other. (d) When the three nuclei are equidistant, the three saddle points become equivalent, each lying along a σ_v-σ_h symmetry plane intersection, a short distance from an H-H internuclear axis. The fourth stationary point is now coincident with the density minimum at the ring centre.

The approach of nuclei can also lead to the <u>disappearance</u> of stationary points and partitioning surfaces. Consider, specifically, a heteronuclear diatomic molecule, AB. As the A-B internuclear distance is decreased, the saddle point between the nuclei will eventually dis-

appear as the charge distribution approaches, in a very real sense, the limiting case of the "united atom". When the nuclear charges on A and B are very different, this will occur at much larger internuclear distances than when they are similar. (Recall the example of FH^+ and NeH^+ mentioned in Section B of this chapter.) When the charges are identical (i.e., in a homonuclear diatomic), the stationary point will persist for all nuclear configurations.

We now consider some of the properties of fragments defined by these surfaces.

1. The partitioning method appears to yield chemically identifiable fragments by maximizing the retention of the distribution of charge and of properties of a fragment when it occurs in different environments. The changes in the charge distribution which occur when a fragment is transferred from one system to another, are largely restricted to the regions of low density surrounding the nuclei. There is considerable evidence that constancy in the charge distribution of a fragment in different systems may account for the near-additivity of properties often observed experimentally -- an additivity which is no less than remarkable considering the tremendous changes in environment which often occur upon transfer of a fragment from one system to another.[91] We return to this point shortly.

2. Each fragment has a well-defined electronic population and energy. The population of a fragment (A), $\bar{N}(A)$, may be obtained by integration of the electronic charge density, $\rho(\underset{\sim}{r})$, over the region of space occupied by (A).

$$\bar{N}(A) = \int_A \rho(\underset{\sim}{r}) d\underset{\sim}{r} \qquad [2.8]$$

An expression for the electronic energy density may be immediately written down in terms of the first- and second-order density matrices, $\rho(\underset{\sim}{r};\underset{\sim}{r}')$ and $\Gamma(\underset{\sim}{r}_1,\underset{\sim}{r}_2;\ \underset{\sim}{r}_1',\underset{\sim}{r}_2')$ as

$$E_e(\underset{\sim}{r}) = -\tfrac{1}{4}\nabla^2\rho(\underset{\sim}{r};\underset{\sim}{r}')_{\underset{\sim}{r}=\underset{\sim}{r}'} + \sum_\alpha(-Z_\alpha/r_\alpha)\rho(\underset{\sim}{r}) + \int\Gamma(\underset{\sim}{r}_1,\underset{\sim}{r}_2)/|\underset{\sim}{r}_1-\underset{\sim}{r}_2|\,d\underset{\sim}{r}_2 \qquad [2.9]$$

where Z_α denotes the charge on the α^{th} nucleus, and r_α denotes the distance from the point $\underset{\sim}{r}$ to that nucleus. The above expression may be abbreviated to

$$E_e(\underset{\sim}{r}) = K(\underset{\sim}{r}) + V'(\underset{\sim}{r}) + V''(\underset{\sim}{r}) \qquad [2.10]$$

where $K(\underset{\sim}{r})$, $V'(\underset{\sim}{r})$ and $V''(\underset{\sim}{r})$ denote the local contributions to the kinetic energy, and the one- and two-electron potential energies, respectively. The electronic energy of a fragment $\overline{E}_e(A)$, may then be obtained by integration of [2.10] over the volume of (A).

$$\begin{aligned}\overline{E}_e(A) &= \int_A K(\underset{\sim}{r})d\underset{\sim}{r} + \int_A V'(\underset{\sim}{r})d\underset{\sim}{r} + \int_A V''(\underset{\sim}{r})d\underset{\sim}{r} \\ &= \overline{K}(A) + \overline{V}'(A) + \overline{V}''(A) \qquad [2.11]\end{aligned}$$

$\overline{V}'(A)$ is equivalent to the attractive interaction of the charge density in (A) with all the nuclei in the system. The two-electron potential energy of (A), $\overline{V}''(A)$ is equivalent to the self-repulsion of the electrons in (A), plus one-half the repulsion of the electrons in (A) with those external to (A).* In general, the six-dimensional integration required

---

* The integration of $\Gamma(\underset{\sim}{r}_1,\underset{\sim}{r}_2)$ over (A) may be written as $[\int_A d\underset{\sim}{r}_1\int_A d\underset{\sim}{r}_2+\int_A d\underset{\sim}{r}_1\int_B d\underset{\sim}{r}_2]\Gamma$ $= \overline{V}'_A(A) + \overline{V}''_B(A) = \overline{V}''(A)$. Similarly, $\overline{V}''(B) = \overline{V}''_B(B) + \overline{V}''_A(B)$. $\overline{V}''(A)$ is the self-repulsion of the electrons in (A), and $\overline{V}''_B(A)$ must equal one-half of the electron-electron repulsion between (A) and (B) since $\overline{V}''_A(B) = \overline{V}''_B(A)$.

to determine $\overline{V}^{nn}(A)$ is rather time-consuming. When Hartree-Fock wavefunctions are employed, the term may be evaluated indirectly (see Appendix IA for details).

In addition to the usual Schrödinger form of the kinetic energy density, $K(\underset{\sim}{r})$, it is possible to define a function, $G(\underset{\sim}{r})$, which upon integration over all space also yields the average electronic kinetic energy, $\overline{T}_e$, of system.[92] $G(\underset{\sim}{r})$ may be written in terms of the natural orbitals[41] of the system, $\{\psi_i\}$, and their occupation numbers, $\{\lambda_i\}$, as

$$G(\underset{\sim}{r}) = \tfrac{1}{2}\sum\lambda_i \nabla\psi_i(\underset{\sim}{r})\cdot\nabla\psi_i(\underset{\sim}{r}) \qquad [2.12]$$

(For a Hartree-Fock wavefunction the natural orbitals are equivalent to the occupied orbitals.) $K(\underset{\sim}{r})$ and $G(\underset{\sim}{r})$, although they both yield the average kinetic energy of the system when integrated over all space, are generally quite different locally and are related by the expression,

$$L(\underset{\sim}{r}) = K(\underset{\sim}{r}) - G(\underset{\sim}{r}) = -\tfrac{1}{4}\nabla^2\rho(\underset{\sim}{r}) \qquad [2.13]$$

$K(\underset{\sim}{r})$ exhibits all those quantum-mechanical peculiarities (i.e., negative and infinite values) which are irreconcilable with the classical concepts of the kinetic energy. These peculiarities are isolated in $L(\underset{\sim}{r})$, and hence $G(\underset{\sim}{r})$ is classical-like to the extent that it is finite and positive for all finite values of $\underset{\sim}{r}$ and tends to zero as $\underset{\sim}{r}$ tends to infinity.

The difference between $\overline{K}(A)$ and $\overline{G}(A)$ for a given fragment, (A), is given by

$$\overline{L}(A) = \overline{K}(A) - \overline{G}(A) = -\tfrac{1}{4}\int_A\int\int\nabla^2\rho(\underset{\sim}{r})d\underset{\sim}{r} \qquad [2.14]$$

The volume integral in the above equation may be transformed into an integral over the surface defining the fragment (A) by means of Green's theorem, and therefore [2.14] reduces to

$$\overline{L}(A) = -\tfrac{1}{4}\int_A\int\int\vec{\nabla}\rho(\underset{\sim}{r})\cdot\vec{n}(\underset{\sim}{r})dS \qquad [2.15]$$

where $\vec{n}(\underset{\sim}{r})$ is the outwardly directed unit vector normal to the surface at $\underset{\sim}{r}$, and the integration is performed over all $\underset{\sim}{r} \in S(\underset{\sim}{r})$. For the partitioning surfaces defined in the preceeding section, the integrand in [2.15] is <u>everywhere</u> zero (recall Equation [2.7]). Therefore, $\overline{L}(A) = 0$ for all fragments defined by these surfaces, and the electronic kinetic energy, $\overline{T}_e(A)$, may be obtained by integration of <u>either</u> $K(\underset{\sim}{r})$ or $G(\underset{\sim}{r})$ over the volume contained by (A).

$$\overline{T}_e(A) = \overline{K}(A) = \overline{G}(A) \qquad [2.16]$$

In the sense that both $\overline{K}(A)$ and $\overline{G}(A)$ are identical for fragments defined according to [2.7], the kinetic energy of these fragments is well-defined.

3. There is substantial evidence that a regional virial theorem may hold for fragments defined according to Equation [2.7]. The existence of such a theorem was first suggested by Bader and Beddall,[43,91] and based primarily on two observations regarding the charge distribution:

(1) The additivity of properties (including the total energy) often observed experimentally appears to be a direct consequence of charge distributions of fragments remaining

unaltered upon transfer between systems;

(2) To the extent that the charge distribution in a region of space remains unaltered upon transfer, so too does the kinetic energy density as defined by $G(\underset{\sim}{r})$.

These two observations, taken together, suggested the existence of a relationship between the total energy of a region of space and the kinetic energy of that region. The relationship between these quantities for the full system is, of course, given by the virial theorem, [1.39]. It was therefore suggested that a regional relationship might parallel [1.39] and take the form

$$-\overline{T}_e(A) = \overline{E}_e(A) - \sum_\alpha \vec{R}_\alpha \cdot \vec{F}_\alpha^{el}(A) \qquad [2.17]$$

where $\overline{T}_e(A)$ and $\overline{E}_e(A)$ are given by Equations [2.16] and [2.11], respectively, and $\vec{F}_\alpha^{el}(A)$ is the electronic force exerted on the α^{th} nucleus by the charge density in (A). The last term in [2.17] will henceforth be referred to as the nuclear virial (see Appendix II), and denoted by $\overline{V}_n(A)$.

Equation [2.17] is not a definitive statement of a fragment virial relationship because of the origin dependence in $\overline{V}_n(A)$.[+] That is, the

---

[+] The nuclear virial for the total system, $\overline{V}_n = -\sum_\alpha \vec{R}_\alpha \cdot \vec{F}_\alpha^{el}$, is origin independent. This is easily seen if one considers a shift in the origin by an amount, $\vec{dR}$. The nuclear virial evaluated at this new origin is then given by $\overline{V}_n' = -\sum_\alpha (\vec{R}_\alpha - \vec{dR}) \cdot \vec{F}_\alpha^{el} = -\sum_\alpha \vec{R}_\alpha \cdot \vec{F}_\alpha^{el} + \vec{dR} \cdot \sum_\alpha \vec{F}_\alpha^{el} = \overline{V}_n + \vec{dR} \cdot \sum_\alpha \vec{F}_\alpha^{el}$. The term $\sum_\alpha \vec{F}_\alpha^{el}$ must equal zero as required for translational invariance of the system (note that $\vec{F}_\alpha^{el}$ is equivalent to the net force on α minus the nuclear force). In general, this is not true when the forces are evaluated only over a portion of the charge density (i.e., $\sum_\alpha \vec{F}_\alpha^{el}(A) \neq 0$), and therefore $\overline{V}_n(A)$ is an origin dependent term.

relationship could conceivably hold for any fragment, (A), providing one chose the proper origin to evaluate $\overline{V}_n(A)$. Shortly after the original proposition, Bader, Beddall and Peslak[44] published a theoretical development of [2.17] which provided an independent condition for the determination of the origin. Further, numerical evidence was presented to show that only for fragments defined by [2.7] does the equality in [2.17] hold.

The development, which we briefly review here, closely parallels Slater's[20] original derivation of the molecular virial theorem. This derivation proceeds directly from Schrödinger's equation, $H(=\hat{T}_e+\hat{V}_e)\psi_e = E_e\psi_e$, which may be written

$$-\tfrac{1}{4}\sum_{l=1}^{3n}(\partial^2\psi_e/\partial q_l^2) + (\hat{V}_e - E_e)\psi_e = 0 \qquad [2.18]$$

where q_l denotes an electronic Cartesian coordinate. By operating on [2.18], Slater was able to show that [2.19]

$$\sum_i \psi_e^* (\partial^2\psi_e/\partial q_l^2) - \tfrac{1}{4}\sum_i \partial/\partial q_l \left[\psi_e^{*\,2}\,\partial/\partial q_l \left(\sum_j q_j \frac{\partial\psi_e/\partial q_j}{\psi_e^*}\right)\right] = -\sum_j q_j(\partial\hat{V}_e/\partial q_j)\psi_e^*\,\psi_e$$

Upon integration over all space, Equation [2.19] yields

$$\overline{S}(=-2\overline{T}_e+\not{\delta}) = \overline{V}(=\overline{V}_e+\overline{V}_n) \qquad [2.20]$$

That is, the first term in [2.19] yields minus twice the kinetic energy of the system, $-2\overline{T}_e$; the second term reduces to a surface term, $\not{\delta}$, to be evaluated at the boundary surface of the integration; the third term (i.e., the r.h.s. of [2.19]) yields the virial for the system, $\overline{V}$, which may be expanded as the sum of the electronic potential energy, $\overline{V}_e$, plus the nuclear virial, $\overline{V}_n$ (see Appendix II for details of this

expansion). When the integration is carried out over all space, $\not{\delta}$ vanishes because of the vanishing of ψ_e at the boundary surface, $q_i = \pm\infty$. One is, therefore, lead directly to the general form of the virial theorem, $-2\overline{T}_e = \overline{V}$ (Equation [1.37]). When the integration is performed only over a fragment of the system, $\not{\delta}$ does not, in general, vanish. It is this term which plays an important part in defining those fragments for which a regional virial theorem holds.

Consider now a system partitioned into two fragments, (A) and (B). The integration over [2.19] may be performed in such a manner as to yield[44]

$$\overline{\overline{S}}(A) + \overline{S}(B) = \overline{V}(A) + \overline{V}(B) \qquad [2.21]$$

$\overline{S}(A)$ is equal to $-2\overline{K}(A) + \not{\delta}(A)$, where $\overline{K}(A)$ is as previously defined (Equations [2.9] - [2.11]), and $\not{\delta}(A)$ is a term to be evaluated over the surface defining (A). The virial of (A), $\overline{V}(A)$, is equal to the electronic potential energy of (A), $\overline{V}_e(A) = \overline{V}'(A) + \overline{V}''(A)$ (again see Equations [2.9] - [2.11]), plus the nuclear virial of (A), $\overline{V}_n(A)$. Equivalent definitions hold for $\overline{S}(B)$ and $\overline{V}(B)$. A non-trivial fragment virial relationship would require that

$$\overline{S}(A) = -2\overline{K}(A) + \not{\delta}(A) = \overline{V}(A) \qquad [2.22]$$

Further, a relationship of the form [2.17] would require that

$$-2\overline{T}_e(A) = \overline{V}(A) \qquad [2.23]$$

$\not{\delta}(A)$ is an origin dependent term through the presence of the q_j in [2.19]. Therefore, so too is $\overline{S}(A)$. Similarly, $\overline{V}(A)$ is origin dependent through the nuclear virial, $\overline{V}_n(A)$ (recall the footnote +, page 50). There is now considerable evidence that for fragments defined according

to [2.7], and only for these fragments, is the origin which causes $\mathcal{G}(A)$ to vanish identical to that which brings the two sides of [2.22] into equality. For these fragments, $\overline{K}(A)$ is equivalent to $\overline{T}_e(A)$ (recall page 49), and therefore, [2.22] is equivalent to [2.23].

To summarize then, in analogy with vanishing of $\mathcal{G}$ over the total system, the vanishing of $\mathcal{G}(A)$ provides an independent condition for the determination of the origin for $\overline{V}_n(A)$. Only fragments defined by [2.7] appear to satisfy [2.23]. The surfaces which enclose these fragments are uniquely defined by a property of the system. Therefore, so too is $\overline{V}_n(A)$ unique, and defined completely by a property of the system.

The non-zero contributions to $\mathcal{G}(A)$ come from the finite portions of the surface defining (A), i.e., from all portions of the surface except those at infinity. In polyatomic molecules, one always encounters interior fragments (i.e., fragments bounded by more than one finite surface) in addition to exterior fragments (fragments bounded by a single finite surface). For example, in BH_3F^-, (B) is an interior fragment bounded by four finite surfaces, three which it shares with the exterior (H) fragments, and one which it shares with the exterior (F) fragment. It is clear from the preceeding discussion that the vanishing of $\mathcal{G}$ for a given finite surface requires the definition of an origin. Thus, the nuclear virial of a fragment requires as many origins for its evaluation as there are finite surfaces bounding it. One may obtain a general expression for $\overline{V}_n(A)$ if one defines it by difference, i.e., $\overline{V}_n(A) = \overline{V}_n - \sum_I \overline{V}^I_n(I)$, where (I) is an exterior fragment sharing its surface with (A), and "I" denotes the origin associated with the vanishing of

$\mathcal{S}$ for the finite surface defining (I). It is then a simple matter to show that

$$\bar{V}_n(A) = -\sum_\alpha \vec{R}^o_\alpha \cdot \vec{F}^{el}_\alpha(A) - \sum_I \vec{r}_I \cdot \sum_\alpha \vec{F}^{el}_\alpha(I) \qquad [2.24]$$

where $\vec{R}^o_\alpha$ denotes the position vector of nucleus α from <u>any</u> origin, "o", and $\vec{r}_I$ denotes the position vector from "o" to "I". When (A) is an exterior fragment, [2.24] reduces to $\bar{V}_n(A) = -\sum \vec{R}^a_\alpha \cdot \vec{F}^{el}_\alpha(A)$, the limiting form of $\bar{V}_n(A)$ which appears in Equation [2.17].

The evidence for a fragment virial theorem is, at present, numerical in nature. No analytical proof for the relationship [2.23] has yet been found. Unfortunately, the hypotheses are rather difficult to check for polyatomic systems such as those reported in the following chapter, because of the larger errors in the total virial theorem, and more especially, in the forces associated with these wavefunctions. We will, therefore, in this work, assume the validity of [2.23] to the extent that we will take $-\bar{T}_e(A) = \bar{E}(A)$ for systems with no net forces acting on the nuclei, i.e., here, systems in their equilibrium geometries. In this case, $\bar{V}_n$ reduces to $\bar{V}_n$, the nuclear repulsion potential, and hence $-\bar{T}_e = \bar{E}$. $\bar{V}_n(\hat{A})$ is then equivalent to that portion of $\bar{V}_n$ assigned to (A), and when added to $\bar{E}_e(A)$, yields the total energy of (A). In that the virial relationship appears to hold for fragments defined by [2.7], we will, henceforth refer to the partitioning scheme as the <u>virial partitioning scheme</u>.

NOTE ADDED IN PROOF:

At press time for this work a paper appeared in the literature on regional stationary principles and virial theorems: [A. Mazziotti, R. G. Parr, G. Simons, J. Chem. Phys., 59, 939 (1973).] These authors have shown that if the Born-Oppenheimer Hamiltonian for a molecular system is averaged over all space for electrons 2,3,...,N, but for electron 1 is averaged only over the volume A, bounded by a surface S, the regional expectation value so defined is stationary with respect to change of a parameter ξ in the exact wavefunction, provided that

$$\int_S [(\partial/\partial \vec{n}_1) P_\xi(1,1')]_{1'=1} \, dS_1 = 0$$

where $\vec{n}$ is a vector normal to S, and for nodeless ψ,

$$P_\xi(1,1') = \int \ldots \int \psi^*(1',2,\ldots,N)\psi(1,2,\ldots,N) \cdot$$

$$(\partial/\partial\xi) \ell n[\psi(1,2,\ldots,N)/\psi^*(1',2,\ldots,N)]\Big|_{\xi=1} \, d\tau_2 \ldots d\tau_N$$

Under this condition a regional virial has been shown to hold for the volume A, in the sense previously described in this work. The above condition differs from the condition given in Equation [2.6], but, in the opinion of these authors, the surfaces defined by it should be very similar to those defined by Equation [2.6].

CHAPTER 3

A SUMMARY OF WAVEFUNCTION COMPUTATIONS

All computations were performed on Control Data Corporation 6400 and Cyber 70 computers with a locally upgraded version of the POLYATOM/2 SCF program system[52] (programs PA20, PA300, and PA40 (PA400 for the open-shell atomic systems)). Those for BH_3, BF_3, BH_4^-, BH_3CO and FHF^- are the best reported to date in terms of the total energy. To the author's knowledge, no previous computations have been performed on BH_3F^- and BF_3H^-.

A. Boron Systems

1. Basis Sets

All wavefunctions for the boron systems employ Huzinaga's[53] (10,6) Gaussian basis sets on the first-row atoms, and his 6s expansion on the hydrogens. The (10,6) sets were contracted to [5,3] as suggested by Dunning.[54] The 6s hydrogen set was contracted 2.2.1.1 for all except the BH_3CO wavefunction, where the contraction was 2.2.2. A complete set of d-type polarization functions (x^2, y^2, z^2, xy, xz, yz) was added to each first-row atom ($\alpha_B = 0.57$; $\alpha_C = 0.92$; $\alpha_O = 0.91$; $\alpha_F = 1.00$); a complete set of p-type polarization functions (x, y, z) was added to each hydrogen ($\alpha_H = 1.00$). Exponents of the polarization function are close to optimum.

In addition, for the negatively charged molecular ions, BH_4^- and BH_3F^-, the sets were further augmented with one diffuse s-type function per atom ($\alpha_B = 0.30$; $\alpha_F = 0.11$; $\alpha_H = 0.032$), and one diffuse

p-type function per first-row atom ($\alpha_B = 0.022$; $\alpha_F = 0.073$). This additional (sp/s) augmentation was done to ensure that the wavefunctions for these molecular ions, with their more diffuse electron distributions, would be of about the same quality as those for the neutral molecules. For the BF_3H^- molecular ion, only the H set was augmented with a diffuse function. The reason for this was partially a fiscal one, for augmentation of the entire basis set would have nearly doubled the already large amount of calculation time required. Further, it was felt that additional flexibility on the H could prove to be more important than on the (BF_3) fragment. If the extra charge density in this molecule was largely localized on the (BF_3) fragment (specifically, on the fluorines), it would be shared among the various constituents, and extra flexibility in the basis set would not be quite as important. If, on the other hand, the extra density was localized largely in the region of the H, additional flexibility here would be almost mandatory.

It was expected that the additional diffuse functions would have little effect on the neutral species. In order to check this, calculations with and without the additional (sp/s) augmentation were performed on B, H, F, BH, BF, and BH_3. It was found that although the additional functions had very little effect on the total electronic energy, they sometimes had an appreciable effect on the various components of that energy (T, V', and V''). For this reason, whenever possible, comparisons are made only between systems and fragments which employ identical basis sets.

A summary of the wavefunctions and the basis sets is given in Tables 3-1 and 3-3. Both the augmented and non-(sp/s) augmented results

are reported for B, H, F and BH_3. The shorthand notation used for the basis sets employed on the first-row atoms, (A), and the hydrogens, (H), is as follows:

A1: Huzinaga-Dunning (10,6) ≡ [5,3] augmented with d functions (α_B = 0.57; α_C = 0.92; α_O = 0.91; α_F = 1.00)

A2: The A1 set plus additional s (α_B = 0.30; α_F = 0.11) and p (α_B = 0.022; α_F = 0.073) functions

H1: Huzinaga (6) ≡ [4] augmented with p functions (α_H = 1.0)

H2: The H1 set plus an additional s function (α_H = 0.032)

H3: Identical to H1 set, except (6) ≡ [3]

2. Geometries

Molecular geometries for the boron systems are given in Table 3-1. Experimental geometries were used for BH,[55] BF_3,[56] BH_3CO,[57] CO,[58] and BF.[59] The BH_3 molecule was found to be of D_{3h} symmetry, in accordance with the work of other authors.[60-62] The B-H bond length in this molecule was optimized with a smaller basis set (Huzinaga[53]-Dunning[54] (9,5/4) ≡ [4,3/2(3.1)]), augmented with a set of p functions on H (α_H = 1.0), and was found to be 2.25 au. Other authors have reported values of 2.25,[60] 2.191,[61] and 2.31 au,[62] using smaller basis sets. A tetrahedral geometry was assumed for BH_4^-. The B-H bond length in this molecule was found to be 2.336 au, again via an optimization procedure using a smaller basis set (Huzinaga[53]-Dunning[54] (9,5/4) ≡ [4,2/3(2.1.1)]). Previous theoretical values are 2.1 ± .2[63] and 2.24 au.[64] The value obtained here is in

good agreement with the experimental value of 2.37 ± .04 au[65] in crystalline Na-, K-, and Rb-BH_4^-.

BH_3F^- and BF_3H^- have not yet been observed experimentally. Both molecules were assumed to be of C_{3v} symmetry. The geometry of the (BH_3) fragment in BH_3F^- was taken to be identical to that of a (BH_3) fragment in BH_4^-; the geometry of the (BF_3) fragment in BF_3H^- was taken as identical to the experimental geometry of a (BF_3) fragment in crystalline BF_4^-.[66] The B-F bond length in BH_3F^- was calculated to be 2.817 au, using the smaller basis set described above for BH_3, augmented with s (α_B = 0.032; α_F = 0.110; α_H = 0.05) and p (α_B = 0.022; α_F = 0.086) functions. The B-H bond length in BF_3H^- was fixed at 2.31 au, an average of the BH_3 and BH_4^- values.

Two calculations are also reported for BH_3 in a bent (C_{3v}) configuration. In one case, the BH_3 geometry is identical to that of the (BH_3) fragment in BH_4^- and BH_3F^-. In the other, the geometry is the same as that for the (BH_3) fragment in BH_3CO.

3. Energetics

The total energies and their components for these systems are listed in Tables 3-2 and 3-3. The dissociation energies for the larger molecules are given in Table 3-4. These were obtained as follows.

(a) BH_3

The Hartree-Fock value for the dissociation energy (D_e^o) of BH (as calculated from Tables 3-2 and 3-3) is 63.40 kcal/mole. This compares to an experimental value of 84.32 kcal/mole.[67] The difference between these two values (20.92 kcal/mole) should serve as a good estimate of the correlation energy correction for the reaction,

$BH(g) \rightarrow B(g) + H(g)$. The Hartree-Fock value for the BH_3 dissociation energy is 233.46 kcal/mole. An estimate of the correlation correction here may be taken as roughly twice that for the BH dissociation, since three electron pairs are broken during the reaction $BH_3(g) \rightarrow B(g) + 3H(g)$, and one new pair is formed in going to the boron ^2P ground state. This yields a D_e^o value of 275.3 kcal/mole for the BH_3 dissociation.

The D_o^o values for dissociation of B_2H_6 into atoms, and into two BH_3 molecules, have previously been estimated as 566.36 kcal/mole[68] and 37.1 kcal/mole,[69] respectively. These two values may be coupled to yield a D_o^o value for the BH_3 dissociation of 264.7 kcal/mole, in reasonable agreement with the D_e^o value reported here.

(b) BF_3

The Hartree-Fock and experimental D_e^o values for BF are 139.23 and 197.9 ± 11.5 kcal/mole,[70] respectively. The Hartree-Fock value for BF_3 is 366.23 kcal/mole. Applying the same reasoning as for BH_3 yields a D_e^o value for BF_3 of 483.6 ± 23.2 kcal/mole. This is in agreement with the experimental D_o^o value of 460.5 kcal/mole reported by Diebler and Liston.[71]

(c) BH_4^-, BH_3F^-, BH_3CO, and BF_3H^-

The dissociation energies reported for these compounds were computed directly from the Hartree-Fock energies. No correlation corrections were made since all species involved are closed shell systems. (Recall the discussion in Chapter I-C.) The value of D_e^o $(BH_3\text{-}H^-)$ = 62.7 kcal/mole is in good agreement with a previously reported theoretical value of 62.0 kcal/mole.[72] Several experimental estimates for $D_o(BH_3\text{-}CO)$

have been given. McCoy and Bauer[73] report $D_o^{300} = 18.8$ kcal/mole; Feldman and Koski[69] give $D_o^{400} = 23.1 \pm 2$ kcal/mole. A previous theoretical calculation with a much smaller (5,3/3) basis set gives $D_e^o = 22.7$ kcal/mole.[74] The value reported here ($D_e^o = 6.3$ kcal/mole) is considerably less than all of these. No previous theoretical or experimental data is available for BH_3F^- and BF_3H^-.

TABLE 3-1. Wavefunctions for the boron systems. Electronic state and configuration, geometry, basis set, orbital energies (including those for the first few virtual orbitals), and total energy are reported. All data is given in atomic units.

MOLECULE	GEOMETRY	BASIS SET	ORBITAL AND TOTAL ENERGIES			
$BH(X\ ^1\Sigma^+)$	$C_{\infty v}$ $R(B\text{-}H) = 2.336$	(A2,H2)	$1\sigma(2)$	- 7.68702	1π	.02615
			$2\sigma(2)$	- .64872	4σ	.05013
			$3\sigma(2)$	- .34744	5σ	.06052
			TOTAL ENERGY	-25.12946		
$BF(X\ ^1\Sigma^+)$	$C_{\infty v}$ $R(B\text{-}F) = 2.391$	(A2)	$1\sigma(2)$	- 26.37833	$5\sigma(2)$	- .40619
			$2\sigma(2)$	- 7.71468	2π	.04046
			$3\sigma(2)$	- 1.69986	6σ	.04861
			$4\sigma(2)$	- .85475	7π	.06950
			$1\pi(4)$	- .74457		
			TOTAL ENERGY	-124.15704		
$BH_3(X\ ^1A_1')$	D_{3h} $R(B\text{-}H) = 2.25$	(A2,H2)	$1a_1'(2)$	- 7.61275	$1a_2''$	.03052
			$2a_1'(2)$	- .70440	$2e'$	.04622
			$1e'(4)$	- .49817	$3a_1'$	.05286
			TOTAL ENERGY	-26.39998		
$BF_3(X\ ^1A_1')$	D_{3h} $R(B\text{-}F) = 2.447$	(A1)	$1e'(4)$	- 26.33840	$4e'(4)$	- .70263
			$1a_1'(2)$	- 26.33837	$1e''(4)$	- .68798
			$2a_1'(2)$	- 7.77811	$1a_2'(2)$	- .66184
			$3a_1'(2)$	- 1.69443	$2a_2''$	.12698
			$2e'(4)$	- 1.64875	$5e'$	.15758
			$4a_1'(2)$	- .86216	$5a_1'$	16162
			$3e'(4)$	- .81931	$3a_2''$	24105
			$1a_2''(2)$	- .76876	$6a_1'$	55407
	TOTAL ENERGY -323.33119					

TABLE 3-1 (Cont.)

MOLECULE	GEOMETRY	BASIS SET	ORBITAL AND TOTAL ENERGIES			
$BH_4^-(X\ ^1A^1)$	T_d R(B-H) = 2.362	(A2,H2)	$1a_1(2)$	- 7.29920	$2t_2$	.15993
			$2a_1(2)$	- .44930	$3a_1$	.17587
			$1t_2(6)$	- .19057	$3t_2$	.24343
			TOTAL ENERGY	-26.98725		
$BH_3F^-(X\ ^1A^1)$	C_{3v} R(B-H) = 2.362 R(B-F) = 2.817 tetrahedral angles	(A2,H2)	$1a_1(2)$	- 25.99917	$5a_1(2)$	- .34647
			$2a_1(2)$	- 7.35960	2e(4)	- .19255
			$3a_1(2)$	- 1.28303	3e	.16021
			$4a_1(2)$	- .49171	$6a_1$	.16266
			1e(4)	- .38109	$7a_1$	.18578
					4e	.23979
			TOTAL ENERGY	-125.95169		
$BH_3CO(X\ ^1A_1)$	C_{3v} R(B-H) = 2.256 R(B-C) = 2.910 R(C-O) = 2.137 θ(H-B-H) = 113.6667 θ(H-B-C) = 104.6064	(A1,H3)	$1a_1(2)$	- 20.71604	1e(4)	- .69375
			$2a_1(2)$	- 11.44063	$7a_1(2)$	- .56298
			$3a_1(2)$	- 7.55433	2e(4)	- .47281
			$4a_1(2)$	- 1.57169	3e	.09743
			$5a_1(2)$	- .90234	$8a_1$	.13737
			$6a_1(2)$	- .79987	4e	.17045
					$9a_1$	.19728
			TOTAL ENERGY	-139.18595		

TABLE 3-1 (Cont.)

MOLECULE	GEOMETRY	BASIS SET	ORBITAL AND TOTAL ENERGIES			
$BF_3H^-(X\ ^1A_1)$	C_{3v} R(B-F) = 2.646 R(B-H) = 2.310 tetrahedral angles	(A1,H2)	1e(4)	- 26.02935	4e(4)	- .40918
			$1a_1(2)$	- 26.02933	5e(4)	- .37746
			$2a_1(2)$	- 7.44597	$1a_1(2)$	- .36087
			$3a_1(2)$	- 1.36842	$6a_1(2)$	- .23973
			2e(4)	- 1.32180	$7a_1$	.20616
			$4a_1(2)$	- .56778	$8a_1$	.33441
			3e(4)	- .48858	5e	.33759
			$5a_1(2)$	- .47729	$9a_1$	.45028
					$10a_1$	.56465
			TOTAL ENERGY	-323.92439		
$BH_3(X\ ^1A_1')$	D_{3h} R(B-H) = 2.25	(A1,H1)	$1a_1'(2)$	- 7.61321	$1a_2''$	.05003
			$2a_1'(2)$	- .70457	2e'	.16743
			1e'(4)	- .49864	$2a_2''$	.24235
			TOTAL ENERGY	-26.39965		
$BH_3(X\ ^1A_1)$	C_{3v} R(B-H) = 2.336 tetrahedral angles (BH_4^-, BH_3F^- geometry)	(A2,H2)	$1a_1(2)$	- 7.63894	$3a_1$	.01314
			$2a_1(2)$	- .69549	2e	.04687
			1e(4)	- .47096	$4a_1$	.05294
			TOTAL ENERGY	-26.35655		
$BH_3(X\ ^1A_1)$	C_{3v} R(B-H) = 2.256 Θ(H-B-H) = 113.6667 (BH_3CO geometry)	(A1,H3)	$1a_1(2)$	- 7.61712	$3a_1$	.03610
			$2a_1(2)$	- .70668	2e	.16730
			1e(4)	- .48781	$4a_1$	.22806
			TOTAL ENERGY	-26.37757		

TABLE 3-1 (Cont.)

MOLECULE	GEOMETRY	BASIS SET
$CO(X\ ^1\Sigma^+)$	$C_{\infty v}$ R(C-O) = 2.132	(A1)

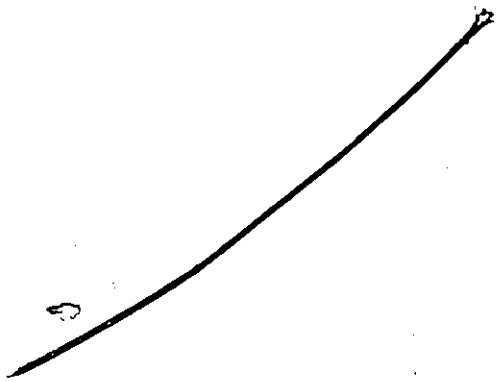

ORBITAL AND TOTAL ENERGIES

$1\sigma(2)$	- 20.67502	$1\pi(4)$	- .64203
$2\sigma(2)$	- 11.36043	$5\sigma(2)$	- .55452
$3\sigma(2)$	- 1.52790	2π	.12330
$4\sigma(2)$	- .80608	6σ	.23958
		3π	.31280

TOTAL ENERGY -112.77631

TABLE 3-2

Wavefunctions for boron systems. Energy components. All data in atomic units.

MOLECULE	$\bar{T}e$	$\bar{V}'$	$\bar{V}''$	$\bar{E}_e$	$\bar{V}_n$	$\bar{E}_T$
$BH(X\ ^1\Sigma^+)$	25.11517	- 62.28857	9.90353	- 27.26987	2.14041	- 25.12946
$BF(X\ ^1\Sigma^+)$	124.09258	-332.96297	65.89275	-142.97762	18.82058	-124.15704
$BH_3(X\ ^1A_1')$	26.38191	- 75.42784	15.20948	- 33.83645	7.43647	- 26.39998
$BF_3(X\ ^1A_1')$	323.27859	-997.95249	238.83919	-435.83471	112.50352	-323.33119
$BH_4^-(X\ ^1A_1)$	26.95203	- 84.33197	20.36974	- 37.01021	10.02296	- 26.98725
$BH_3F^-(X\ ^1A_1)$	125.84904	-363.47647	82.20022	-155.42721	29.47552	-125.95169
$BH_3CO(X\ ^1A_1)$	139.08345	-438.70362	103.92992	-195.69025	56.50430	-139.18595
$BF_3H^-(X\ ^1A_1)$	323.90807	-1016.44830	252.52796	-440.01227	116.08788	-323.92439
$^aBH_3(X\ ^1A_1)$	26.38139	- 75.42355	15.20605	- 33.83612	7.43647	- 26.39965
$^bBH_3(X\ ^1A_1)$	26.18230	- 74.59938	14.93219	- 33.48489	7.12833	- 26.35655
$^cBH_3(X\ ^1A_1)$	26.36083	- 75.40184	15.22111	- 33.81990	7.44233	- 26.37757
$CO(X\ ^1\Sigma^+)$	112.66207	-310.87489	62.92244	-135.29038	22.51407	-112.77631

a non-(sp/s) augmented basis set

b geometry same as (BH_3) in BH_4^- and BH_3F^-

c geometry same as (BH_3) in BH_3CO

TABLE 3-3

Atomic wavefunctions. Basis sets and energy components. All data in atomic units.

SPECIES	BASIS SET	$\bar{T}_e$	$\bar{V}'$	$\bar{V}''$	$\bar{E}_e$
$B(X^2P)$	(A2)	24.52893	- 56.89503	7.83764	-24.52847
$B(X^2P)$	(A1)	24.52979	- 56.89811	7.83987	-24.52844
$F(X^2P)$	(A2)	99.38703	-238.61639	39.82263	-99.40673
$F(X^2P)$	(A1)	99.41936	-238.67845	39.85269	-99.40644
$F^-(X^1S)$	(A2)	99.43554	-243.45075	44.56022	-99.45499
$H(X^2S)$	(H1),(H2),(H3)	.49994	- .99988	0.	- .49994
$H^-(X^1S)$	(H2)	.49048	- 1.37792	.40009	- .48736

TABLE 3-4

Some Calculated Dissociation Energies†

REACTION	D_e^o(kcal/mole)
$BH_3(g) \rightarrow B(g) + 3H(g)$	275
$BF_3(g) \rightarrow B(g) + 3F(g)$	484 ± 24
$BH_4^-(g) \rightarrow BH_3(g) + H^-(g)$	62.7
$BH_3F^-(g) \rightarrow BH_3(g) + F^-(g)$	60.7
$BH_3CO(g) \rightarrow BH_3(g) + CO(g)$	6.3
$BF_3H^-(g) \rightarrow BF_3(g) + H^-(g)$	66.4

† Dissociation energies are for 0°K and do not include a zero-point vibrational energy correction.

B. Bifluoride Reaction

1. Basis sets

All computations on the bifluoride systems were performed with Csizmadia's[75] (13,7/4) Gaussian basis set, augmented with a set of p functions on hydrogen ($\alpha_H = 1.00$). This set was used in uncontracted form (except during geometry optimizations, where the contraction was to [4,2/2]), thus providing a rather large amount of (sp) flexibility.

2. Geometries

Four configurations along the linear reaction path for $HF(g) + F^-(g) \rightarrow FHF^-(g)$ are reported in Tables 3-5 and 3-6, along with results of calculations on F, F^-, and HF. The HF geometry is the experimental one.[67] The geometries of the FHF^- ion were all optimized with the contracted basis set described above.

The FHF^- ion, in its equilibrium geometry, was found to be of $D_{\infty h}$ symmetry, with an F-F distance of 4.24 au. This is consistent with other recent theoretical values[76-79] which range from 4.20 to 4.34 au. The most recent experimental value is 4.331 ± .008 au[80] in crystalline Na-, K-, and NH_4-HF_2.

3. Energetics

The total energy obtained for the equilibrium configuration of the bifluoride ion (see Table 3-5) is surprisingly low, even though no polarization functions were added to the fluorines. The value is ~ 6 kcal/mole below the previously reported best value,[76] and lies only .01 au above the estimated Hartree-Fock energy.[76]

From the data of Table 3-6, the value of $D_e^o(FH\text{-}F^-)$ is computed

to be 43.2 kcal/mole. This value compares well with other recent theoretical values[77-79] which range from 40 to 52 kcal/mole. Experimental estimates of the hydrogen bond energy in this molecule have varied from ~ 27-58 kcal/mole. The best estimate to date is probably that of Harrell and McDaniel[81] (37 ± 2 kcal/mole). The reaction apparently proceeds with no activation energy.

TABLE 3-5. Wavefunctions for the bifluoride systems. Electronic state and configuration, geometry, orbital energies (including those for the first few virtual orbitals), and total energy are reported. All data is given in atomic units.

MOLECULE	GEOMETRY	ORBITAL AND TOTAL ENERGIES			
$FHF^-(X\ ^1\Sigma^+)$	$C_{\infty v}$ R(F-F) = 7.000 R(F-H) = 1.743	$1\sigma(2)$	- 26.14543	$1\pi(4)$	- .50024
		$2\sigma(2)$	- 25.84359	$2\pi(4)$	- .20182
		$3\sigma(2)$	- 1.45289	$6\sigma(2)$	- .20012
		$4\sigma(2)$	- 1.09412	7σ	.38340
		$5\sigma(2)$	- .61356	8σ	.49720
				3π	.51967
		TOTAL ENERGY	-199.53871		
$FHF^-(X\ ^1\Sigma^+)$	$C_{\infty v}$ R(F-F) = 6.000 R(F-H) = 1.772	$1\sigma(2)$	- 26.11234	$1\pi(4)$	- .46877
		$2\sigma(2)$	- 25.85667	$6\sigma(2)$	- .21623
		$3\sigma(2)$	- 1.41673	$2\pi(4)$	- .21567
		$4\sigma(2)$	- 1.10859	7σ	.42231
		$5\sigma(2)$	- .57857	8σ	.51798
				3π	.53788
		TOTAL ENERGY	-199.55074		
$FHF^-(X\ ^1\Sigma^+)$	$C_{\infty v}$ R(F-F) = 5.000 R(F-H) = 1.849	$1\sigma(2)$	- 26.05847	$1\pi(4)$	- .41689
		$2\sigma(2)$	- 25.88114	$6\sigma(2)$	- .24609
		$3\sigma(2)$	- 1.35604	$2\pi(4)$	- .24320
		$4\sigma(2)$	- 1.13956	7σ	.47131
		$5\sigma(2)$	- .52348	8σ	.54505
				3π	.56498
		TOTAL ENERGY	-199.56908		

TABLE 3-5 (Cont.)

MOLECULE	GEOMETRY	ORBITAL AND TOTAL ENERGIES			
†$FHF^-(X\ ^1\Sigma_g^+)$	$D_{\infty h}$ R(F-F) = 4.240 R(F-H) = 2.120	$1\sigma_u(2)$	- 25.95724	$1\pi_u(4)$	- .33475
		$1\sigma_g(2)$	- 25.95721	$1\pi_g(4)$	- .30649
		$2\sigma_g(2)$	- 1.26839	$3\sigma_u(2)$	- .28489
		$2\sigma_u(2)$	- 1.21478	$4\sigma_g$	.50840
		$3\sigma_g(2)$	- .47591	$4\sigma_u$	.56528
				$2\pi_u$	.29316
		TOTAL ENERGY	-199.58098		
†$HF(X\ ^1\Sigma^+)$	$C_{\infty v}$ R(H-F) = 1.7328	$1\sigma(2)$	- 26.29532	$1\pi(4)$	- .65047
		$2\sigma(2)$	- 1.60675	$4c$	.20993
		$3\sigma(2)$	- .75455	5σ	.38103
				2π	.38356
		TOTAL ENERGY	-100.05694		
$F^-(X^1S)$	---	$1s(2)$	- 25.82006	$3s$	.60049
		$2s(2)$	- 1.06719	$3p$	.68573
		$2p(6)$	- .17465		
		TOTAL ENERGY	-99.45519		

† equilibrium geometry

TABLE 3-6. Wavefunctions for bifluoride systems.

Energy components. All data is in atomic units.

SPECIES		$\bar{T}$	$\bar{V}'$	$\bar{V}''$	$\bar{E}_e$	$\bar{V}_n$	$\bar{E}_T$
$FHF^-(X\ ^1\Sigma^+)$	$R_{F-F} = 7.000$	199.45835	-521.90732	104.46332	-217.98565	18.44694	-199.53871
$FHF^-(X\ ^1\Sigma^+)$	$R_{F-F} = 6.000$	199.42610	-526.59272	106.90821	-220.25841	20.70767	-199.55074
$FHF^-(X\ ^1\Sigma^+)$	$R_{F-F} = 5.000$	199.41676	-533.30850	110.39893	-223.49281	23.92373	-199.56908
$FHF^-(X\ ^1\Sigma_g^+)$	$R_{F-F} = 4.240$	199.62705	-541.17419	114.37182	-227.17532	27.59434	-199.58098
$HF(X\ ^1\Sigma^+)$		100.01833	-250.58037	45.31119	-105.25084	5.19391	-100.05694
$F^-(X^1S)$		99.46902	-243.56453	44.64032	- 99.45519	---	- 99.45519

CHAPTER 4

APPLICATIONS OF THE VIRIAL PARTITIONING METHOD

We now employ the virial partitioning scheme outlined in Chapter 2 to a study of the changes in the charge and energy distributions which occur during Lewis acid-base reacitons. Section A opens the chapter with a discussion of BH, BF, BH_3, and BF_3. This section is intended to acquaint the reader with the concepts of fragments and fragment properties, and how they may be used in the description and interpretive study of chemical systems. The analyses of the Lewis acids, BH_3 and BF_3, are preparative to the study of their complexes. In Section B we discuss the four complexes, BH_3-H^-, BH_3-F^-, BH_3-CO, and BF_3-H^-, particularly with respect to the charge redistributions which occur upon complex formation, and the reasons underlying them. In Section C we look at the changes which occur during hydrogen bond formation in the reaction: $FH + F^- \rightarrow FHF^-$. Finally, Section D concludes the chapter with a discussion of transferability of virially partitioned fragments between molecular systems, and the possibility of employing them in quantum-mechanical calculations. All data given in the tables and quoted in the text are in atomic units, unless explicitly stated otherwise.

The notation which will be used has, for the most part, been previously defined. It will sometimes be convenient to break the electron-nuclear attractive potential of a fragment, $\overline{V}'(A)$, into its internal and external components. The internal component, denoted as $\overline{V}'_{int}(A)$, is simply the attractive interaction of the charge density in (A) with the nucleus (or nuclei) contained by (A). The external component, $\overline{V}'_{ext}(A)$, is the interaction of that density with nuclei exterior to (A). The electron-electron repulsion potential, $\overline{V}''(A)$, may be divided in a similar manner. The internal component, $\overline{V}''_{int}(A)$, is the self-repulsion of the charge density in (A). The external component, $\overline{V}''_{ext}(A)$, is equal to one-half the repulsion of the charge density in (A) with the charge density external to it. (The other half is assigned to the external fragments.)

Note also that the virial of a fragment will always be denoted with a script $\overline{\mathcal{V}}$, whereas the potential energy will be denoted by a non-script $\overline{V}$. The electronic component of the virial, $\overline{\mathcal{V}}_e$, is always equivalent to the sum of $\overline{V}'$ and $\overline{V}''$. The nuclear component, $\overline{\mathcal{V}}_n$, reduces to the nuclear repulsion potential, $\overline{V}_n$, plus a net force term (the virial of the external forces) when a molecule is not at its equilibrium geometry. (See Appendix II for details.) As stated earlier, we will in this work assume the operation of a fragment virial theorem, $-2\overline{T}_e(A) = \overline{\mathcal{V}}(A)$, and for equilibrium geometries take $-\overline{T}_e(A)$ as equal to the total energy of the fragment, $\overline{E}(A)$.

Finally, we define the net charge on a fragment as $C(A) = Z_A - N(A)$, where Z_A denotes the total nuclear charge interior to (A), and $N(A)$ denotes the electronic population of (A).

TABLE 4-1. Fragment populations and energies for the boron systems.

The values of $-\bar{E}/\bar{T}_e$ reported for each system were used to scale the $\bar{T}_e$ values prior to calculation of the energy changes listed in Tables 4-2 and 4-3. All values are given in atomic units (1 au = 627.71 kcal/mole).

SPECIES	FRAGMENT	N	$\bar{T}_e$	$\bar{V}'$	$\bar{V}''$	$\bar{E}_e$	$^{\dagger}\bar{V}_{nn}$	
	(B)	4.2177	24.2077	- 56.4297	7.9601	- 24.2619	.0542	$\bar{E}$ = - 25.1295
BH	(H)	1.7823	.9075	- 5.8589	1.9434	- 3.0080	2.1005	$-\bar{E}/\bar{T}_e$ = 1.000569
	TOTAL	6.0000	25.1152	- 62.2886	9.9035	- 27.2699	2.1547	
	(B)	2.8630	23.7532	- 55.5266	8.0381	- 23.7352	- .0180	$\bar{E}$ = - 26.4000
BH_3	(H)	1.7123	.8762	- 6.6338	2.3905	- 3.3671	2.4908	$-\bar{E}/\bar{T}_e$ = 1.000685
	TOTAL	8.0000	26.3819	- 75.4278	15.2095	- 33.8364	7.4545	
	(B)	4.0673	24.0940	- 67.2971	13.4300	- 29.7732	5.6792	$\bar{E}$ = -124.1570
BF	(F)	9.9327	99.9986	-265.6658	52.4628	-113.2044	13.2058	$-\bar{E}/\bar{T}_e$ = 1.000519
	TOTAL	14.0000	124.0926	-332.9630	65.8928	-142.9776	18.8850	
	(B)	2.4079	23.3657	- 76.4334	18.6147	- 34.4531	11.0874	$\bar{E}$ = -323.3312
BF_3	(F)	9.8640	99.9710	-307.1730	73.4082	-133.7939	33.8229	$-\bar{E}/\bar{T}_e$ = 1.000163
	TOTAL	32.0000	323.2786	-997.9525	238.8392	-435.8347	112.5561	
	(B)	2.9848	23.6908	- 57.0323	9.2500	- 24.0915	.4007	$\bar{E}$ = - 26.9872
BH_4^-	(H)	1.7538	.8153	- 6.8249	2.7799	- 3.2297	2.4144	$-\bar{E}/\bar{T}_e$ = 1.001307
	(BH_3)	8.2462	26.1367	- 77.5071	17.5898	- 33.7805	7.6438	
	TOTAL	10.0000	26.9520	- 84.3320	20.3697	- 37.0102	10.0582	

TABLE 4-1 (Cont.)

SPECIES	FRAGMENT	$\bar{N}$	$\bar{T}_e$	$\bar{V}'$	$\bar{V}''$	$\bar{E}_e$	$\bar{V}_n$	
								$\bar{E}$ = -125.9517
	(B)	2.7860	23.5646	- 63.6580	12.5847	- 27.5087	3.9440	
	(H)	1.7638	.8441	- 10.2877	4.4732	- 4.9703	4.1262	
BH_3F^-	(BH_3)	8.0773	26.0969	- 94.5211	26.0045	- 42.4197	16.3228	$-\bar{E}/\bar{T}e$ = 1.000816
	(F)	9.9227	99.7521	-268.9554	56.1958	-113.0075	13.2554	
	TOTAL	18.0000	125.8490	-363.4765	82.2002	-155.4272	29.5782	
								$\bar{E}$ = -139.1860
	(B)	2.9629	23.7984	- 66.7334	13.6511	- 29.2839	5.4856	
	(H)	1.6379	.8265	- 10.9733	4.6272	- 5.5197	4.6932	
	(BH_3)	7.8765	26.2779	- 99.6534	27.5326	- 45.8430	19.5651	$-\bar{E}/\bar{T}_e$ = 1.000737
BH_3CO	(C)	4.8210	37.0542	-112.6456	25.2542	- 50.3372	13.2831	
	(O)	9.3025	75.7514	-226.4046	51.1431	- 99.5100	23.7586	
	(CO)	14.1235	112.8056	-339.0502	76.3973	-149.8473	37.0417	
	TOTAL	22.0000	139.0835	-438.7036	103.9299	-195.6903	56.6068	
								$\bar{E}$ = -323.9244
	(B)	2.5044	23.3516	- 76.7708	19.1654	- 34.2538	10.9022	
	(F)	9.9114	99.8841	-307.3162	75.0780	-132.3541	32.4700	
BF_3H^-	(BF_3)	32.2385	323.0038	-998.7194	244.3994	-431.3161	108.3123	$-\bar{E}/\bar{T}_e$ = 1.000050
	(H^-)	1.7615	.9042	- 17.7289	8.1285	- 8.6961	7.7919	
	TOTAL	34.0000	323.9081	-1016.4483	252.5280	-440.0123	116.1042	
								$\bar{E}$ = - 26.3996
	(B)	2.8696	23.7585	- 55.5590	8.0488	- 23.7517	- .0068	
	(H)	1.7101	.8743	- 6.6215	2.3857	- 3.3615	2.4872	$-\bar{E}/\bar{T}_e$ = 1.000692
$^aBH_3$	TOTAL	8.0000	26.3814	- 75.4236	15.2060	- 33.8361	7.4547	

TABLE 4-1 (Cont.)

SPECIES	FRAGMENT	$\overline{N}$	$\overline{T}_e$	$\overline{V}'$	$\overline{V}''$	$\overline{E}_e$	$\overline{V}_n$	
								$\overline{E}$ = - 26.3776
	(B)	2.9235	23.7720	- 55.7592	8.1244	- 23.8627	.0907	
	(H)	1.6922	.8629	- 6.5476	2.3656	- 3.3191	2.4561	$-\overline{E}/\overline{T}_e$ = 1.000635
a,b BH_3	TOTAL	8.0000	26.3608	- 75.4018	15.2211	- 33.8199	7.4591	
								$\overline{E}$ = - 26.3566
	(B)	3.0365	23.7632	- 55.9706	8.1824	- 24.0251	.2619	
	(H)	1.6545	.8064	- 6.2096	2.2499	- 3.1533	2.4569	$-\overline{E}/\overline{T}_e$ = 1.006655
c BH_3	TOTAL	8.0000	26.1823	- 74.5994	14.9322	- 33.4849	7.3026	
								$\overline{E}$ = -112.7763
	(C)	4.6416	36.7947	- 98.0187	18.8442	- 42.7820	5.9873	
	(O)	9.3584	75.8673	-212.8562	44.4805	- 92.5083	16.6410	$-\overline{E}/\overline{T}_e$ = 1.001014
CO	TOTAL	14.0000	112.6621	-310.8749	62.9224	-135.2904	22.6283	

a Non-(sp/s) augmented basis set. The results for BH_3CO should be compared to those for this wavefunction.

b The geometry here is identical to that of a (BH_3) fragment in BH_3CO.

c The geometry here is identical to that of the (BH_3) fragments in BH_4^- and BH_3F^-.

† Calculated by difference. $\overline{V}_n = -\overline{E}_e - \overline{T}_e$.

A. A Comparison of BH, BH_3, BF, and BF_3

The fragment populations and energy components for all the boron system are given in Table 4-1. The changes in fragment properties on bond formation in the above compounds are summarized in Table 4-2. All values are relative to the constituent atoms in their ground states. Contour maps of the charge distributions and partitioning surfaces for BH and BH_3 are shown in Fig. 4-1. Those for BF and BF_3 appear in Fig. 4-2.

The formation of BH from its constituent atoms is marked by the transfer of .78 electrons (e) from (B) to (H). In BH_3 the transfer drops to .71 e per (H), a result which one might well expect as the (B) fragment loses more and more of its valence density. In BF one observes a larger transfer of .93 e, consistent with the so-called "electronegativity" difference between F and H. The transfer in BF_3 drops to .86 e per (F), paralleling the BH to BH_3 change. Thus, in both BH_3 and BF_3 the (B) fragment is highly electron-deficient. This deficiency is more pronounced in BF_3 where the (B) fragment has a net charge of +2.59, compared with +2.14 in BH_3. [It is instructive at this point to compare these net charges with those obtained via a Mulliken population analysis -- +1.10 for BF_3 and +0.14 for BH_3. It is even more instructive to compare these population analysis results with those of other authors. Schwartz and Allen[82] give +1.39 for BF_3 and -.57 for BH_3; Armstrong and Perkins[83] quote +.82 for their (5,2) BF_3 wavefunction and +1.42 for their (7,3) BF_3 wavefunction. The tremendous fluctuations in $\bar{N}(A)$ values calculated via the Mulliken scheme are not observed when the method proposed in this work is used.

Figure 4-1. Electronic charge distributions and partitioning surfaces for BH and BH_3. Both the σ_h and σ_v symmetry planes are shown for BH_3. Solid crosses denote in-plane nuclei; dotted crosses denote out-of-plane nuclei. Contour values are as listed in Fig. 2-1.

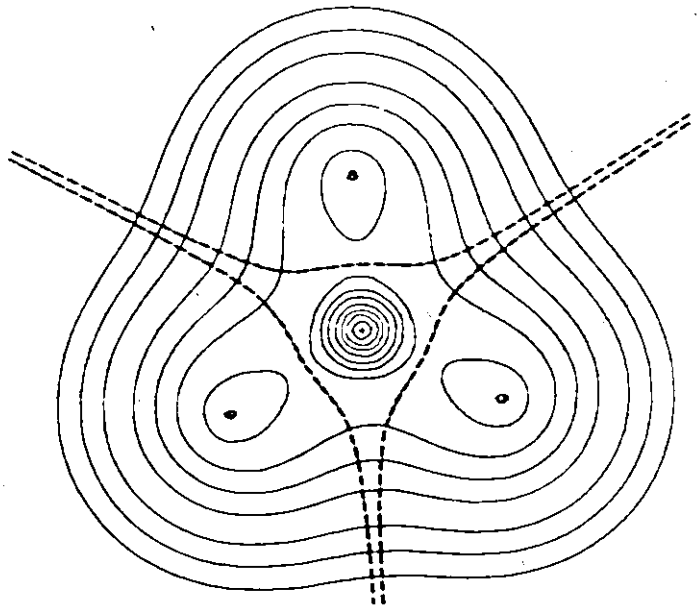

BH_3

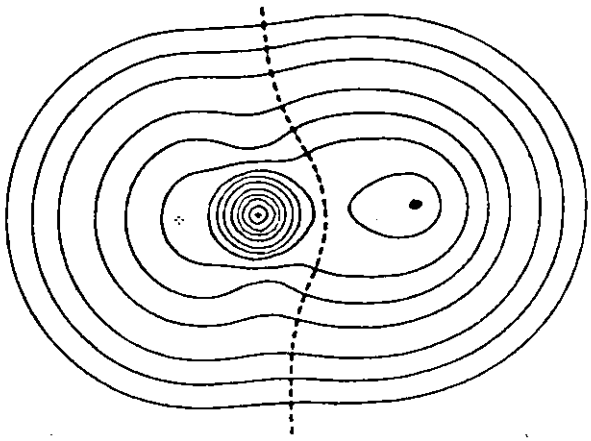

BH_3

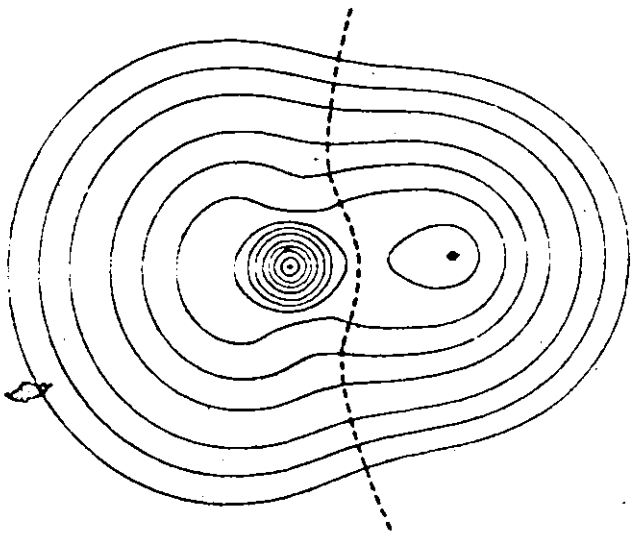

BH

Figure 4-2. Electronic charge distributions and partitioning surfaces for BF and BF_3. Both the σ_h and σ_v symmetry planes are shown for BF_3. Solid crosses denote in-plane nuclei; dotted crosses denote out-of-plane nuclei. Contour values are as listed in Fig. 2-1.

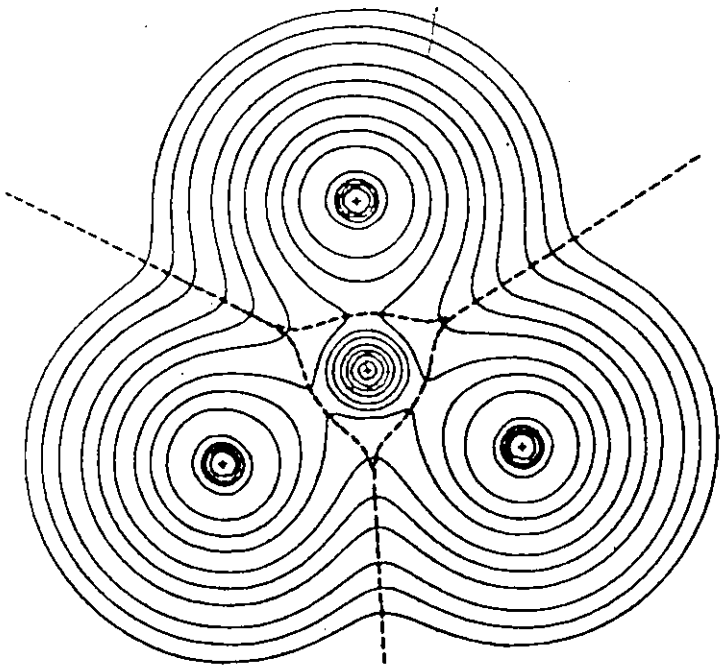

BF_3

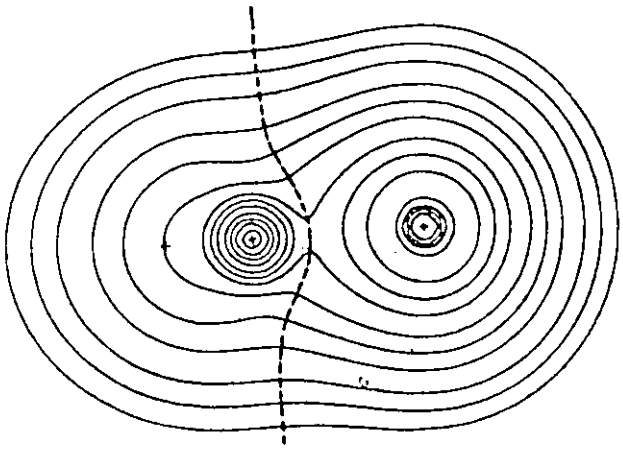

BF_3

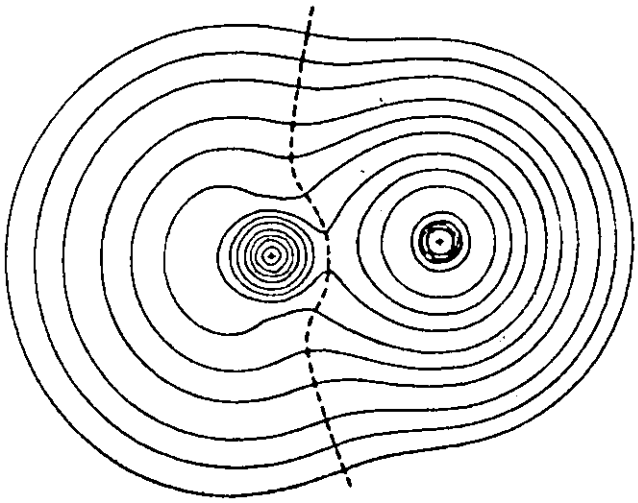

BF

TABLE 4-2. Changes in fragment populations and energies on bond formation in BH, BH_3, BF, and BF_3.

All values are relative to constituent atoms. Both the internal and external contributions to the change in $\overline{V}'$ are reported. $\Delta\overline{E}$ is given in kcal/mole; all other energy changes are in atomic units (1 au = 627.71 kcal/mole).

MOLECULE	FRAGMENT	$\Delta\overline{N}$	$^{+}\Delta\overline{E} = -\Delta\overline{T}$ (kcal/mole)	$\Delta\overline{V}'_{int}$	$\Delta\overline{V}'_{ext}$	$\Delta\overline{V}'$	$\Delta\overline{V}'$	$\Delta\overline{E}_e$	$^{++}\Delta\overline{V}_n$
	(B)	- .782	193	1.987	- 1.521	.465	.122	.267	.040
BH	(H)	.782	-256	- .744	- 4.115	- 4.859	1.943	- 2.508	2.100
	TOTAL	---	- 63	1.243	- 5.636	- 4.394	2.066	- 2.241	2.140
	(B)	-2.137	476	5.129	- 3.761	1.369	.201	.793	- .034
BH_3	(H)	.712	-237	- .718	- 4.916	- 5.634	2.391	- 2.867	2.490
	TOTAL	---	-233	2.976	- 18.510	- 15.533	7.372	- 7.808	7.436
	(B)	- .933	265	2.471	- 12.873	- 10.402	5.592	- 5.245	5.667
BF	(F)	.933	-404	- 5.915	- 21.133	- 27.049	12.640	- 13.798	13.154
	TOTAL	---	-139	- 3.445	- 34.006	- 37.451	18.232	- 19.042	18.821
	(B)	-2.592	727	6.939	- 26.475	- 19.535	10.775	- 9.925	11.084
BF_3	(F)	.864	-365	- 5.718	- 62.776	- 68.495	33.555	- 34.387	33.806
	TOTAL	---	-366	-10.215	-214.804	-225.019	111.441	-113.087	112.503

† The $\Delta\overline{E}$ values were calculated from "scaled" $\overline{T}_e$ values. The appropriate $\overline{T}_e$ values in Tables 3-3 and 4-1 were multiplied by $-\overline{E}/\overline{T}_e$ prior to the differencing operation. This was done to ensure that the fragment energy changes summed to give the correct total energy change. Had this not been done, the $\Delta\overline{E}$ values would have included cummulative virial theorem errors for the systems. Values are not corrected for electron correlation.

†† Calculated by difference. $\Delta\overline{V}_n = -\Delta\overline{E}_e - \Delta\overline{T}_e$.

Compare, for example, the values for the two BH_3 wavefunctions reported in Table 4-1. The Mulliken method yields C(B) values of +.27 and +.14 for the smaller and larger wavefunctions, respectively. The partitioning scheme proposed here gives +2.13 and +2.14. Comparisons between Gaussian wavefunctions obtained in this laboratory and Slater wavefunctions of other authors give similar results.]

Consider now the energies of formation (from atoms in their electronic ground states) of these compounds. We begin with some general considerations. The virial theorem for an atom takes the form $-\overline{T}_e = \overline{E}$. For a molecule in its equilibrium geometry (no net forces acting on the nuclei), the form of the theorem is identical. Therefore, one may immediately write

$$-\Delta\overline{T}_e = \Delta\overline{E} \qquad [4.1]$$

where $\Delta\overline{T}_e$ denotes the change in the kinetic energy on bond formation (i.e., the kinetic energy of the molecule minus the kinetic energies of its constituent atoms) and $\Delta\overline{E}$ denotes the change in total energy on bond formation. In order for a molecule to be stable relative to its constituent atoms, $\Delta\overline{E}$ must, of course, be negative. Thus, one has the well-known result that a positive value for $\Delta\overline{T}_e$ indicates an increase in stability, whereas a negative $\Delta\overline{T}_e$ indicates a decrease. Alternately, [4.1] may be written as

$$-2\Delta\overline{T}_e = \Delta\overline{V}' + \Delta\overline{V}'' + \Delta\overline{V}_n \qquad [4.2]$$

where $\Delta\overline{V}'$, $\Delta\overline{V}''$ and $\Delta\overline{V}_n$ denote the changes in the electron-nuclear, electron-electron, and nuclear-nuclear components of the potential energy, respectively, upon bond formation. Therefore, in order for a

system to achieve stability ($\Delta\bar{T}_e > 0$), we must have $\Delta\bar{V}' + \Delta\bar{V}'' + \Delta\bar{V}_n < 0$. Upon bond formation $\Delta\bar{V}' < 0$, $\Delta\bar{V}'' > 0$, and $\Delta\bar{V}_n > 0$. Whether or not a system can achieve stability depends upon whether the charge redistribution accompanying bond formation is such that the overall decrease in $\bar{V}'$ is sufficient to offset the destabilizing increases in $\bar{V}''$ and $\bar{V}_n$. That is, for an increase in stability one must have $|\Delta\bar{V}'| > \Delta\bar{V}'' + \Delta\bar{V}_n$. The extent by which $|\Delta\bar{V}'|$ exceeds $\Delta\bar{V}'' + \Delta\bar{V}_n$ is given by $2\Delta\bar{T}_e$.

Since the partitioning procedure yields fragments which separately obey the virial relationship, we have, in addition to [4.1] and [4.2],

$$-\Delta\bar{T}_e(A) = \Delta\bar{E}(A) \qquad [4.3]$$

and

$$-2\Delta\bar{T}_e(A) = \Delta\bar{V}'(A) + \Delta\bar{V}''(A) + \Delta\bar{V}_n(A) \qquad [4.4]$$

where, for example, $\Delta\bar{T}_e(A)$ is the kinetic energy of the fragment (A) in the molecule minus its value in the free atom, and similarly for the other properties. Thus, a positive $\Delta\bar{T}_e(A)$ immediately implies an increase in the stability of (A), whereas a negative $\Delta\bar{T}_e(A)$ implies a decrease in stability. The reason for any change in the stability of (A) in a given situation may be traced directly to the values of $\Delta\bar{V}'(A)$, $\Delta\bar{V}''(A)$ and $\Delta\bar{V}_n(A)$.

Table 4-2 summarizes these values for BH, BH_3, BF and BF_3. In addition to the total values for $\Delta\bar{V}'(A)$, the internal and external components, $\Delta\bar{V}'_{int}(A)$ and $\Delta\bar{V}'_{ext}(A)$ are given. $\Delta\bar{V}_{int}(A)$ measures the change in the attractive interaction of the charge density in (A) with

its internal nucleus, upon transition from free atom to molecular fragment. $\Delta\bar{V}'_{ext}(A)$ is equivalent to the interaction of the density in (A) with the nuclei external to it in its new molecular environment, an interaction not experienced by the free atom. With these definitions in mind, we now proceed.

We first note that in all four molecules, the (B) fragment has undergone a decrease in stability (relative to a B atom in its ground state). The overall stability of these molecules may therefore be attributed directly to increases in the stabilities of the (H) and (F) fragments -- increases which are more than sufficient to counteract the destabilization experienced by the (B) fragment. Why does a fragment stabilize or destabilize in a given bonding situation? We consider first the BH molecule. Recall that the (B) fragment in this molecule has lost a considerable amount of electronic charge (0.78 e). This is immediately reflected by a positive $\Delta\bar{V}'_{int}(B)$ value of 1.99. The attractive interaction between the charge density remaining in the (B) fragment and the external H nucleus, $\Delta\bar{V}'_{ext}(B)$, is only -1.52, not sufficient to counterbalance the increase in $\bar{V}'_{int}(B)$. Overall then, $\Delta\bar{V}'(B)$ is positive. Whenever a fragment has a positive $\Delta\bar{V}'$, it invariably undergoes a decrease in stability. $\Delta\bar{V}''(A)$ and $\Delta\bar{V}_n(A)$ are generally positive and destabilizing. Thus, a negative value of $\Delta\bar{V}'(A)$ is mandatory if a fragment is to have any chance of stabilizing itself.† In BH, $\bar{V}''(B)$ undergoes an increase of .12. Thus, the decrease

---

† A negative value for $\Delta\bar{V}''(A)$ is most unlikely upon bond formation. It would require (1) that (A) lose a substantial amount of charge density and (2) that the decrease in $V''_{int}(A)$ associated with this loss not be outweighed by the positive external repulsion term, $V''_{ext}(A)$. The lowest value of $\Delta V''(A)$ yet observed is +.053 for the (Be) fragment in BeH.[45] Occasionally, one does observe negative $\Delta\bar{V}_n(A)$ values upon bond formation (eg. the (B) fragment in BH_3). However, these are always small in magnitude and have never led to stability.

in the self-repulsion of the (B) electrons due to the loss of charge density, $\Delta\bar{V}'_{int}(B)$, is outweighed by the repulsion between the charge density in the (B) fragment and the density external to it.† $\bar{V}_n(B)$ also undergoes a small increase (.04) upon bond formation. Thus, all three components of $\bar{V}(B)$ contribute to the destabilization of the (B) fragment in BH. The extent of this destabilization is given by $-\Delta\bar{T}_e(B)$, and is therefore equal to 193 kcal/mole.

The nuclear virial of a fragment requires some additional comment. It is determined primarily by the extent to which the charge density in a fragment counteracts the nuclear repulsion forces. The direction and magnitude of the forces exerted on the nuclei by the charge density in various spatial regions is characteristic of the binding in the system.[50,93]

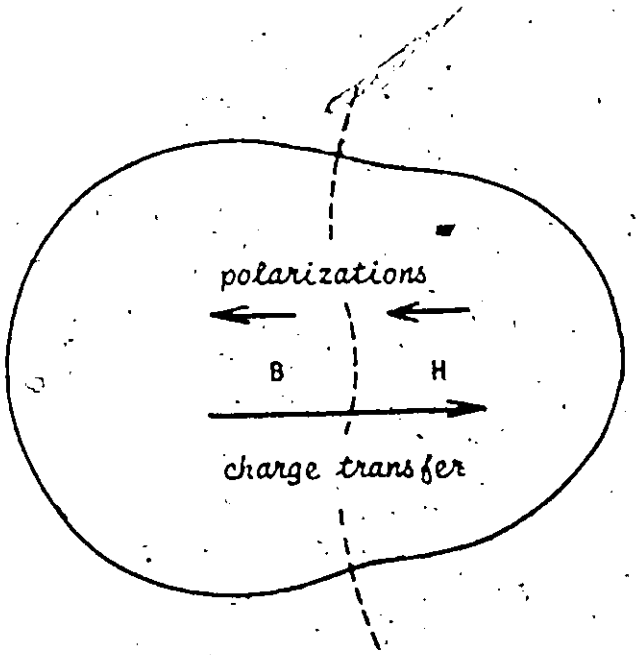

† The internal and external components of $\Delta\bar{V}'(A)$ are not reported here. Unfortunately, there is no way of obtaining $\bar{V}'_{int}(A)$ apart from a time-consuming, six-dimensional integration of $\Gamma(r_1,r_2)/|r_1-r_2|$ over the fragment, (A). Recall that the total values of $\bar{V}'(A)$ reported here were obtained by an alternate method (see Appendix IA, Eq. [A1.10]).

For example, in BH, because of the net charge transfer from (B) to (H), the (B) fragment is positively charged and, as a whole, exerts a net antibinding (repulsive) force on the H nucleus. In order to counterbalance this, the charge density in the (H) fragment is polarized inwards (towards the B-H bond), and thus exerts a net binding force on its own nucleus. Similarly, the (H) fragment is negatively charged, and thus exerts a net binding (attractive) force on the B nucleus. In order to counterbalance this, the (B) density is polarized away from the B-H bond, and thus exerts a net antibinding force on its own nucleus. This back-polarization is evident in the contour map of the BH charge distribution (refer to Fig. 4-1). In summary, the charge density in the (B) fragment does little to counteract the nuclear repulsive forces. It exerts an antibinding force on its own nucleus, and because of the loss of charge density, a relatively small binding force on the H nucleus. The origin defined by the partitioning surface in BH is near the bond midpoint. Thus, the binding force, $\vec{F}_H^{el}(B)$, gives a positive contribution to the nuclear virial of the (B) fragment (i.e., $-\vec{R}_H \cdot \vec{F}_H^{el}(B) > 0$), and the antibinding force, $\vec{F}_B^{el}(B)$, gives a negative contribution (i.e., $-\vec{R}_B \cdot \vec{F}_B^{el}(B) < 0$). The two contributions are nearly equal in magnitude and almost cancel. Thus, $\bar{V}_n(B)$ [$\equiv \Delta\bar{V}_n(B)$] is reduced to a relatively small value (.04).

We now return to BH. The stabilization energy in this molecule comes entirely from the (H) fragment. The charge transfer to this fragment results in a decrease in its internal $\bar{V}'$ ($\Delta\bar{V}'_{int}(H) = -.74$). There is also a significant stabilization from the interaction of the (H) density with the +5 charge of the B nucleus ($\Delta\bar{V}'_{ext}(H) = -4.12$), and

therefore $\overline{V}'(H)$ undergoes a significant decrease upon bond formation ($\Delta\overline{V}'(H) = -4.86$). [It is interesting to note that the charge density transferred from (B) to (H) interacts with the B nucleus almost as strongly on (H) as when it was on (B). The portion of $\Delta\overline{V}'_{ext}(H)$ attributable to the transferred electrons should be approximately equal to $(\Delta\overline{N}(H)/\overline{N}(H)) \times \Delta\overline{V}'_{ext}(H) = -1.81$, since there are no core electrons in the (H) fragment. The interaction of this same density when on the B atom is approximately given by $-\Delta\overline{V}'_{int}(B) = -1.99$.] $V''(H)$ undergoes an increase, internally as well as externally, because of the charge transfer to (H). Further, the bulk of the nuclear repulsion forces are balanced by the charge density in (H). It exerts a binding force on its own nucleus, plus a relatively large binding force on the B nucleus due to its net negative charge. The stabilizing decrease in $\overline{V}'(H)$ is more than sufficient to balance the destabilizing increases in $\overline{V}''(H)$ and $\overline{V}_n(H)$. $\Delta\overline{T}_e(H)$ is therefore positive, and $\Delta\overline{E}(H)$ negative. The (H) fragment is stabilized by 256 kcal/mole, an amount which is more than sufficient to counterbalance the 193 kcal/mole destabilization of the (B) fragment. Thus, the molecule as a whole is stable by 63 kcal/mole, relative to the separated atoms.

The results for BH_3, BF and BF_3 are similar to those for BH. In each case the (B) fragment loses charge density and is destabilized. Thus, the entire stabilization of these molecules comes from the (H) and (F) fragments. The changes in BH_3 closely parallel those in BH. Note that the loss of 2.14 e from the (B) fragment once again causes a large increase in its internal $\overline{V}'$, an increase which is not counterbalanced by the external interactions with the H nuclei. Therefore, $\Delta\overline{V}'$

for this fragment is again positive. $\Delta\overline{V}''(B)$ is again only slightly positive due to the large depletion of charge density, and subsequent decrease in the internal electron-electron repulsions. These values, coupled with the small contribution from $\Delta\overline{V}_n(B)$, once again yield a negative $\Delta\overline{T}_e(B)$ value and, hence, a positive $\Delta\overline{E}(B)$. In BF and BF_3, the changes are somewhat masked because of the larger nuclear charge of F. The loss of charge density from (B) is still evident in the positive $\Delta\overline{V}'_{int}(B)$ values. However, the negative values of $\Delta\overline{V}'_{ext}(B)$ are now much larger in magnitude because of the stronger interaction with the F nucleus (or nuclei), and $\Delta\overline{V}'(B)$ is overall negative and stabilizing. This, however, is not sufficient to balance the larger destabilizing increases in $\overline{V}''(B)$ and $\overline{V}_n(B)$. [Note particularly the much larger increases in $\overline{V}''(B)$ relative to those in BH and BH_3. Although the internal component of this quantity undergoes a decrease similar to those in BH and BH_3, the high repulsion between the (B) and (F) charge densities causes V''(B) to undergo a much more substantial increase than in BH and BH_3.]

We point out here that the value of $\Delta\overline{V}'_{int}$ (and also of $\Delta\overline{V}''_{int}$) for any fragment, $(A)_i$, should reflect not only the charge transfer to or from (A), but also any <u>net expansion or contraction</u> of the charge density in (A). The reader should note that we make a careful distinction between contraction and a simple loss of charge density, as we do between expansion and a simple gain of charge density. A loss of charge density from (A) will result in an <u>increase</u> in $\overline{V}'_{int}(A)$, whereas a net contraction of the charge density in (A) will result in a <u>decrease</u> in $\overline{V}'_{int}(A)$. Similarly, a gain of charge density by (A) will cause

TABLE 4-3. $\Delta\bar{E}/|\Delta\bar{N}|$, $\Delta\bar{V}'_{int}/\Delta\bar{N}$, and $\bar{r}$ values for the (B), (H), and (F) fragment of Table 4-2. $\bar{r}$ is an approximate measure of the tightness with which transferred electrons are, or were, bound in a fragment (see text for explanation).

FRAGMENT	MOLECULE	$\Delta\bar{N}$	$\Delta\bar{E}/\lvert\Delta\bar{N}\rvert$ (kcal/mole-electron)	$\Delta\bar{V}'_{int}/\Delta\bar{N}$ (au/mole-electron)	$\bar{r}$ (au)
(B)	BH	- .782	247	-2.539	1.97
	BF	- .933	284	-2.649	1.89
	BH_3	-2.137	222	-2.400	2.08
	BF_3	-2.592	280	-2.677	1.87
(H)	BH	.782	-327	- .951	1.05
	BH_3	.712	-333	-1.007	.99
(F)	BF	.933	-433	-6.342	1.42
	BF_3	.864	-422	-6.618	1.36

$\overline{V}'_{int}(A)$ to decrease, whereas a net expansion of its charge density will cause it to increase. Thus, net contractions or expansions can reinforce or counteract the effects of charge transfer. Simple charge transfers are always reflected by negative $\Delta\overline{V}'_{int}(A)/\Delta\overline{N}(A)$ ratios. When a net contraction or expansion counteracts the effect of the charge transfer, the magnitude of this ratio will decrease. In extreme cases, the ratio may even be positive. The above effects are largely absent for the compounds studied in this section, and the $\Delta\overline{V}'_{int}(A)/\Delta\overline{N}(A)$ ratios parallel the charge transfers very closely. There is, however, one significant exception.

Table 4-3 lists the values of $\Delta\overline{V}'_{int}/\Delta\overline{N}$ for the (B), (H), and (F) fragments of Table 4-2. Also reported are values of $\overline{r}$, measures of the average distance between the nucleus in a fragment and the charge density transferred to or from that fragment. [e.g., The (B) fragment in BH has lost .782 e. The resultant increase in $\overline{V}'_{int}(B)$ of 1.987 is equivalent to that which would result from a loss of .782 electrons distributed over the surface of a nucleus-centred sphere of radius 1.97 au.] First note that the $|\Delta\overline{V}'_{int}/\Delta\overline{N}|$ ratios are relatively constant for a given fragment. For example, in BF_3, $|\Delta\overline{V}'_{int}(F)/\Delta\overline{N}(F)| = 6.618$ au/electron. In BF, this decreases slightly to 6.342 au/electron. The decrease is to be expected. When more and more charge density is transferred to a fragment, it will accumulate in more outlying regions of the fragment. Thus, in BF_3, the .864 electrons transferred to (F) are, on the average, a distance of 1.36 au from the F nucleus. In BF, a larger charge transfer of .933 electrons occurs, and the average distance between the transferred charge and the F nucleus increases to 1.42 au. This

is immediately reflected by a decrease in $|\Delta\bar{V}'_{int}(F)/\Delta\bar{N}(F)|$. Note that the (H) fragments, upon transition from BH_3 to BH show a similar trend. Consider now the (B) fragments. The four molecules are, in order of increasing loss of charge density from the (B) fragment: $BH < BF < BH_3 < BF_3$. Accordingly, one would expect the values of $\bar{r}(B)$ to show a continual decrease from BH to BF_3, and the $|\Delta\bar{V}'_{int}(B)/\Delta\bar{N}(B)|$ values to show a continual increase (the charge density stripped from the (B) fragment comes from areas ever closer to the B nucleus). The $\bar{r}(B)$ values in the above $BH \rightarrow BF_3$ series are: 1.97, 1.89, 2.08, 1.87. The $|\Delta\bar{V}'(B)/\Delta\bar{N}(B)|$ values in the same series are: 2.54, 2.65, 2.40, 2.68. Note that in both cases the third value (the BH_3 value) is out of place. Thus, in BH_3, $\bar{V}'_{int}(B)$ does not increase to the extent one would expect on the basis of the charge loss alone. The increase has been counteracted by a contraction of the charge density in the (B) fragment. This has a considerable effect on the total energy change experienced by this fragment. Table 4-3 also lists the $\Delta\bar{E}/|\Delta\bar{N}|$ ratio for each fragment, or what could be called the <u>stabilization</u> (or destabilization) <u>efficiency</u> of a fragment (i.e., the total energy change experienced by a fragment per electron lost or gained, as the case may be). In BH_3, the $\Delta\bar{E}/|\Delta\bar{N}|$ ratio for the (B) fragment is significantly less than in BH (222 kcal/mole-electron opposed to 247 kcal/mole-electron). Thus, the (B) fragment undergoes considerably less destabilization per electron lost in BH_3 than in BH. Compare this to the relatively constant $\Delta\bar{E}/|\Delta\bar{N}|$ ratio for the (B) fragment in BF and BF_3.

This effect accounts directly for two observations: (1) the

bond length in BH_3 (2.250 au) is actually shorter than that in BH (2.336 au), and (2) the B-H bond strength in BH_3 (78 kcal/mole) is greater than that in BH (63 kcal/mole). This difference in bond strength is further enhanced by the (H) fragments, which have a slightly greater stabilization efficiency in BH_3 (-333 kcal/mole-electron) than in BH (-327 kcal/mole-electron) -- probably due to the larger net positive charge on the (B) fragment in BH_3, and subsequently, the greater stabilizing effect it has on the (H) fragments in this molecule. Contrast this to the results for BF and BF_3, where the B-F bond length is greater in BF_3 (2.447 au) than in BF (2.391 au), and the B-F bond strength is less (122 kcal/mole in BF_3, as opposed to 139 kcal/mole in BF). The lower B-F bond strength in BF_3, relative to BF, results from a decrease in the stabilization efficiency of the (F) fragment. That is, the $\Delta\bar{E}/|\Delta\bar{N}|$ ratio for (F) in BH is -433 kcal/mole-electron, as compared to -422 kcal/mole-electron in BF_3. Note that this is directly opposed to the trend in the $\Delta\bar{V}_{int}/\Delta\bar{N}$ values for (F), and is probably a result of significant repulsions between the (F) fragments in BF_3.

In summary then, the B-H bond strength is greater in BH_3 than in BH because (1) the (B) fragment undergoes a net contraction and (2) the stabilization efficiency of the (H) fragments is greater, a result which is largely due to the higher positive charge on the neighbouring (B) fragment in BH_3. The B-F bond strength in BF_3 is less than in BF because the stabilization efficiency of the (F) fragments has decreased due to substantial repulsions between them. These repulsions in BF_3 overide the effect of the larger positive charge on the (B) fragment. The variation in bond strengths is not specific to the wavefunctions reported here. The experimental values show

the same trends (see Chapter 3-A-3).

Table 4-3 also reveals a number of other interesting features. The average value of $\bar{r}$ for density transferred to an (H) fragment is $\sim$ 1 au. The same value for density transferred <u>from</u> a (B) fragment increases to $\sim$ 2 au. The $\bar{r}$ value for density transferred <u>to</u> an (F) fragment has a surprisingly low value of $\sim$ 1.4 au. Therefore, any charge density transferred to (F) is bound very tightly, and does not accumulate, as one might expect, in the outlying regions of the fragment. The $|\Delta\bar{V}'_{int}/\Delta\bar{N}|$ value for this fragment is, therefore, anomalously high. This is the basis of the high electron affinity of the F atom, and also accounts for the significantly greater stabilizing ability of the (F) fragment ($\sim$ -430 kcal/mole-electron) than the (H) fragment ($\sim$ -330 kcal/mole-electron) in these compounds.

A glance at the changes in the energy components listed in Table 4-2 once again reiterates what might be called "the curse of theoretical chemistry", i.e., that the total energy change in any chemical reaction is an extremely delicate balance of very large competing effects. Whether or not a compound can achieve stability relative to its component parts depends upon whether or not the electronic charge density can shift and polarize in such a manner so that the final change in $\bar{V}'$ is sufficient to counterbalance the tremendous destabilizing increases in $\bar{V}''$ and $\bar{V}_n$. One of the most attractive features of the partitioning method proposed here is that it allows one to discuss the large changes in the electronic potential energy components in terms of individual fragment changes. A fragment virial theorem further defines a partitioning of the nuclear repulsive

potential and allows one to assign to each fragment a total energy. The total energy change in any chemical reaction may then be viewed as a balance of fragment energy changes, all of which are of reasonable chemical magnitude.

B. Four Lewis Acid-Base Complexes: BH_3-H^-, BH_3-F^-, BH_3-CO and BF_3-H^-

The generalized (or Lewis) acid-base reaction

$$A + :B \rightarrow A:B$$

is probably the most important of all chemical reactions, in that almost all molecules can be dissected (mentally at least) into constituent acids and bases. Hence, a considerable effort has been expended in developing a method of predicting the relative stabilities of A:B complexes from the properties of A and :B. Earlier work centred on developing a scale of acid and base strength and hence predicting the stability of any complex on the basis of the strengths of its components. The problem here is that the relative strength of an acid or base (however one may define strength) is invariably a sensitive function of the reference base or acid to which it is coordinated. Thus, relative to some base, :B, A may be a stronger acid than A'; relative to a new base, B', this order may well be reversed.

In 1963, Pearson[85] put forth his principle of hard and soft acids and bases (HSAB). The useful qualitative rule he proposed was that "hard acids prefer to coordinate with hard bases and soft acids prefer to coordinate with soft bases." Hard acids and bases have been qualitatively defined as possessing a number of related

properties, the basic one being a tightly held valence charge density which is not easily distorted or removed. In the case of a hard acid this is often associated with small size and a high positive charge. Soft acids and bases have the opposite properties. One of the original reasons for undertaking a study of the above four complexes was to determine whether or not there was any correlation between the stability of an acid-base complex and the relative hardness or softness of its constituents, and if so, to relate it to the changes in the charge and energy distributions accompanying bond formation. Under Pearson's scheme, H^- and CO are classed as soft bases and F^- is classed as hard. BH_3 and BF_3 have been classed as soft and hard acids, respectively, largely due to a predicted difference in the effective charges on the (B) fragment in the two systems ($\sim +3$ in BF_3 and $<< +3$ in BH_3).[94] The partitioning results obtained here substantiate this predicted trend (recall C(B) = +2.59 in BF_3 and +2.14 in BH_3). Note also the small size of (B) in BF_3 (Fig. 2-2) relative to (B) in BH_3 (Fig. 2-1).

The fragment populations and energy components for these systems have been listed in Table 4-1. The changes in these quantities upon complex formation (relative to their values in the free acid and base reactants) are summarized in Table 4-4. We begin with two general observations. First, all complexes, with the exception of BH_3CO, have nearly identical stabilities of $\sim$ 60 kcal/mole. The low stability of BH_3CO ($\sim$ 6 kcal/mole) is consistent with experimental results (recall Chapter 3-A-3). Indeed, the fact that this compound is stable at all, whereas BF_3CO is not, has been rationalized on the basis of soft-soft and hard-soft interactions in the two cases, respectively.[94]

Figure 4-3. Electronic charge distributions and partitioning surfaces for the molecules: BH_4^-, BH_3F^-, BH_3CO, and BF_3H^-. All molecules are shown in a σ_v symmetry plane. Solid crosses denote in-plane nuclei; dotted crosses denote out-of-plane nuclei. The Lewis acid fragment (BH_3 or BF_3) is always on the left and the Lewis base on the right. Contour values are as listed in Fig. 2-1.

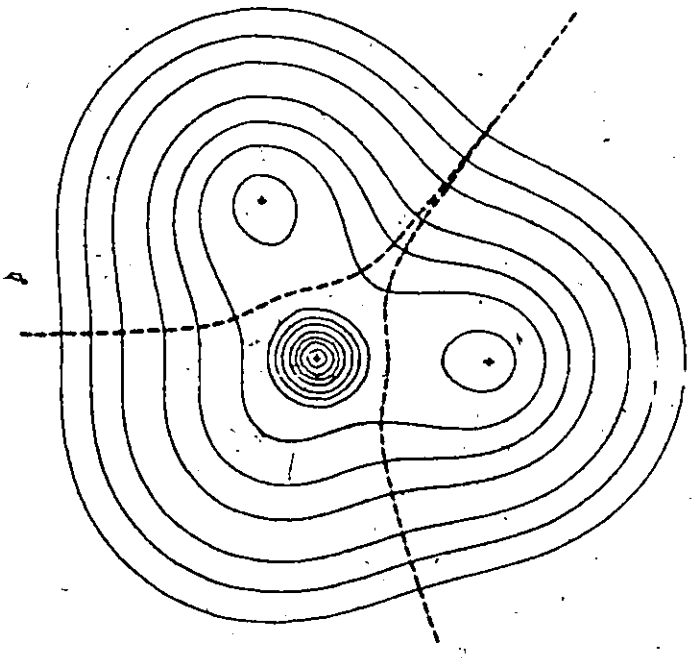

BH_4^-

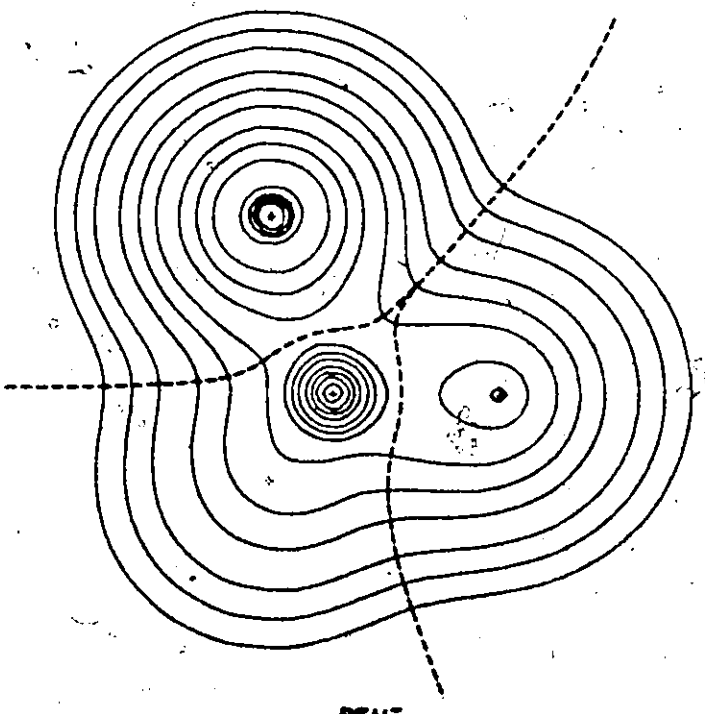

BF_3H^-

Figure 4-3 (Continued)

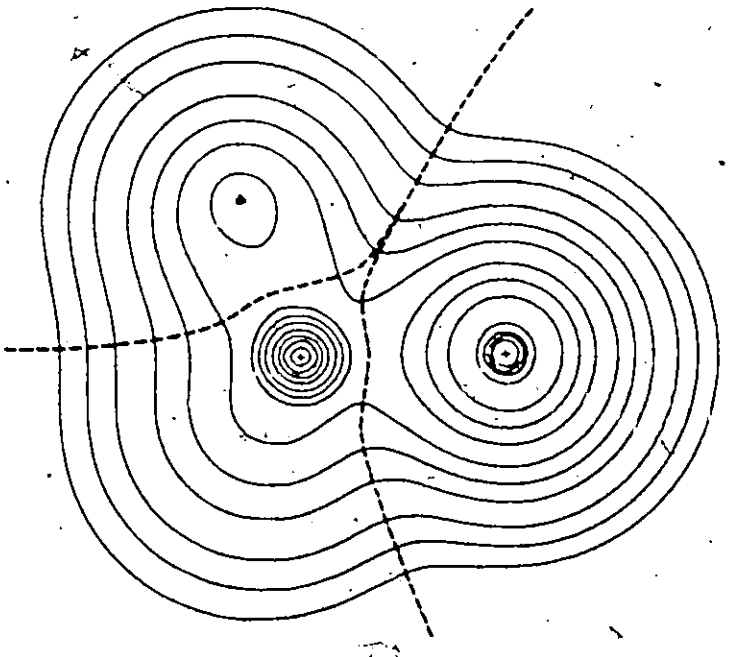

BH_3F^-

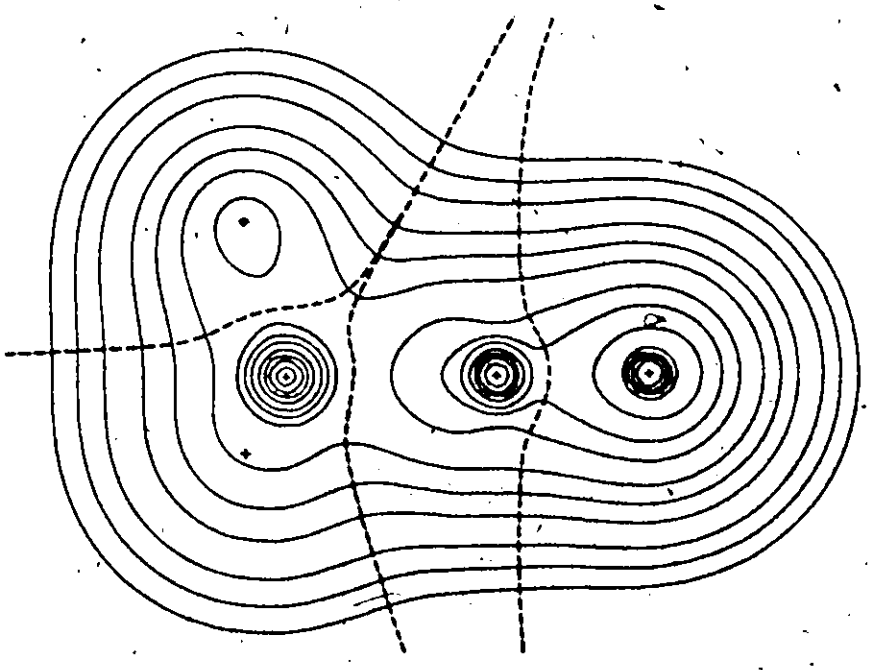

BH_3CO

TABLE 4-4. Changes in fragment populations and energies on formation of the Lewis acid-base complexes, BH_3-H^-, BH_3-F^-, BH_3-CO, and BF_3H^-.

All values are relative to BH_3 and the appropriate base (or fragments thereof). All data is in atomic units, with the exception of the $\Delta\bar{E}$ values which are given in kcal/mole (1 au = 627.71 kcal/mole).

MOLECULE	FRAGMENT	$\Delta\bar{N}$	$^{\dagger}\Delta\bar{E} = -\Delta\bar{T}$ (kcal/mole)	$\Delta\bar{V}'$	$\Delta\bar{V}''$	$\Delta\bar{E}_e$	$^{\dagger\dagger}\Delta\bar{V}_{nn}$
	(B)	.122	29.9	- 1.506	1.212	- .356	.404
	(H)	.041	37.9	- .191	.389	.137	- .077
BH_3-H^-	(BH_3)	.246	143.8	- 2.079	2.380	.056	.173
	(H^-)	-.246	-206.5	- 5.447	2.380	- 2.742	2.413
	TOTAL	---	- 62.7	- 7.526	4,760	- 2.686	2.586
	(B)	- .077	116.6	- 8.131	4.547	- 3.773	3.959
	(H)	.051	20.1	- 3.654	2.083	- 1.603	1.635
BH_3-F^-	(BH_3)	.077	176.9	-19.093	10.795	- 8.583	8.865
	(F^-)	- .077	-237.5	-25.505	11.636	-13.553	13.174
	TOTAL	---	- 60.7	-44.598	22.431	-22.136	22.039
	(B)	.093	- 25.7	-11.174	5.602	- 5.532	5.491
	(H)	- .072	30.0	- 4.352	2.241	- 2.158	2.206
BH_3-CO	(BH_3)	- .123	64.2	-24.230	12.326	-12.007	12.109
	(C)	.179	-156.6	-14.627	6.812	- 7.555	7.306
	(O)	- .056	86.0	-13.548	6.663	- 7.002	7.139
	(CO)	.123	- 70.6	-28.175	13.475	-14.557	14.444
	TOTAL	---	- 6.3	-52.405	25.801	-26.564	26.554

TABLE 4-4 (Cont.)

MOLECULE	FRAGMENT	$\Delta\overline{H}$	$^{+}\Delta\overline{E} = -\Delta\overline{T}$ (kcal/mole)	$\Delta\overline{V}'$	$\Delta\overline{V}''$	$\Delta\overline{E}_e$	$^{++}\Delta\overline{V}_n$
	(B)	.097	10.5	- .337	.551	.199	- .183
	(F)	.047	61.6	- .143	1.670	1.440	- 1.342
BF_3-H^-	(BF_3)	.238	195.3	- .767	5.560	4.519	- 4.207
	(H^-)	- .238	-261.6	-16.351	7.729	- 8.209	7.792
	TOTAL	---	- 66.4	-17.118	13.289	- 3.690	3.584

+ The $\Delta\overline{E}$ values were calculated using scaled $\overline{T}_e$ values from Table 4-1. The scaling procedure was identical to that described for the $\Delta\overline{E}$ values in Table 4-2.

++ Calculated by difference. $\Delta\overline{V}_n = -\Delta\overline{E}_e - \Delta\overline{T}_e$.

In a sense, it is surprising that the stabilities of BH_3-H^-, BH_3-F^- and BF_3-H^- show so little disparity. It is perhaps questionable whether BH_3 should really be classed as a soft acid, as the (B) fragment does have a substantial positive charge. On the basis of this property alone, it is probably not as different from BF_3 as Pearson predicted.[94] However, H^- and F^- lie very much at opposite ends of the hardness-softness scale. Thus, one might well expect some differences to show up, particularly in comparing BH_3-H^- and BH_3-F^-. Of course, the relative stabilities predicted here are specific to the gas phase. The energy of a fragment in a molecule is a sensitive function of its environment, and could be significantly effected upon solvation. Thus, a soft solvent could conceivably stabilize both the acid and base fragments of a soft-soft combination, whereas a hard solvent could stabilize both fragments of a hard-hard combination. A soft-hard combination might undergo stabilization of one component, and possibly even destabilization of the other component, in either a hard or soft solvent. Thus, experimental dissociation energies taken in solvents could yield different results than gas-phase measurements.

The second general observation we make is that upon complex formation, the base always undergoes an increase in stability, whereas the acid undergoes a decrease. For example, in BH_3-F^- the (F) fragment is stabilized by 237 kcal/mole relative to the free F^- ion, and the (BH_3) fragment is destabilized by 177 kcal/mole relative to the free acid, BH_3. These observations also apply to other Lewis acid-base adducts studied in this laboratory,[90] including

the $FH\text{-}F^-$ complex to be discussed in Section C of this chapter. With these opening remarks, we now examine the four complexes in greater detail.

Compare, first, $BH_3\text{-}H^-$ and $BH_3\text{-}F^-$. Although these two complexes are of almost identical stability (relative to their acid and base constituents), the manner in which they achieve it is quite different. The relative hardness and softness of the F^- and H^- ions, respectively, is well-reflected in the charge transfers to BH_3. In $BH_3\text{-}H^-$ the H^- loses .25 e; in $BH_3\text{-}F^-$ the F^- ion loses only .08 e, in accordance with its tightly held charge distribution and high electronegativity. However, the most striking difference between the two complexes is in the disposition of the transferred charge. In $BH_3\text{-}H^-$, this charge is fairly evenly distributed, with .12 e going to the (B) fragment and .04 e to each (H). In $BH_3\text{-}F^-$, the charge lost by F^- is transferred <u>entirely</u> to the (H) fragments, along with an <u>additional</u> .08 e from the (B) fragment. This is the only one of the four complexes in which the (B) fragment actually loses charge density. One would expect that, if anything, this fragment should gain charge density, particularly because of its high net positive charge. That is, charge density transferred to (B) would experience the full +5 charge of the B nucleus, but only the repulsion of 2.14 electrons in that fragment. From this point of view, a charge transfer to (B) would be energetically favourable in that $V'_{int}(B) + V''_{int}(B)$ would decrease. Charge transferred to an (H) fragment, on the other hand, would experience the repulsion of 1.71 electrons in that fragment -- a significantly greater destabilizing

effect than the stabilizing interaction with the +1 charge of the H nucleus. That charge is transferred solely to the (H) fragments in BH_3-F^- may be explained only on the basis of a strong replusive interaction between the electrons in the (B) and (F) fragments. That is, the (F) fragment literally forces the charge density in the (B) fragment back to the (H) fragments in order that the system as a whole may achieve maximum stability.†

The properties of the (F) fragment explain a large amount of fluorine chemistry, and in particular, its often encountered anomalous behaviour. The dominant property of this fragment which has been consistently observed in this laboratory is a strong resistance to change. In the compounds studied here, the population of the (F) fragment is always between 9.7 e and 10.0 e. Compare this with the variance in the populations of the (B) and (H) fragments (Tables 4-1 and 4-7). Further, the charge density is very tightly held (recall the earlier discussion of the $\Delta\bar{V}'_{int}(F)$ values for BF and BF_3). This is reflected even in the contour maps of the density distributions, where the (F) fragment always looks very much like a fluoride ion and the contours near the partitioning surface exhibit a distinct "pinched" effect (see Figs. 4-2, 4-3, and later, Fig. 4-4). The reason for this is purely an energetic one. Transfers of charge density from (F), or large polarizations of the (F) density

---

† The reader should note that the total $\Delta\bar{V}'$ and $\Delta\bar{V}''$ values reported in Table 4-4 do not reflect the effects of the charge transfers directly. They are net values and include all new interactions of the charge density in a fragment after the charge transfers have taken place.

cost dearly in terms of the energy. Thus, when the charge distribution shifts to stabilize the system, the (F) fragment literally forces the changes to occur in other parts of the molecule. Further, since the (F) fragment always has a net negative charge, there is a substantial repulsive interaction between (F) and the charge density in neighbouring fragments.

This high resistance to change, and strong repulsive interaction with neighbouring fragments also explains why in BF_3H^-, one observes a charge transfer of only .24 e from H^- to BF_3 -- nearly identical to the .25 e transferred from H^- to BH_3 in BH_3-H. Again, on the basis of electron deficiency, one would expect a larger charge transfer to BF_3 than BH_3 because of the larger positive charge on the (B) fragment. The strong repulsion between the electrons in the (F) and (B) fragments severely limits the charge transfer to BF_3. Once again, any significant polarization of the charge density in the (F) fragments which would alleviate the additional repulsions due to the transfer, has unfavourable energetic consequences. This is the reason BF_3 is not a better electron acceptor than BH_3, and therefore not as strong a Lewis acid as was once believed.[87]

The destabilizing repulsions between (F) and its neighbouring fragments are also evident in the $\Delta\bar{E}$ values for these fragments. Recall from Table 4-2 that the (B) fragment in BH_3 has been destabilized by 476 kcal/mole. In BF_3, the destabilization is 727 kcal/mole -- well in excess of what could be rationalized on the basis of the greater loss of charge density from (B) in BF_3. In the formation of BH_3-F^-, the (B) undergoes an additional destabilization of 117 kcal/mole,

considerably greater than the 30 kcal/mole destabilization observed in BH_3-H^-. This is partially offset by the (H) fragments, which experience a further destabilization of only 20 kcal/mole in BH_3-F^-, as opposed to 38 kcal/mole in BH_3-H^-. The difference here may largely be attributed to the higher net positive charge on (B) in BH_3-F^- (+2.21, as opposed to +2.01 in BH_3-H^-). The addition of H^- to BF_3 causes only a small further destabilization of the (B) fragment (11 kcal/mole), and the bulk of the (BF_3) destabilization in BF_3-H^- comes from the (F) fragments (62 kcal/mole per fragment). The destabilizations of the (H) and (F) fragments in BH_3 and BF_3 which occur upon complex formation are largely due to the change in geometry. That is, when BH_3 and BF_3 change from a planar to a bent configuration, the H-H and F-F distances decrease, and hence the repulsions between the terminal fragments increase. Note how much larger the destabilization is for the (F) fragments in BF_3 than for the (H) fragments in BH_3.

The $\Delta\bar{V}'_{int}/\Delta\bar{N}$ values for these compounds are summarized below in Table 4-5. [Values for $\Delta\bar{V}'_{int}(B)/\Delta\bar{N}(B)$ are not reported. The integrations in these molecules were performed only over the exterior fragments and the properties of (B) were obtained by difference. Hence, no breakdown of $\bar{V}'(B)$ into internal and external components was possible.]

TABLE 4-5. $\Delta\bar{V}'_{int}/\Delta\bar{N}$ ratios for exterior fragments in BH_4^-, BH_3F^-, BF_3H^-, and BH_3CO. Values are given in au/electron.

	(H)	.527		(F)	-.626
BH_3-H^-	(H^-)	1.293	BF_3H^-	(H)	1.669
	(H)	-.120		(H)	-.779
BH_3-F^-	(F)	8.736	BH_3CO	(CO)	-7.206

Note that H^- and F^-, although they both lose charge density upon forming adducts with BH_3 and BF_3, have positive $\Delta\overline{V}_{int}/\Delta\overline{N}$ ratios. Thus, the fragments both undergo considerable contractions upon bond formation which are sufficient to offset the increases in $\overline{V}_{int}$ resulting from the loss of charge density. Note also that contraction of H^- is stronger when it is bound to BF_3 than when bound to BH_3, presumably because of the larger positive charge on the (B) fragment in BF_3. The charge transfer to (B) in BH_3-H^- appears to cause a significant expansion in the terminal (H) fragments of BH_3. Note that the nearly identical transfer to (B) in BF_3-H^- does not cause any expansions in the (F) fragments, a result which is again consistent with earlier observations regarding this fragment, and its strong resistance to change.

Finally, consider BH_3-CO. The results for this molecule provide a rather striking contrast with those for the other three. It is by far the least stable of the set. Further, the charge transfers which occur upon its formation are completely different from those observed for the others. Recall that the (B) fragment in BH_3 has a net charge of +2.14. The (C) fragment in the CO molecule has a net charge of +1.36. Thus, formation of BH_3CO involves the "joining" of two positively charged fragments. In order to stabilize the complex, electrons are transferred from <u>both</u> the (H) and (O) fragments to the (B) and (C) fragments. Each (H) fragment donates .07 e, and (O) donates .06 e. The population of the (B) fragment increases by .09 e; that of the (C) fragment increases by .18 e. It is interesting to note that the overall charge transfer in the

complex is from BH_3 to CO. Thus, the Lewis acid, BH_3, actually loses charge density and the Lewis base, CO, gains charge density. The weakness of CO as a Lewis base is therefore well reflected by its behaviour here.

Note that this is the only one of the four complexes in which the energy of the (B) fragment actually decreases upon bond formation ($\Delta\bar{E}(B) = -26$ kcal/mole), a result of the charge transfer to the fragment and its subsequent interaction with the positively charge neighbouring (C) fragment. Similarly, the increase in stability of CO is due to an increase in stability of its (C) fragment ($\Delta\bar{E}(CO) = -157$ kcal/mole), which again gains charge density and experiences a substantial stabilizing interaction with the positively charge (B) fragment. These effects counteract the destabilizations experienced by the (H) and (O) fragments. Although the complex does achieve stability, it is by a very small margin. The $\Delta\bar{V}_{int}/\Delta\bar{N}$-ratios (Table 4-5) for the fragments do not indicate any significant fragment expansions or contractions upon bond formation. The loss of charge density by the (H) fragments is reflected by increases in $\bar{V}_{int}(H)$, as is the gain by CO reflected by a decrease in $\bar{V}_{int}(CO)$.

The transfer of electrons from the (H) fragments is interesting in that it substantiates previous predictions and rationalizations of the ability of (H), in certain circumstances, to donate charge via the "hyperconjugative" mechanism of electron release.[88] Graham and Stone[87] have rationalized the stability of BH_3CO on the basis of overlap of the π orbitals of C with those of a "pseudo-atom" consisting of the three H atoms acting in concert. The net result of this overlap

would be a charge transfer from (H) to (C), an effect analogous to the hyperconjugative release of density often invoked by organic chemists. A similar effect has also been observed in this laboratory for the isoelectronic molecule CH_3CN.[90] The (C) fragment of CN^- (isoelectronic with CO) is again positively charged (C(C) = +.78), and the formation of CH_3CN is again characterized by a small loss of charge density from the (H) fragments. In CH_3F, a molecule isoelectronic with BH_3F^-, this transfer does not occur. These results suggest that the (H) fragments tend to release density when BH_3 or CH_3 is bonded to a net positively charged fragment, and not when bonded to a net negatively charged fragment. These results are also consistent with the predictions of Pople and Beveridge[84] based on their method of population analysis.

A comparison of BH_3F^- with the isoelectronic CH_3F, and of BH_3CO with its isoelectronic counterpart, CH_3CN, provides a striking illustration of the importance of the stabilizing effect of $\overline{V}'$, and of how it effects the charge distribution. The populations of the fragments in these compounds are summarized in Table 4-6. The transition

TABLE 4-6. $\overline{N}(A)$ values for two sets of isoelectronic molecules: (1) BH_3F^- and CH_3F; (2) BH_3CO and CH_3CN.

	BH_3F^-	CH_3F	BH_3CO	CH_3CN
(B) or (C)	2.786	5.297	2.963	5.787
(H)	1.764	.995	1.638	.958
(F)	9.923	9.717		
(C) of (CO) or (CN)			4.821	4.896
(O) or (N)			9.302	8.444

from the charge distribution in BH_3F^- to that in CH_3F may be made simply by increasing the charge on the B nucleus by +1 (plus a minor geometry change). This results in the migration of 2.51 e to the new (C) fragment. As one would expect, the major portion of this comes from the (H) fragments (2.31 e), and the (F) fragment donates a relatively small amount (.20 e). A transition from BH_3CO to CH_3CN involves an increase in the nuclear charge of B by +1, and an equivalent decrease in that of O. Again this causes a strong migration of 2.82 e to the new (C) fragment, mostly from the (H) fragments which each lose .68 e. The (O) fragment, upon transition to (N), loses .86 e and the population its neighbouring (C) fragment remains relatively constant.

In summary then, the properties of the Lewis acids, BH_3 and BF_3 are not so much determined by the properties of their (B) fragments, as by the properties of their terminal (H) and (F) fragments. BF_3 is not as strong an electron-acceptor as one might expect on the basis of the high positive charge on (B). The strong repulsive interaction between the electrons of the (F) fragments and those of the (B) fragment severely limit the extent of charge transfer to this acid. It appears that charge transfers, and even <u>total</u> energy changes experienced by the individual fragments upon complex formation, can be rationalized (and predicted) solely on the basis of changes in the electron-nuclear attractive forces and electron-electron repulsive forces experienced by the fragments. It is apparent that the latter play an extremely important part in the chemistry of fluorine.

We close this section with an application of these findings

to a problem in organic chemistry. The halogens in general, and fluorine in specific, have long been known for their anomalous behaviour as substituents on aromatic rings.[88] In benzene, most electron-withdrawing substituents deactivate the ring towards electrophillic substitution, and are meta directing. The halogens, however, are ortho-para directing. Further, the order of deactivation is F < Cl < Br < I, the opposite from what one would expect on the basis of the relative electronegativities of the halogens. This has generally been explained in one of two ways. The first argues that although the halogens withdraw electrons from the ring, there is a concomitant back-donation from the π orbitals of the halogen to those of the ring.[88] It is argued that the extent of back-donation depends upon the degree of overlap between the filled outer p_π orbitals of the halogen and the $2p_\pi$ orbitals of the ring carbon to which it is bonded. This overlap should decrease in the order, F > Cl > Br > I, due to increasing carbon-halogen bond length, and increasing disparity between the sizes of the carbon and halogen p_π orbitals. Thus, since the C-F bond is the shortest of the four, and the p_π orbitals of F the most similar to those of C, the feedback of electrons should be greatest in the case of fluorine. The second explanation argues that there is a repulsive interaction between the outer p_π orbitals of halogen and the $2p_\pi$ orbitals of the ring, particularly those of the carbon to which the halogen is bonded.[89] This repulsion should have the effect of pushing the aromatic π electrons away from the substituted position, and lead to charge build up at the ortho and para positions.

The results obtained in this work strongly substantiate the

latter hypothesis. The (F) fragment in fluorobenzene should exhibit very similar properties to the (F) fragments studied here. It can be expected to have a net negative charge (C(F) ∿-.7), a tightly bound charge density; and exert a strong repulsion on the electrons of the adjacent carbon. Some of the charge density on this (C) fragment will be forced onto the neighbouring ortho (C) fragments, thus leaving it with a net positive charge. This effect should decrease in the order (F) > (Cl) > (Br) > (I) for the following reason. The tightness with which the halogen electrons are held, and hence, the sensitivity of the energy to small changes in the charge distributions of halogen fragments, can be expected to decrease in the order (F) > (Cl) > (Br) > (I). Thus, a (Cl) fragment is more capable of undergoing internal changes in order to counteract external stress (such as electron repulsion) than is an (F) fragment which will force most charge redistributions to occur in other parts of the molecule. This "fragment maleability" should increase in the order (F) < (Cl) < (Br) < (I). These results are in agreement with those of Politzer and Timberlake.[86] These authors have evaluated the overlap and electron repulsion integrals, between valence π orbitals on C and X (X = F, Cl, Br, I). The relative magnitudes of the overlap integrals do not support the back-donation theory. The trend in the electron repulsion integrals, however, does lend considerable support to the repulsion theory.

We also point out that the activation-deactivation sequence around the ring (and hence, the activation of the para position) may also be explained on the basis of inter-fragment electron repulsions. The lowest external electron-electron repulsion terms ($\bar{V}'_{ext}$) between

neighbouring fragments should arise when the populations of those fragments show the greatest disparity (e.g., if R denotes the distance between the effective centroids of charge in two fragments, (A) and (B), then N(A) x N(B)/R is largest when N(A) = N(B), and smallest when they show the greatest disparity). On the basis of this term alone, one should observe "population alternation" around a ring, since it leads to a lower energy. The changes in the internal components of $\overline{V}'(C)$ and $\overline{V}''(C)$ with variations in N(C) will, of course, play an important part in the charge distributions in neighbouring (C) fragments. Nevertheless, providing the mean population of the (C) fragments was such that the variation of the sum of these internal components with N(C) was fairly small, an alternating arrangement of populations could be more stable than a non-alternating one. Charge alternation has also been predicted to occur in aliphatic chains by Pople and Beveridge.[84]

C. The Formation of the Bifluoride Ion

We now apply the partitioning method to a study of the Lewis acid-base reaction,

$$FH(g) + F^-(g) \rightarrow FHF^-(g)$$

primarily to illustrate a number of additional features of the method not generally encountered upon application to static systems. The fragment populations and energy components for FH, F^-, and four configurations along the linear reaction coordinate are reported in Table 4-7. The changes in fragment properties which occur during

the course of the reaction are summarized in Table 4-8. All changes are given relative to the F^- ion and the FH molecule (or its constituent fragments). The charge distributions and partitioning surfaces are pictured in Fig. 4-4. Throughout this section, the F^- base fragment will be denoted as (F^-), and the fluorine fragment of the FH molecule as (F).

One of the most attractive features of the partitioning method is that whenever a charge distribution undergoes a continuous change, so too do the partitioning surfaces and the fragments they define. Thus, it is possible to follow the course of a chemical reaction by monitoring changes in fragment properties. The bifluoride reaction proceeds with a continuous decrease in energy until the system reaches its symmetric equilibrium geometry, and achieves a total stabilization energy (relative to separated reactants) of 43 kcal/mole. Note (Table 4-8) how smoothly the fragment properties change as the reaction proceeds to completion. During the course of the reaction, the incoming fluorine ion continually loses charge density to the FH molecule (specifically, to the (F) fragment of FH), to a maximum of .104 e at equilibrium geometry. In accordance with the results for the Lewis acid-base reactions studied in the previous section, the base again increases in stability ($\Delta\bar{E}(F^-)$ = -142 kcal/mole), and the acid decreases in stability ($\Delta\bar{E}$(FH) = 99 kcal/mole).

One interesting feature of this reaction is that at some point during the final stages of the reaction, the partitioning surface between the (F) and (H) fragments in (FH) disappears, and then reappears. That is, at one point the charge distribution in (FH)

Figure 4-4. Electronic charge distributions and partitioning surfaces for FH, F^-, and four linear configurations along the potential surface for the reaction: $FH + F^- \rightarrow FHF^-$. Contour values are as listed in Fig. 2-1.

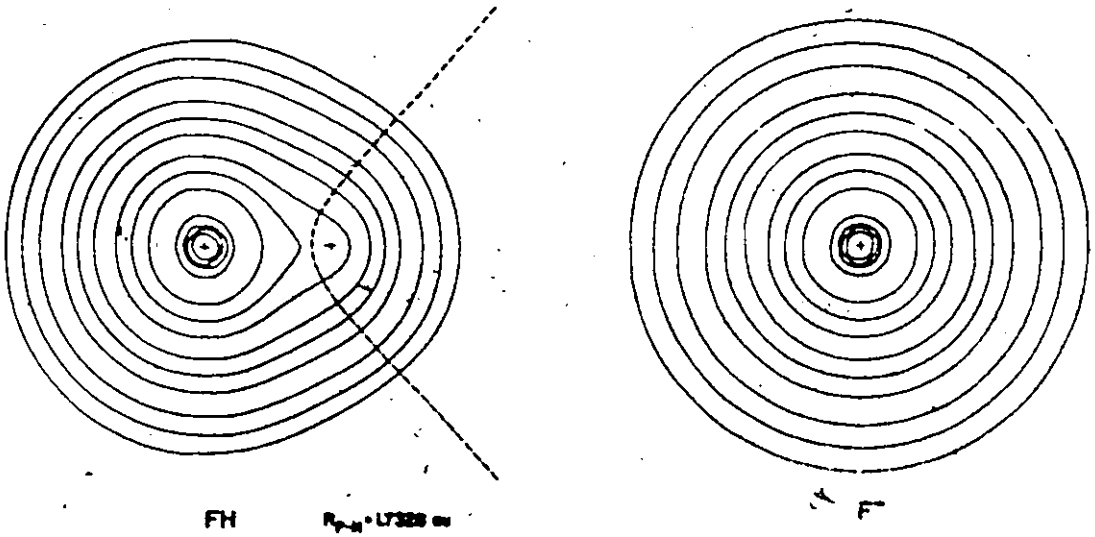

FH R_{F-H} = 1.7328 Å F^-

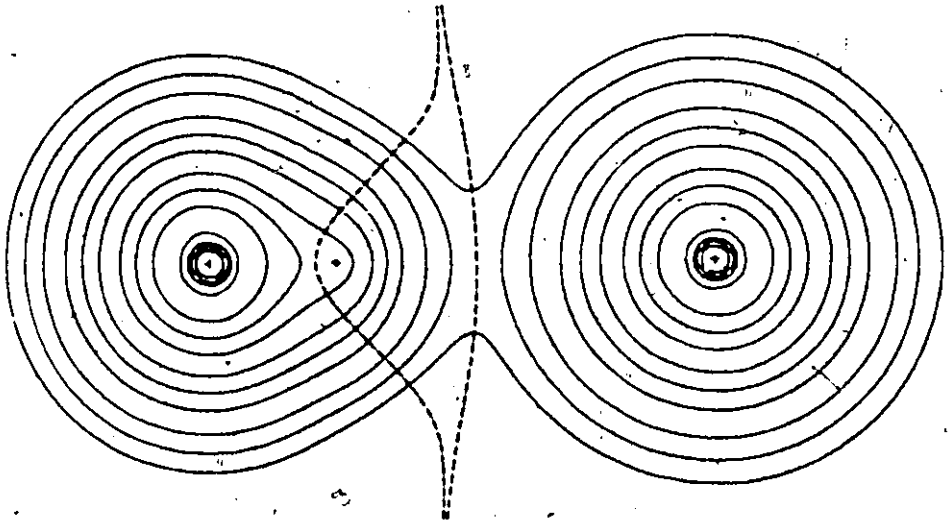

R_{F-H} = 1.763 Å FHF^- R_{F-F} = 2.000 Å

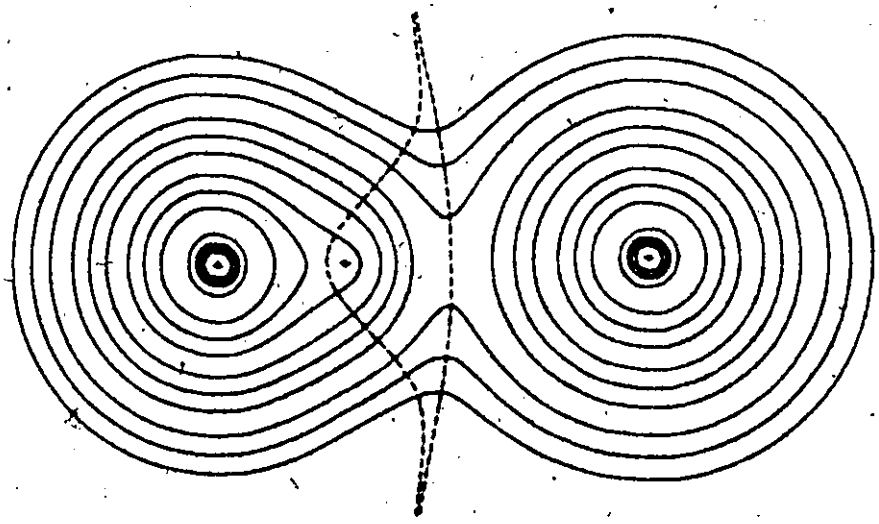

R_{F-H} = 1.772 Å FHF^- R_{F-F} = 2.000 Å

Figure 4-4 (Continued)

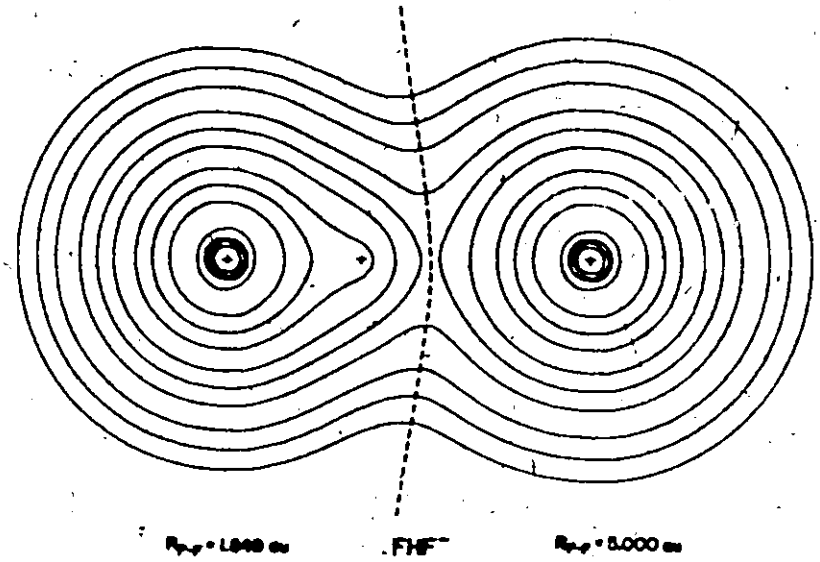

R_{F-F} = 1.948 au FHF⁻ R_{F-F} = 5.000 au

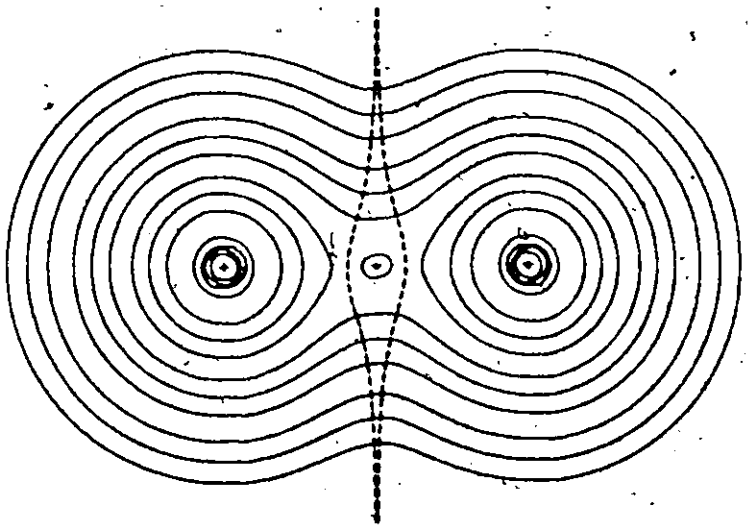

R_{F-H} = 2.180 au FHF⁻ R_{F-H} = 4.240 au

TABLE 4-7. Fragment populations and energies for four linear configurations of the bifluoride ion, the HF molecule (R = 1.7328 au), and the F^- ion.

The incoming F^- ion is always denoted as (F^-); the fluorine fragment in (HF) is denoted as (F). In addition, the ratio $-\bar{E}/\bar{T}$ is reported for equilibrium configurations. All data is in atomic units. The four FHF^- configurations are denoted as follows:

(1) R_{F-F} = 7.000 au; R_{F-H} = 1.743 au
(2) R_{F-F} = 6.000 au; R_{F-H} = 1.772 au
(3) R_{F-F} = 5.000 au; R_{F-H} = 1.849 au
(4) R_{F-F} = 4.240 au; R_{F-H} = 2.120 au

FRAGMENT	$\bar{N}$	$\bar{T}_e$	$\bar{V}'_{int}$	$\bar{V}'_{ext}$	$\bar{V}'$	$\bar{V}''$	$\bar{E}_e$	$\bar{V}_n$
FHF^- (1) $\bar{E}$ = -199.5387								
(F^-)	9.9924	99.4393	-243.4855	-14.7509	-258.2364	51.8558	-106.9412	7.5019
(H)	.2171	.2326			- 1.7412	.6665	- .8421	.6185
(F)	9.7905	99.7864	-243.6865	-18.2432	-261.9297	51.9410	-110.2024	10.4160
(FH)	10.0075	100.0190			-263.6709	52.6075	-111.0444	11.0254
TOTAL	20.0000	199.4583			-521.9073	104.4633	-217.9856	18.5273
FHF^- (2) $\bar{E}$ = -199.5507								
(F^-)	9.9805	99.4387	-243.4654	-17.3254	-260.7908	53.0629	-108.2892	8.8505
(H)	.2056	.2172			- 1.7338	.6696	- .8470	.6298
(F)	9.8139	99.7702	-243.7400	-20.3281	-264.0681	53.1756	-111.1222	11.3520
(FH)	10.0194	99.9874			-265.8019	53.8453	-111.9692	11.9818
TOTAL	20.0000	199.4261			-526.5927	106.9082	-220.2584	20.8323
FHF^- (3) $\bar{E}$ = -199.5691								
(F^-)	9.9481	99.4642	-243.4815	-21.0180	-264.4995	54.7610	-110.2744	10.8102
(FH)	10.0519	99.9526			-268.8090	55.6380	-113.2184	13.2658
TOTAL	20.0000	199.4168			-533.3085	110.3989	-223.4928	24.0760

TABLE 4-7 (Cont.)

FRAGMENT	$\bar{N}$	$\bar{T}_e$	$\bar{V}'_{int}$	$\bar{V}'_{ext}$	$\bar{V}'$	$\bar{V}'$	$\bar{E}_e$	$\bar{T}_n$
†FHF^- (4) $\bar{E}$ = -199.5810 $-\bar{E}/\bar{T}_e$ = .999769								
(F)	9.8959	99.7038	-243.9248	-25.6215	-269.5463	56.7330	-113.1085	13.4057
(H)	.2083	.2194			- 2.0816	.9060	- .9564	.7370
(FH)	10.1041	99.9232			-271.6279	57.6388	-114.0659	14.1427
TOTAL	20.0000	199.6270			-541.1742	114.3718	-227.1753	27.5483
†HF $\bar{E}$ = -100.0569 $-\bar{E}/\bar{T}_e$ = 1.000386								
(F)	9.7418	99.7520	-243.4088	- 5.5966	-249.0053	44.7777	-104.4756	4.7236
(H)	.2582	.2663			- 1.5751	.5335	- .7752	.5089
TOTAL	10.000	100.0183			-250.5804	45.3112	-105.2508	5.2325
F^- $\bar{E}$ = -99.4552 $-\bar{E}/\bar{T}_e$ = .999861								
TOTAL	10.0000	99.4690	-243.5645	----	-243.5645	44.6403	- 99.4552	.0138

† Equilibrium geometry

†† Calculated by difference. $\bar{V}_n = -\bar{E}_e - \bar{T}_e$

TABLE 4-8. Changes in fragment populations and energies during the reaction FH(g) + F^-(g) → FHF^-(g).

The four linear configurations along the reaction path are as denoted in Table 4-5. The changes quoted for (F^-) are all relative to the free F^- ion; those for (FH) and its constituent (F) and (H) fragments are relative to the FH molecule in its equilibrium geometry, and its constituent fragments. All data is given in atomic units.†

FRAGMENT	CONFIGURATION	$\Delta\bar{N}$	$\Delta\bar{T}_e$	$\Delta\bar{V}'_{int}$	$\Delta\bar{V}'_{ext}$	$\Delta\bar{V}'$	$\Delta\bar{V}''$	$\Delta\bar{E}_e$	$\Delta\bar{V}_n$
(F^-)	(1)	- .007	-.030	.079	-14.751	-14.612	7.215	- 7.486	7.516
	(2)	- .019	-.030	.099	-17.325	-17.226	8.423	- 8.834	8.864
	(3)	- .052	-.005	.083	-21.018	-20.935	10.121	-10.819	10.824
	(4)	- .104	.226 (142)†	-.360	-25.621	-25.982	12.093	-13.654	13.429
(FH)	(1)	.007	.001			-13.090	7.296	- 5.794	5.793
	(2)	.019	-.031			-15.221	8.534	- 6.718	6.749
	(3)	.052	-.066			-18.229	10.327	- 7.968	8.034
	(4)	.104	-.157 (-99)†			-21.047	12.328	- 8.815	8.972
(F)	(1)	.049	.034	-.278	-12.647	-12.924	7.163	- 5.727	5.693
	(2)	.072	.018	-.331	-14.731	-15.063	8.398	- 6.647	6.629
	(3)	---	---	---	---	---	---	---	---
	(4)	.154	-.110 (-69)†	-.516	-20.025	-20.541	11.955	- 8.634	8.744
(H)	(1)	- .041	-.034			- .166	.133	- .067	.101
	(2)	- .053	-.049			- .159	.136	- .072	.121
	(3)	---	---	---	---	---	---	---	---
	(4)	- .050	-.047 (-30)†			- .507	.373	- .181	.228

TABLE 4-8 (Cont.)

FRAGMENT	CONFIGURATION	$\Delta\bar{N}$	$\Delta\bar{T}_e$	$\Delta\bar{V}'_{int}$	$\Delta\bar{V}'_{ext}$	$\Delta\bar{V}'$	$\Delta\bar{V}''$	$\Delta\bar{E}_e$	$\Delta\bar{V}_n$
TOTAL	(1)	0.	-.029			-27.762	14.512	-13.279	13.308
	(2)	0.	-.061			-32.448	16.957	-15.552	15.613
	(3)	0.	-.070			-39.164	20.447	-18.787	18.857
	(4)	0.	.069 (43)†			-47.029	24.420	-22.469	22.400

† The $\Delta\bar{T}_e$ values for the equilibrium configuration were calculated using scaled $\bar{T}_e$ values from Table 4-7. The scaling procedure was identical to that described for the data in Table 4-2. Note that only at equilibrium geometry do the $\Delta\bar{T}_e$ values reflect the stability of the system and its constituent fragments. At non-equilibrium geometries these values always include a contribution from the net forces acting on the nuclei. Bracketed values are in kcal/mole (1 au = 627.71 kcal/mole).

†† Calculated by difference. $\Delta\bar{V}_n = -\Delta\bar{E}_e - \Delta\bar{T}_e$.

becomes so dominated by the F nucleus that the stationary point (density minimum) along the F-H internuclear axis vanishes. The disappearance of this stationary point is actually foreshadowed by the changes in fragment populations. During the reaction, both (F^-) and (H) lose charge density to (F). In the early stages of the reaction, the (H) fragment actually transfers more density to (F) than does (F^-). Thus, at R_{F-F} = 7 au, (F^-) has lost .007 e, whereas (H) has lost .041 e. By the time R_{F-F} reaches 6 au, (F^-) has transferred .019 e and (H) has transferred .053 e. In the FH molecule, the population of the (H) fragment is only .258 e, and the (H) fragment barely has sufficient control over the charge density to define its own fragment. In the bifluoride reaction, it has transferred ~ 25% of this density to (F) when the F-F distance is still 6 au. Thus, it is hardly surprising that the (H) fragment as such should disappear by the time R_{F-F} = 5 au. (Recall the lack of a partitioning surface in FH^+, discussed earlier in Chapter 2.) During the final stages of the reaction, (F^-) transfers considerably more charge to (FH), and some of this is actually transferred to the region of the proton. The reappearance of the (H) fragment is due largely to the shift of the proton away from the F nucleus in (FH) to a point where it finally regains sufficient control over the charge density to redefine its fragment.

The changes in the internal components of $\bar{V}'(F)$ and $\bar{V}'(F^-)$ provide some interesting information about this reaction. As the (F) fragment gains charge, $\bar{V}'_{int}(F)$ undergoes a continuous decrease from -243.409 au in FH to -243.925 au in the equilibrium configuration

of FHF^-. The ratio $\Delta\bar{V}^{!}_{int}(F)/\bar{N}(F)$ is $\sim$ -7 au/e during the initial stages of the reaction. During the remainder it drops to $\sim$ -2.3 au/e, suggesting that the electronic charge is being transferred to the outer regions of the fragment and that it is undergoing a slight expansion. Contrast this result with that for the approaching (F^-). Since this fragment continually loses charge density during the course of the reaction, one would expect $\bar{V}^{!}_{int}(F^-)$ to show a continuous increase. Up to R_{F-F} = 6 au this is indeed the case. However, from this point on, it undergoes a sharp <u>decrease</u>, and at equilibrium geometry is actually .360 au below its value in the free ion. Thus, the (F^-) fragment undergoes a considerable contraction during the final stages of the reaction. This contraction is also evident in the contour maps (Fig. 4-4), although the small scale makes it rather difficult to see.

It is always possible to follow changes in the <u>electronic</u> energies of fragments during the course of a reaction. However, this is not true of the <u>total</u> energy. The reason for this is that at non-equilibrium configurations of the nuclei, $\bar{T}_e$ always includes a contribution from the net forces, $\vec{F}_\alpha$, acting on the nuclei. Thus, the virial theorem for any general nuclear configuration of the bifluoride ion must be written, $-\bar{T}_e = \bar{E} - \sum_\alpha \vec{R}_\alpha \cdot \vec{F}_\alpha$. The FH molecule and the F^- ion, to which the Δ values in Table 4-8 are referenced, both satisfy the relationship, $-\bar{T}_e = \bar{E}$, since the net force term is zero. Thus, the relationship between $\Delta\bar{T}_e$ and $\Delta\bar{E}$ is given by

$$-\Delta\bar{T}_e = \Delta\bar{E} - \sum_\alpha \vec{R}_\alpha \cdot \vec{F}_\alpha \qquad [4.5]$$

Note (Table 4-8) that $\Delta\bar{T}_e$ for the system indicates an increase in stability only for the equilibrium configuration of FHF^-, even though the total energy undergoes a continual decrease throughout the entire course of the reaction. This is the expected result. The net force term, $-\sum_\alpha \vec{R}_\alpha \cdot \vec{F}_\alpha$, in Equation [4.5] is positive on the attractive portion of the potential curve, and therefore makes a negative contribution to $\Delta\bar{T}_e$. For the three non-equilibrium configurations in Table 4-8, this contribution is greater in magnitude than that from $\Delta\bar{E}$, and thus leads to a negative value of $\Delta\bar{T}_e$.

The difference between the (H) fragment in the bifluoride ion, and the (H) fragments in the systems discussed earlier is striking. In the boron compounds, the population of (H) was always within a few per cent of 1.7 e. In FH, this has dropped to .26 e. Upon reaction of FH with F^-, the (H) fragment loses an additional .05 e. Thus, in the equilibrium configuration of FHF^-, the population of (H) is a mere .21 e. The (F) fragments are near-fluoride ions with populations of 9.90 e apiece. To describe the FHF^- complex as two fluoride ions held together by a bare proton is, therefore, not far off the mark. In the light of the earlier discussions of the (F) fragment, its strong resistance to change and repulsive interactions with its neighbours, it is surprising that FHF^- should exist at all. Relative to two free fluoride ions, it is stable by 421 kcal/mole -- a rather convincing demonstration of the power of a lowly proton.

D. Constancy and Transferability of Molecular Fragments

One of the most striking features of fragments defined according

to [2.7] is the extent to which they often remain unaltered upon transfer between systems. Consider, for example, the (H) fragment in BH and BH_3. Reference to Fig. 4-1 shows that the fragment appears to be nearly identical in the two systems. Accordingly, one finds (Table 4-1) that the population and kinetic energy of the fragment differ by only .07 e and .03 au (19 kcal/mole), respectively. Since both systems are at their equilibrium geometries, a fragment virial theorem implies that the total energy of the fragment also differs by 19 kcal/mole, and the total virial by 38 kcal/mole. The environment of the fragment is, of course, quite different in the two cases, as reflected in the individual contributions to the virial. $\overline{V}'(H)$ differs by 486 kcal/mole, $\overline{V}''(H)$ by 280 kcal/mole, and $\overline{V}_n(H)$ by 245 kcal/mole. Similar observations hold for the (F) fragment in BF and BF_3. The charge distributions (Fig. 4-2) are again very similar. $\overline{N}(F)$ and $\overline{T}_e(F)$ $(= -\overline{E}(F) = -\frac{1}{2}\overline{V}(F))$ differ by .07 e^- and 17 kcal/mole, respectively. The individual contributions to the total virial show much larger deviations, now ranging from $\sim$ 13000 kcal/mole in the case of $\overline{V}''(F)$ and $\overline{V}_n(F)$, to $\sim$ 26000 kcal/mole for $\overline{V}'(F)$. Thus, a simultaneous near-constancy in $\rho(\underset{\sim}{r})$, $\overline{N}$, $\overline{T}_e$ and $\overline{V}$ is maintained in spite of large changes in the individual contributions to the total virial.

Fragments, then, appear to remain unchanged to the extent that their total virials remain unchanged, and specifically, the total external contribution to the virials. Further, whenever a fragment is transferred from one environment to another, the changes it undergoes appear to be such as to minimize the change in its virial. For example, consider an (H) fragment in BH_3. Upon addition of H^- to form BH_4^-,

the electron-electron repulsion, $\overline{V}'(H)$, undergoes a disproportionate increase because of the excess negative charge on H^-. Reference to Figs. 2-1 and 2-3 shows that the charge distribution of (H) in BH_4^- is more diffuse than in BH_3 (more so than one would expect on the basis of a population increase of only .04 e^-), thus lowering the internal contribution to $\overline{V}'(H)$. Further, by small polarizations of $\rho'(\underline{r})$, the (H) share of the nuclear virial is actually decreased, an uncommon result when nuclei are added to a system. Finally, the small increase in $\overline{N}(H)$ causes an additional drop in $\overline{V}'(H)$, and thus the change in the total virial of the (H) fragment is reduced to a relatively small value. Analogous results apply to (F) in BF_3 when H^- is added to form BF_3H^-. Note that upon addition of CO to BH_3, where the adjacent (C) has a positive charge, $\overline{V}'(H)$ undergoes a disproportionate decrease. This is the only case in which (H) actually loses charge density, thus counteracting the decrease.

The near-constancy of $\overline{N}$, $\overline{T}_e$ and $\overline{V}$ often observed for fragments is largely a consequence of the surface definition, [2.7]. The most noticable changes in the charge distribution occur in the areas of lowest density between the fragments. The partitioning surfaces pass directly through these regions, minimizing the amount of the change assigned to each fragment, and hence, maximizing the retention of fragment identity. Any other surfaces would either include portions of the charge distribution which changed too much upon transfer, or neglect those regions which remained relatively constant.

We have noted here that when $\overline{N}(A)$ remains nearly constant upon transfer, so does the charge distribution, $\rho(\underline{r})$, in (A). It has been pointed out by this laboratory[43] that when $\overline{T}_e(A)$ remains unchanged

so too does the kinetic energy density as defined by $G(\underset{\sim}{r})$. Even more striking is the observation that changes in $\rho(\underset{\sim}{r})$ parallel changes in $G(\underset{\sim}{r})$ very closely. This suggests that both $\rho(\underset{\sim}{r})$ and $G(\underset{\sim}{r})$ are determined by some total field, and that a fragment will undergo the least change upon transfer between systems when the field experienced by the fragment remains nearly constant in the two systems. The fragment virial theorem previously discussed in Chapter 2-C, suggests the total virial field, $V(\underset{\sim}{r})$, as defined by

$$V(\underset{\sim}{r}) = V'(\underset{\sim}{r}) + V''(\underset{\sim}{r}) + V_n(\underset{\sim}{r}) \qquad [4.6]$$

where $V'(\underset{\sim}{r})$, $V''(\underset{\sim}{r})$, and $V_n(\underset{\sim}{r})$ are as previously defined (Chapter 2-C). Indeed, it has been demonstrated[43] that the virial field, $V(\underset{\sim}{r})$, over a fragment exhibits the same degree of constancy as do $\rho(\underset{\sim}{r})$ and $G(\underset{\sim}{r})$, whereas the components of $V(\underset{\sim}{r})$ -- $V'(\underset{\sim}{r})$, $V''(\underset{\sim}{r})$, and $V_n(\underset{\sim}{r})$ -- generally undergo substantial changes upon fragment transfer.

The variations in fragment properties for the boron systems of Table 4-1 are summarized in Table 4-9. Note particularly the small variations in $\overline{N}$ and $\overline{T}_e$ for the (F) fragment. In a virial field language one would say that an (F) fragment is characterized by a strong internal virial field -- one that few other fragments can compete with. The total virial field experienced by (F) in a given environment is, therefore, so strongly dominated by this internal component that its properties remain virtually unchanged. The (H) fragment, on the other hand, has a very weak internal virial field. This is particularly evident if one compares the properties of (H) in the boron systems with its properties in the bifluoride systems.

TABLE 4-9. Variation in properties of exterior (H) and (F) fragments, and of mono-, tri-, and tetra-valent (B) fragments. Values are abstracted from the results in Table 4-1. All data in atomic units.

	$\overline{N}$	$\overline{T}_e$	$\overline{V}'$	$\overline{V'}$	$\overline{V}_n$	$\overline{V}$
-(H)	1.71 ± 4.2%	.86 ± 5.9%	- 11.79 ± 50%	5.04 ± 61%	4.95 ± 58%	- 1.71 ± 5.9%
-(F)	9.90 ± 0.35%	99.87 ± 0.12%	-286.49 ± 8%	63.77 ± 18%	23.51 ± 44%	-199.75 ± .12%
-(B)	4.14 ± 1.8%	24.15 ± 0.24%	- 61.86 ± 9%	10.70 ± 26%	2.87 ± 98%	- 48.30 ± .24%
-(B)<	2.72 ± 11.6%	23.57 ± 0.86%	- 65.98 ± 32%	13.33 ± 40%	5.54 ± 100%	- 47.14 ± .86%
>(B)<	2.75 ± 8.8%	23.58 ± 0.95%	- 66.90 ± 15%	14.21 ± 35%	5.65 ± 93%	- 47.15 ± .95%

the external virial field experienced by (H) in the boron compounds is very similar. Thus, $\bar{N}(H) = 1.71 \pm 4.2\%$ and $\bar{T}_e(H) = 0.86$ au $\pm 5.9\%$ throughout the series. In FHF^-, the external virial field experienced by (H) changes dramatically; $\bar{N}(H)$ drops to 0.21 and $\bar{T}_e(H)$ drops to 0.27 au. The weak internal virial field of (B) is also evident in Table 4-7. Note the fluctuations, particularly in $\bar{N}(B)$, as the external virial field changes. Especially, note the differences between the mono- and poly-valent (B) fragments.

The near constancy of a given fragment in similar bonding situations (and especially, in similar virial fields) suggests that it may be possible to employ fragments in the construction of larger molecules. That is, one can envision a bank of standard fragment charge distributions. In order to construct a given molecule, one would simply select from that bank those fragments which exhibit maximum similarity (both in terms of fragment "valence", and the total field experienced) to those in the molecule under construction. Such a process would be feasible if one could (a) properly join the fragments and (b) calculate all properties of a system from its charge distribution.

Both problems may have solutions. The "marriage" of fragments is probably best handled by some self-consistent procedure. Suppose that one knew the exact form of a charge density-virial field relationship. One could begin by placing all fragments in their proper respective positions in the new molecule. A first correction to the charge in (A) could then be calculated from the new external virial field experienced by (A) from the other fragments. One would then proceed in a similar fashion for (B), (C), (D), and so on down the line. After the first

corrections to $\rho(\underset{\sim}{r})$ for each fragment had been obtained, the second iterative cycle could begin, using the corrected fragment charge distributions to calculate the second cycle corrections. This procedure could be repeated until convergence in $\rho(\underset{\sim}{r})$ was achieved, and the new molecular charge distribution obtained. Of course, a number of problems would have to be solved (apart from that of first finding a charge density-field relationship). For example, the boundary surfaces of the fragments would not match at the beginning of the iterative procedure and a method of defining the fragments throughout the calculation would be necessary. Also, the total number of electrons would not sum to give the correct integral figure at the beginning. Presumably, if the starting fragments were well-chosen, a small scaling procedure, either prior to or during the calculation, could be employed. Of course, the constraint of conservation of charge would have to be imposed.

The problem of relating the charge distribution to the energy is an unsolved, but heavily studied problem.[95] From the theorem of Hohenberg and Kohn[96] it is known that the energy must be a unique functional of the charge density. Unfortunately, the exact functional form of this relationship is not yet known.

CHAPTER 5

CONCLUDING SUMMARY

The virial partitioning method outlined in this work is a viable and practical method for the study of chemical systems. The partitioning surfaces and the fragments they define are fully and uniquely determined by the topographical features of the electronic charge distribution -- an observable property of the system. For this reason, the method is of high generality, and may be applied to any chemical system, irrespective of its complexity or the form of the wavefunction which describes it..

The properties of any system may be summarized, in a well-defined and non-arbitrary manner, in terms of the gross properties of its constituent fragments. The observable properties in chemistry are one- and two-electron properties. That portion of any one-electron property assigned to a fragment, (A), may be obtained by performing the appropriate integration only over the volume of space occupied by that fragment. Thus, if $\hat{\Omega}_1(\underline{x})$ denotes the operator associated with some one-electron property, $\overline{\Omega}_1$, and $\rho(\underline{x},\underline{x}')$ denotes the first-order (or one-electron) density matrix for the system, then $\overline{\Omega}_1(A)$ is given by

$$\overline{\Omega}_1(A) = \int_A \hat{\Omega}_1(\underline{x}) \cdot \rho(\underline{x},\underline{x}')_{\underline{x}=\underline{x}'} d\underline{x} \qquad [5.1]$$

Similarly, if $\hat{\Omega}_2(\underline{x}_1,\underline{x}_2)$ denotes the operator associated with a two-electron property, $\overline{\Omega}_2$, and $\Gamma(\underline{x}_1,\underline{x}_2;\underline{x}_1',\underline{x}_2')$ denotes the second-order

(two-electron) density matrix for the system, then $\bar{\Omega}_2(A)$ is given by

$$\bar{\Omega}_2(A) = \int_{\substack{\text{all}\\\text{space}}} \delta \int_A \Omega_2(\underset{\sim}{x}_1,\underset{\sim}{x}_2)\cdot\Gamma(\underset{\sim}{x}_1,\underset{\sim}{x}_2;\underset{\sim}{x}_1',\underset{\sim}{x}_2')\Big|_{\substack{\underset{\sim}{x}_1=\underset{\sim}{x}_1'\\ \underset{\sim}{x}_2=\underset{\sim}{x}_2'}} d\underset{\sim}{x}_1 d\underset{\sim}{x}_2 \qquad [5.2]$$

where one integration is performed over all space, and the other is carried out only over that portion of the space occupied by (A).

In this work we have been primarily concerned with the electronic population of a given fragment, and the components of its electronic energy. Changes in the one- and two-electron components of the potential energy provide a valuable insight into the reasons behind any redistribution of the charge density which takes place during a chemical reaction. Changes in the internal components of these quantities provide a useful measure of any net expansions or contractions undergone by a fragment in the course of a reaction.

There is a considerable growing body of evidence that these fragments each satisfy a regional virial theorem. This implies that when the nuclear configuration is such that there are no net forces acting on the nuclei (i.e., when a system is at its equilibrium geometry, or in the transition state of a reaction), the <u>total</u> energy of a fragment is equal to the negative of its kinetic energy. This immediately defines a partitioning of the nuclear repulsion potential, something which could not previously be done in a non-arbitrary manner.

Whenever a charge distribution undergoes a continuous change, so too do the partitioning surfaces and the fragments they define. Thus, the partitioning method is dynamic in that it may be applied

to study chemical reactions as well as static systems. The changes which occur during the course of a reaction may be followed by monitoring the properties of the fragments involved. It should be noted that, although we have been concerned solely with isolated molecules, there is no reason why the partitioning method could not be employed in the description and study of large chemical systems such as crystals or polymers. The properties of the surfaces which partition isolated molecules are identical to the properties of those which partition the various members of any ensemble of molecules, atoms, or ions from each other. Thus, through this method it is possible to associate a well-defined region of space, and well-defined properties with each constituent of an ensemble.

To view a molecule as a collection of fragments is quite different from the traditional picture -- a picture in which the concept of a chemical "bond" plays such an important role. The partitioning surfaces bisect what are normally considered to be chemical bonds. In view of the tremendous amount of experimental evidence regarding near-constancy of group properties, the fragment picture does not appear to be an unreasonable one. Concepts such as bond additivity are not at variance with the fragment approach. When additivity of bond properties is observed, it simply means that the properties of the two "bonding" fragments are very similar in different situations, and the "non-bonding" fragments undergo only minor changes when the bond is formed.

One of the most interesting properties of the fragments is the extent to which they often remain unaltered upon transfer between

systems. This suggests the possibility of employing these fragments directly in quantum-mechanical calculations. It has been suggested in this laboratory that the charge density at each point in space is determined by some total field acting at that point (Chapter 4-D). If there is indeed a charge density-field relationship, and if its exact form were known, it might be possible to perform "self-consistent-fragment" [SC(F)] calculations. In such a calculation, one would select from some bank of standard fragment charge distributions, those fragments expected to exhibit the strongest similarity to those in the molecule under study, and through some iterative procedure continually correct the charge distributions of the fragments for the effects of their new environment. This possibility, although highly speculative in nature, does have some exciting consequences. Under the present method of calculating molecular wavefunctions, the time required is approximately proportional to the fourth power of the number of electrons in the system. Thus, on a machine such as the CDC 6400, whereas the calculation on BH_3 reported in Chapter 3 required approximately 45 minutes of central processor time, a projected calculation of the same quality on C_6H_6 would require over 300 hours. Granted, the CDC 6400 is about a factor of ten slower than the best machines available today. However, computer technology as we now know it is rapidly approaching its upper limit. Thus, under the present framework, "ab initio" quantum-mechanical calculations on larger systems -- particularly those of biological importance -- will simply never be feasible. In order to study these molecules within any rigorous framework, a new approach to quantum chemistry is necessary. A fragment approach may well be

the answer.

The study in Chapter 4 is far from exhaustive. Only when the partitioning method has been applied to a large number of chemical systems, will its full potentialities (and shortcomings) be realized. In view of the tremendous amount of time and effort which is now expended on obtaining molecular wavefunctions, it seems only reasonable that an equivalent amount of time and effort go into extracting from these wavefunctions, useful and physically meaningful information. The virial partitioning method appears to be a very promising means to this end.

APPENDIX I

INTEGRATION OVER MOLECULAR FRAGMENTS

A. The Quadrature Method

The three-dimensional integration over molecular fragments was accomplished with the method of Gaussian quadrature.[97(a)] The quadrature over a given fragment was defined in terms of a nucleus-centred, spherical coordinate system, since this best suited the near-spherical character of the molecular charge distribution and its related properties around any of the nuclei. For the spherical coordinate system defined in Fig. AI-1, the integral of a function, $f(r,\theta,\phi)$,

$$\int_{\phi_1}^{\phi_2}\int_{\theta_1}^{\theta_2}\int_{R_1}^{R_2} f(r,\theta,\phi)r^2\sin\theta\,dr\,d\theta\,d\phi \qquad [AI.1]$$

is replaced by a discrete summation,

$$\Delta\phi\,\Delta\theta\,\Delta R \sum_{k=1}^{n_\phi}\sum_{j=1}^{n_\theta}\sum_{i=1}^{n_r} f(r_i,\theta_j,\phi_k)r_i^2\sin\theta_j\, w_i w_j w_k \qquad [AI.2]$$

where $\Delta\phi = |\phi_2-\phi_1|$, $\Delta\theta = |\theta_2-\theta_1|$, and $\Delta R = |R_2-R_1|$; n_ϕ, n_θ, and n_r are the number of points used in the quadrature over the ϕ, θ, and r coordinates, respectively; and w_k, w_j, and w_i are the weighting factors for the integrand at $\phi = \phi_k$, $\theta = \theta_j$, and $r = r_j$, respectively -- coordinates which are calculated from another corresponding set of weighting factors, v_k, v_j, and v_i.

In the integration program we distinguish between two sets of right-handed Cartesian coordinate systems: (1) the integration coordinate system (ICS) and (2) the molecular coordinate system (MCS).

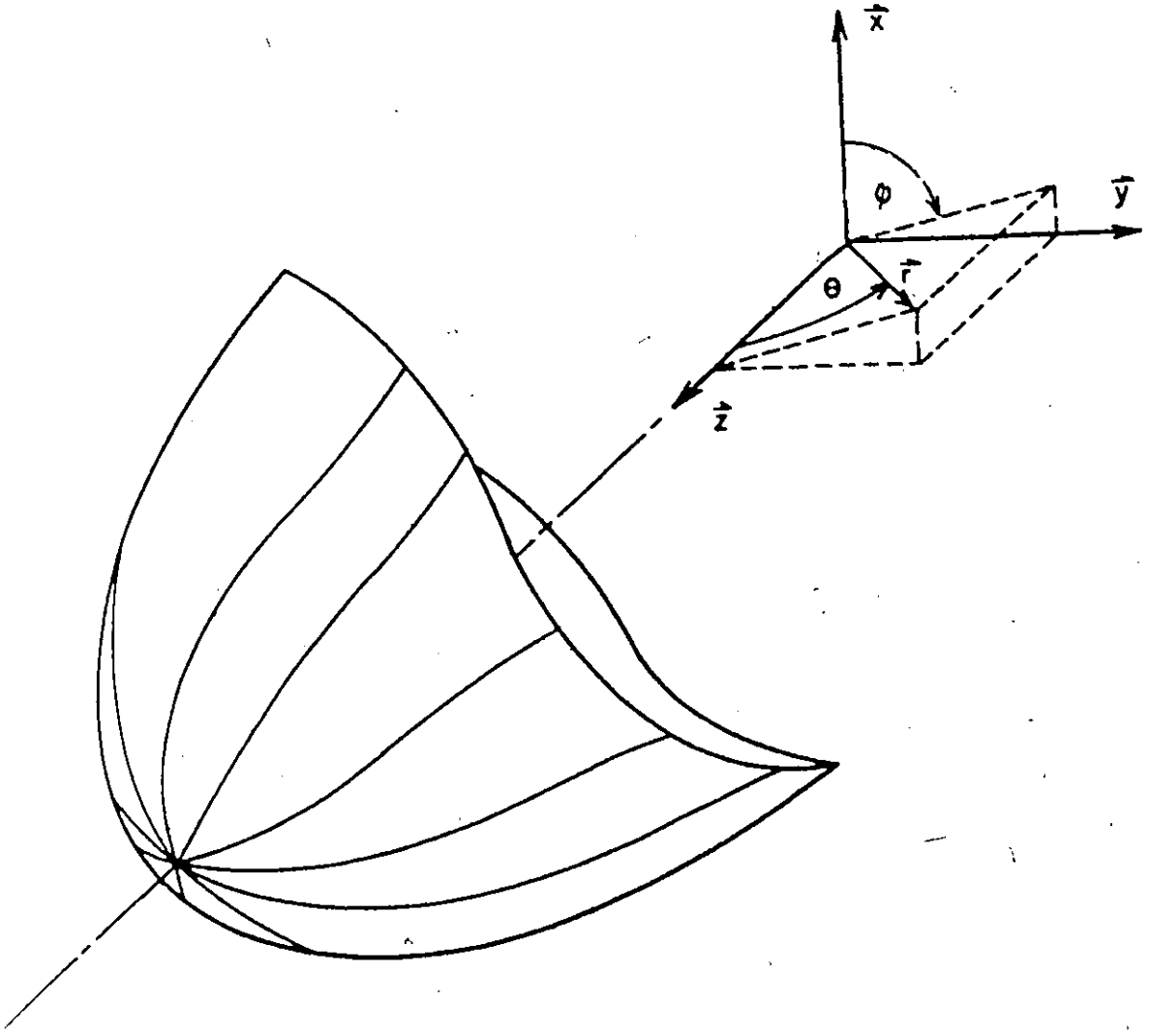

Figure A1-1. A typical partitioning surface and some of the gradient paths which traverse it. The orientation of the ICS, and its relation to the spherical coordinate system used in the quadrature is shown.

The ICS, illustrated in Fig. AI-1, is the system in terms of which the coordinates (r_i, θ_j, ϕ_k) in the quadrature formula [AI.2] are defined. The MCS is the system in terms of which the molecular wavefunction is specified. Transformation from one system to another is accomplished by means of translation and rotation matrices

$$\begin{pmatrix} x \\ y \\ z \end{pmatrix}_{MCS} = R \begin{pmatrix} x \\ y \\ z \end{pmatrix}_{ICS} + \begin{pmatrix} x_o \\ y_o \\ z_o \end{pmatrix}_{MCS} \qquad [AI.3]$$

$$\begin{pmatrix} x \\ y \\ z \end{pmatrix}_{ICS} = R^{-1} \begin{pmatrix} x-x_o \\ y-y_o \\ z-z_o \end{pmatrix}_{MCS} \qquad [AI.4]$$

The rotation matrix, R, and its inverse, R^{-1}, are calculated from the Eulerian angles [98] which rotate the ICS into the same "attitude" as the MCS (i.e., $\vec{x}_{ICS} // \vec{x}_{MCS}$, $\vec{y}_{ICS} // \vec{y}_{MCS}$, $\vec{z}_{ICS} // \vec{z}_{MCS}$). The elements of the translation matrix (x_o, y_o and z_o) are the coordinates of the origin of the ICS, relative to the MCS. By convention, the origin of the ICS is always taken at a nucleus contained by the fragment being integrated, and the z axis of the ICS always points to a stationary point in the surface defining the fragment (i.e., to a point in the charge distribution, $\rho(\underset{\sim}{r})$, where $\vec{\nabla}\rho(\underset{\sim}{r}) = 0$). The program can handle only one partitioning surface at a time. Fragments bounded by more than one surface must be integrated in sections.

Under the above conventions (refer to Fig. AI-1), each value of ϕ_k in [AI.2] defines a plane which contains the z axis of the ICS, and intersects the partitioning surface. The three-dimensional quadrature over (r,θ,ϕ) may then be viewed as a series of two-dimensional

quadratures over (r,θ). The area over which each two-dimensional quadrature is performed is defined by the position of the plane, ϕ_k, and the intersection of that plane with the partitioning surface.

A typical plane is shown in Fig. AI-2. In order to facilitate an accurate quadrature with a minimum number of points, each plane was divided into several regions. These regions were integrated separately, and the results then summed to give the totals for each plane. Regions were denoted as type 1, 2, 3, 4a, or 4b, according to their surface dependence. If we denote the boundaries of a type n region as R_1^n, R_2^n, θ_1^n, and θ_2^n, then the surface dependence may be summarized as follows (refer to Fig. AI-2):

(1) Type 1 -- no surface dependence

(2) Type 2 -- $R_2^2 = r(\theta,\phi)$

(3) Type 3 -- $R_2^3 = r(\theta_1^3,\phi)$

(4) Type 4a-- $\theta_1^{4a} = \theta(r,\phi)$ and $R_1^{4a} = r(\theta_1^3,\phi)$

(5) Type 4b-- $\theta_1^{4b} = \theta(r,\phi)$

The actual specification of surface-independent regional boundaries (eg., R_1^2, θ_1^2, and θ_2^2 for a type 2 region) was based on both the shape of the partitioning surface, and the spatial distribution of the functions to be integrated. Both showed little enough variation with ϕ to warrant using the same surface-independent regional boundaries for each quadrature plane, ϕ_k. A specific example of region specification is given in Sec. C of this appendix.

We now summarize the properties calculated by the integration program. For Hartree-Fock wavefunctions, the properties may all be expressed in terms of the occupied orbitals, $\{\phi_i\}$.

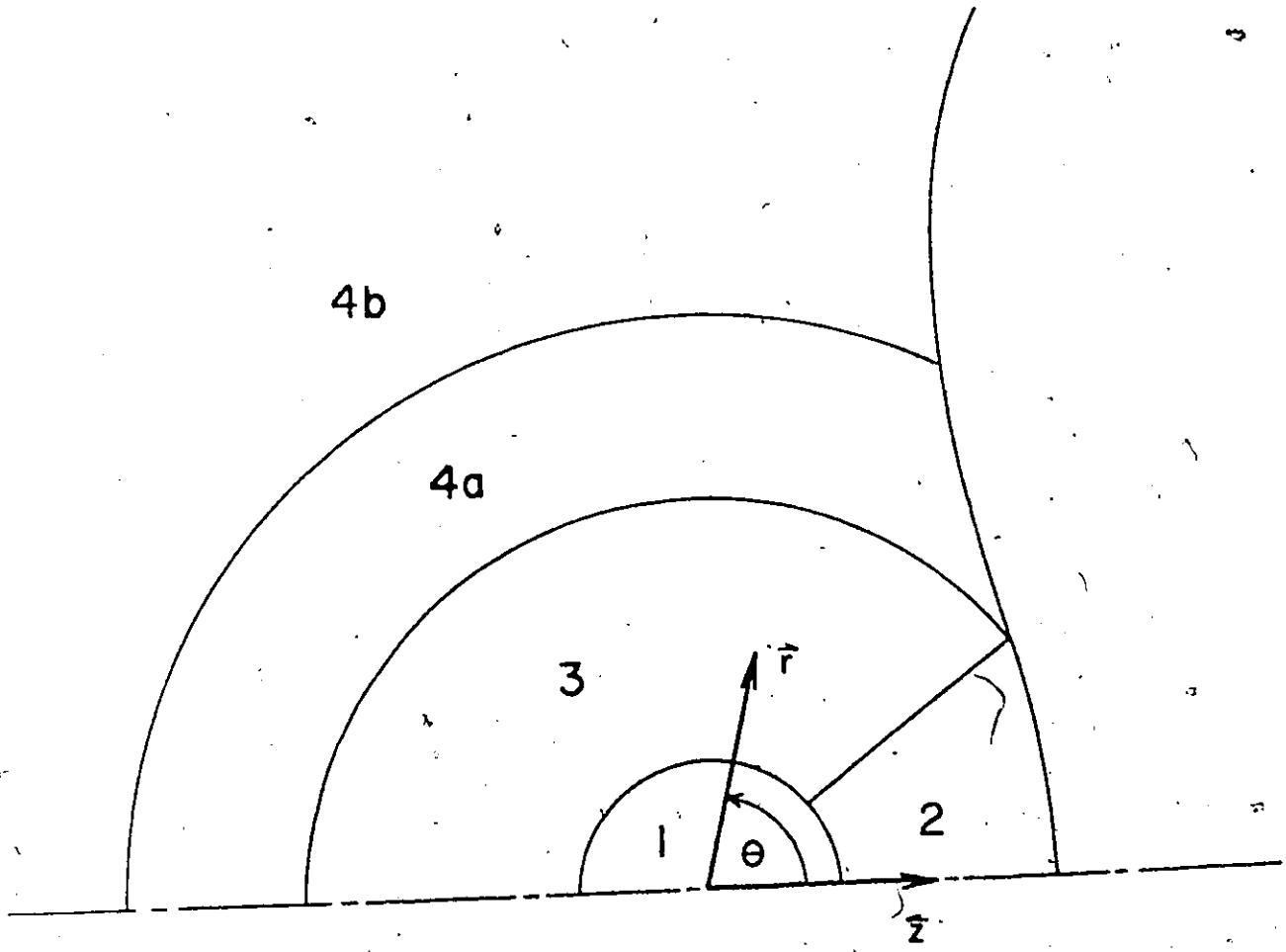

Figure A1-2. The intersection of a partitioning surface with a quadrature plane, ϕ_k, and a representative division of that plane into type 1, 2, 3, 4a, and 4b regions.

$$\rho(\underset{\sim}{r}) = \sum_i \lambda_i \phi_i^2(\underset{\sim}{r}) \qquad [A1.5]$$

$$K(\underset{\sim}{r}) = -\tfrac{1}{2}\sum_i \lambda_i \phi_i(\underset{\sim}{r}) \nabla^2 \phi_i(\underset{\sim}{r}) \qquad [A1.6]$$

$$G(\underset{\sim}{r}) = \tfrac{1}{2}\sum_i \lambda_i \vec{\nabla}\phi_i(\underset{\sim}{r}) \cdot \vec{\nabla}\phi_i(\underset{\sim}{r}) \qquad [A1.7]$$

$$L(\underset{\sim}{r}) = K(\underset{\sim}{r}) - G(\underset{\sim}{r}) \qquad [A1.8]$$

$$V'(\underset{\sim}{r}) = -\rho(\underset{\sim}{r}) \sum_\alpha (Z_\alpha / r_\alpha) \qquad [A1.9]$$

$$V''(\underset{\sim}{r}) = \tfrac{1}{2}\sum_i (\epsilon_i \rho_i(\underset{\sim}{r}) - k_i(\underset{\sim}{r}) - v_i'(\underset{\sim}{r})) \qquad [A1.10]$$

$$E_e(\underset{\sim}{r}) = K(\underset{\sim}{r}) + V'(\underset{\sim}{r}) + V''(\underset{\sim}{r}) \qquad [A1.11]$$

$$\vec{F}_\alpha^{el}(\underset{\sim}{r}) = V'(\underset{\sim}{r}) \vec{r}_\alpha / r_\alpha^2 \qquad [A1.12]$$

The notation employed in [A1.5] through [A1.12] has, for the most part, been previously defined (Eqs. [1.36], [2.3], [2.9], [2.10], [2.12], and [2.13]). Note that $V''(\underset{\sim}{r})$ was not evaluated from the expression given in [2.9]. Such a procedure would prove to be rather time-consuming because of the integration required. In [A1.10], $\rho_i(\underset{\sim}{r})$, $k_i(\underset{\sim}{r})$ and $v_i'(\underset{\sim}{r})$ denote the orbital components of $\rho(\underset{\sim}{r})$, $K(\underset{\sim}{r})$ and $V'(\underset{\sim}{r})$, respectively (i.e., single terms in [A1.5], [A1.6], and [A1.9]); ϵ_i denotes the energy eigenvalue of the i^{th} molecular orbital. This alternate expression for $V''(\underset{\sim}{r})$ may be readily derived from Eq. [1.25] by multiplying through from the left by $\phi_i(1)$. Note that this expression is specific to closed-shell systems.

Theoretically, the value of $\bar{L}$ over a fragment, (A), defined by [2.7] should, of course, be zero. For this reason, it proved to be a useful check on the accuracy of both the quadrature and the surface calculation. In practice, $\bar{L}(A)$ normally ranged from 10^{-6} to 10^{-4} au.

B. Determination of Partitioning Surfaces

Integration over all but the type I regions requires a knowledge of certain specific points along the intersections of the partitioning surface with the quadrature planes, ϕ_k. Operationally, the partitioning surfaces are defined by the collection of gradient paths which originate and terminate at stationary points in the charge distribution. In isolated molecules, these paths generally originate at infinity, and terminate at saddle points.

A representative partitioning surface, the saddle point it contains, and several of the gradient paths which traverse it is illustrated in Fig. AI-1. The method of surface calculation used was to evaluate several of the paths of steepest descent from the saddle point, as traced by the vectors, $-\vec{\nabla}\rho(\underset{\sim}{r})$. Points on the partitioning surface lying between these gradient paths were determined by interpolation. Of course, it is impossible to begin calculation of a gradient path at the saddle point, since $\vec{\nabla}\rho(\underset{\sim}{r})$ is a null vector there. In practice, the starting points for the paths of steepest descent were taken 10^{-6} au from the saddle point, in a ring centred at that point, perpendicular to the z axis of the ICS. Each path to be calculated was specified by its initial ϕ coordinate.

The outer limits of the integration were generally taken to be 10 au from the origin of the ICS. Hence, calculation of the gradient paths was also terminated here. In general, 1000-1500 points were evaluated along each path. Each successive point along a given path was determined by a linear extrapolation along the vector, $-\vec{\nabla}\rho(\underset{\sim}{r})$, calculated at the previous point. The spacing between points is much

more critical near a saddle point than it is some distance away. This is because the direction of a gradient path often changes quite rapidly near a saddle point. It is imperative that one stay as close as possible to the path during the initial stages of its calculation. If one wanders too far from the correct gradient path at this point, it can cause serious errors in the remainder of its calculation. Also, the local values of the properties [A1.5] through [A1.12] are much larger near a saddle point than they are some distance from it. Hence, it is more important to have an accurate partitioning surface here than it is farther out. The initial spacing between points was generally taken somewhere between 10^{-8} and 10^{-6} au. This was incremented at each successive point via an arithmetic progression. The progression was redefined each time the gradient path crossed a regional boundary. A spacing of 10^{-1} au was found to be quite satisfactory near the outer boundaries of the integration. The example given in Sec. C of this appendix should clarify the entire procedure.

We now turn to the problem of interpolating between the gradient paths to obtain the surface coordinates required by the Gaussian quadrature scheme. For what follows, it is important that the reader be quite clear about the notation. R_1^n, R_2^n, θ_1^n, and θ_2^n will again denote the r and θ boundaries of a type n region. Coordinates of points defined by the Gaussian quadrature formula will be denoted as r_I, θ_J, and ϕ_K, whereas general coordinates will appear without subscripts. Functional relationships among coordinates will appear in

parentheses. For example, $R_2^2 = r(\theta,\phi)$ indicates that the R_2 boundary of a type 2 region is a function of both θ and ϕ.

The r and ϕ coordinates of some representative gradient paths are plotted in Fig. AI-3. Paths 1 and 5 lie in neighbouring symmetry planes and their ϕ coordinates remain constant. The dotted vertical line labelled $\phi = \phi_k$ represents one of the ϕ planes defined by the quadrature formula. The methods of determining the intersections of the partitioning surface with any plane, $\phi = \phi_k$, were as follows.

(a) Type 2 regions -- Here, we must find the values of $R_2^2 = r(\theta_j,\phi_k)$ for each plane, ϕ_k. Consider a specific $\theta = \theta_j$ as illustrated in Fig. AI-3. Each gradient path was evaluated until its θ coordinate exceeded θ_j. The coordinate, (r,θ_j,ϕ), was calculated for each path using a three-point Lagrangian interpolation formula,[97(b)] based on the last three coordinates obtained for each path. The method of splines[99] was then used to obtain cubic polynomial fits to the function, $R_2^2 = r(\theta_j,\phi)$, in the intervals between the gradient paths. These polynomials were then used to calculate $R_2^2 = r(\theta_j,\phi_k)$ for each plane, ϕ_k. The process was repeated for each ϕ_j.

(b) Type 3 regions -- For these regions we require only the intersections, $R_2^3 = r(\theta_1^3,\phi_k)$, along the line labelled $\theta = \theta_2^2 = \theta_1^3$ in Fig. AI-3. The procedure was identical to that described for type 2 regions.

(c) Type 4a regions -- These are the most troublesome regions.

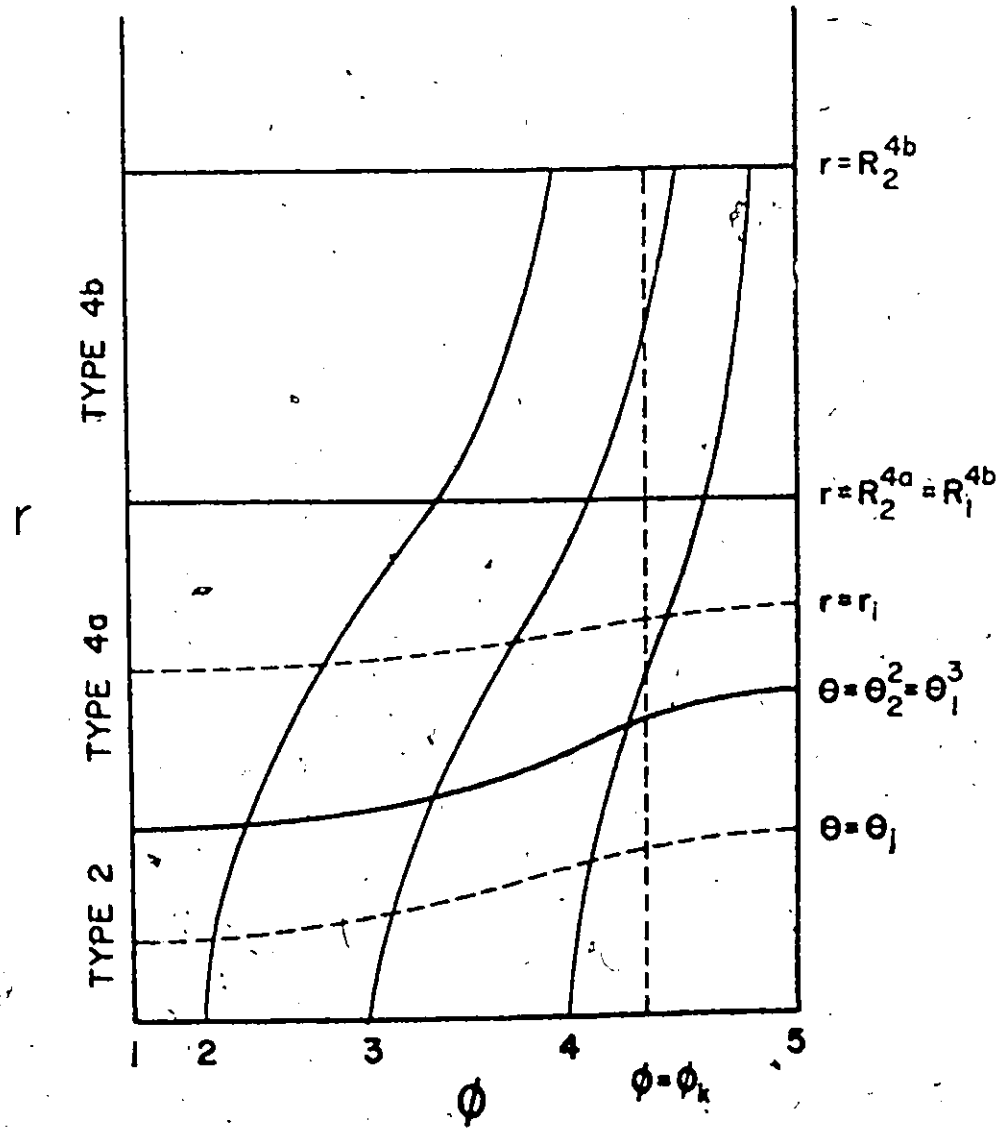

Figure A1-3. A plot of the (r,θ) coordinates of some typical gradient paths as they pass through type 2, 4a, and 4b regions. Paths 1 and 5 lie in neighbouring symmetry planes. $\theta = \theta_k$ denotes a plane defined by the quadrature formula.

Here we need to evaluate the boundary coordinates, $\theta_1^{4a}(r_i,\phi_k)$. The difficulty is that R_1^{4a} is a function of ϕ, as depicted by the line labelled $\theta = \theta_2^2 = \theta_1^3$ in Fig. AI-3. Hence, the values of r_i from the quadrature formula are different for different values of ϕ. Consider a typical $r_i(\phi)$ as illustrated in Fig. AI-3. We eventually require an equation for $\theta_1^{4a} = \theta(r_i,\phi)$ where r_i is itself a function of ϕ. The method was as follows. As before, each gradient path was evaluated until its r coordinate exceed r_i. Of course, now the value of r_i at the crossover depends upon ϕ. Each time a point on a gradient path was calculated, the polynomial fit to $R_2^3 = r(\theta_1^3,\phi)$, previously calculated for type 3 regions, was used to obtain the value of R_1^{4a} at the value of ϕ defined by the point on the gradient path. This, coupled with R_2^{4a}, was used to evaluate r_i. If the r coordinate of the gradient path exceeded r_i, then the coordinate (r_i,θ,ϕ) was determined with the three-point Lagrangian interpolation formula. The interpolation was based on the differences, $(r-r_i)$, for the last three points on the path. This procedure was repeated for each gradient path. The method of splines was then used to obtain a fit to the function $\theta_1^{4a} = \theta(r_i,\phi)$ in each interval. The polynomials obtained were used to calculate $\theta_1^{4a} = \theta(r_i,\phi_k)$ for each plane, ϕ_k. The process was repeated for each r_i.

(d) Type 4b regions -- the value of $R_1^{4b} (= R_2^{4a})$ is now constant and the r_i are no longer functions of ϕ. The method was the same as that for type 4a regions, except that R_1^{4b}, and hence r_1, no longer needed to be re-evaluated for each point on the gradient paths.

C. An Example: The (F) Fragment of BH_3F^-

In order to clarify some of the points in the preceeding sections, we now take a specific example -- integration over the F fragment in BH_3F^-. The orientations of the ICS and MCS are shown in Fig. AI-4. Note that the ICS is centred on the F nucleus, and that its $\vec{z}$ axis points directly to the stationary point in the partitioning surface (in this case, the point of minimum density on the B-F axis). The $\vec{x}$ axis of the ICS (the axis in the $\phi = 0$ plane) was chosen to lie in the symmetry plane containing the $\vec{y}$ axis of MCS. The Eulerian angles relating the two coordinates systems were specified as (90°, 180°, 0°). [The convention used in the partitioning program was that the rotations be performed around the $\vec{z}$, $\vec{x}'$, and finally, the $\vec{z}''$ axis of the ICS.]

The BH_3F^- molecule and its (F) fragment are both of C_{3v} symmetry. For this reason, it is necessary to perform the integration only over one-sixth of the fragment -- a wedge-shaped section lying between any two symmetry planes. The boundaries for the integration over the ϕ coordinate were therefore chosen as $\phi_1 = 0°$ and $\phi_2 = 60°$. A 5-point quadrature grid was used between these boundaries.

Each integration plane, ϕ_K, was divided into six regions. The region types, boundaries, the number of points used in the quadrature over r and θ, and the initial grids and grid increments for the gradient

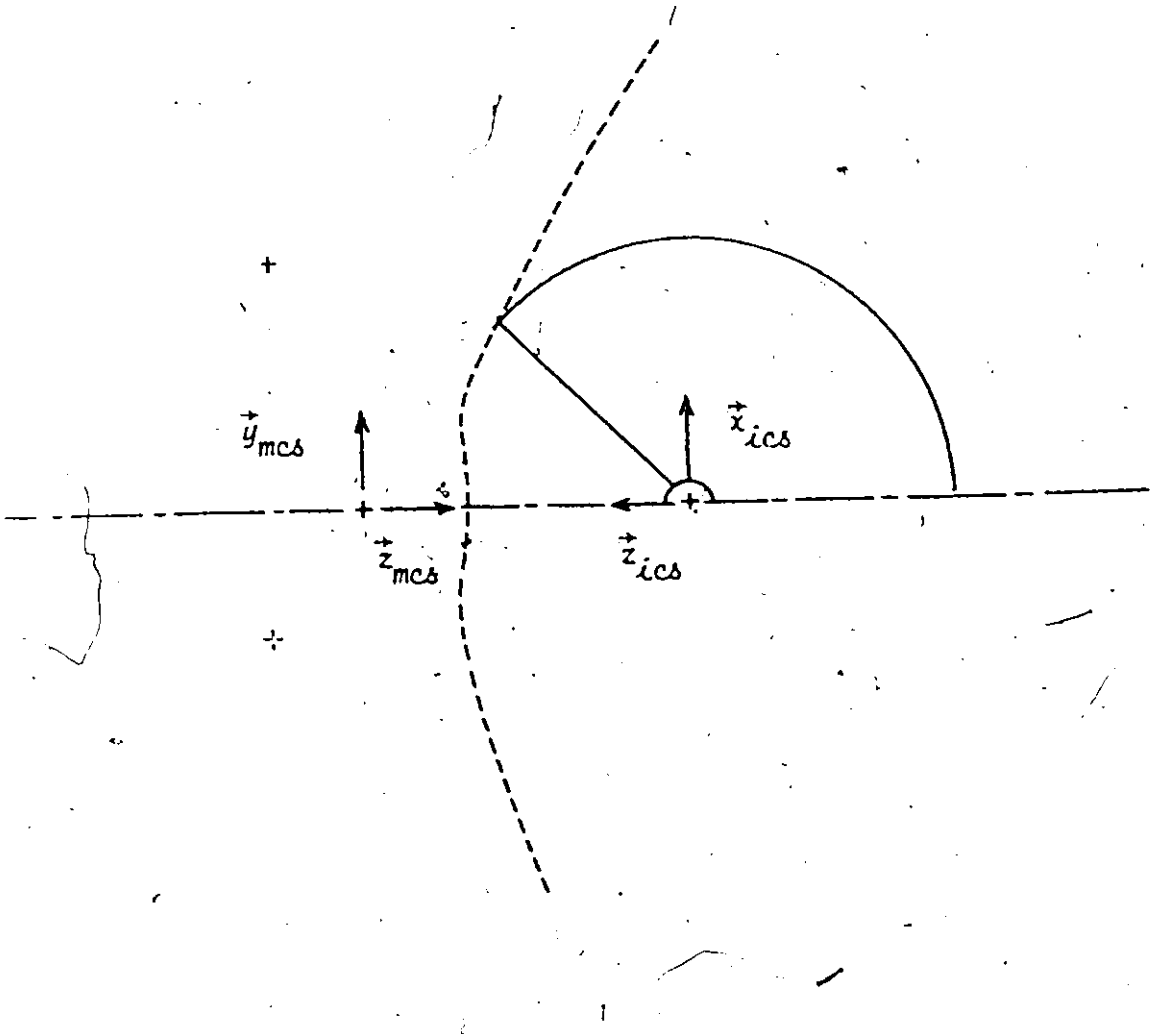

Figure A1-4. Specification of quadrature regions for integration over the (F) fragment of BH_3F^-. Solid crosses denote nuclei in the plane (left to right: H, B, and F); the broken cross denotes the projection of the two out-of-plane H nuclei. The dotted line denotes the intersection of the (F) partitioning surface with the C_{3v} plane shown. The two inner type 1 regions and the outer boundary of the type 4 region are not shown. The positions and orientations of the ICS and MCS are given. Both coordinate systems are right-handed.

each calculations in these regions, are listed below.

TYPE	R_1	R_2	n_r	θ_1	θ_2	n_θ	GRID	INCR
1	0.	0.006	10	0.	180.	10	----	----
1	0.006	0.06	16	0.	180.	10	----	----
1	0.06	0.3	16	0.	180.	10	----	----
2	0.3	----	24	0.	45.	16	1.0E-4	3.6E-6
3	0.3	----	24	45.	180.	16	1.0E-4	0.
4	----	10.0	16	---	180.	16	1.0E-3	6.8E-5

Only the boundary of the outermost type 1 region is illustrated in Fig. AI-4. The boundaries of the inner regions were determined from the behaviour of the functions K and G around the nucleus. A scaled plot of ρ, K, and G at fluorine along the C_3 symmetry axis is given in Fig. AI-5. The plot is typical of first-row nuclei and Gaussian basis sets. It becomes successively more spread-out for nuclei with smaller charges. There is generally little angular variation of the distribution. For first-row nuclei, the R_2 boundary of the first type 1 region was always chosen roughly coincident with the maximum in the G function. The r boundaries of the second type 1 region were chosen such that the shoulder in the G function was approximately in the centre of the region. Boundaries of type 2, 3, and 4 regions were chosen in accordance with the shape of the partitioning surface in the various φ quadrature planes. It is sometimes necessary to choose "compromise" regional boundaries when the surface varies significantly with φ. As can be seen from Fig. AI-4, the surface for BH_3F^- shows little variation with φ. The section of the surface below the C_3 axis is identical to the surface at $\phi_2 = 60°$. As φ varies from 0°

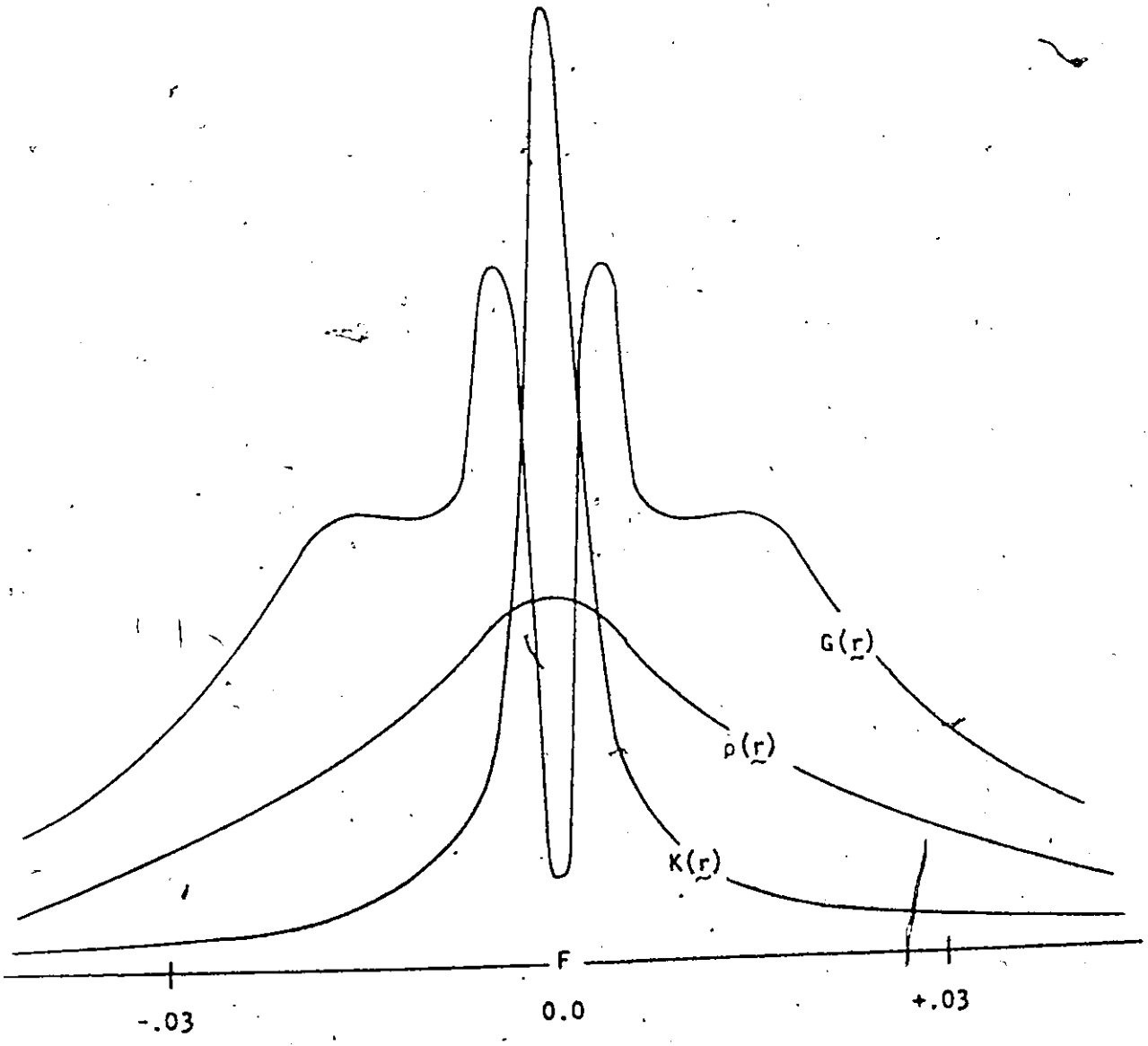

Figure A1-5. Behaviour of $\rho(\underset{\sim}{r})$, $K(\underset{\sim}{r})$, and $G(\underset{\sim}{r})$ within .03 au of the F nucleus in BH_3F^-. The three functions are drawn to different scale factors in the diagram. At the F nucleus, $\rho(\underset{\sim}{r}) \sim 4.3 \times 10^2$ au, $K(\underset{\sim}{r}) \sim 1.7 \times 10^6$ au, and $G(\underset{\sim}{r}) \sim 2.1 \times 10^2$ au. The value of $G(\underset{\sim}{r})$ at its peak is $\sim 1.8 \times 10^4$ au; at its shoulder, $G(\underset{\sim}{r}) \sim 1.4 \times 10^4$ au. This type of behaviour is specific to wavefunctions constructed from Gaussian basis sets. When a Slater basis set is employed, $\rho(\underset{\sim}{r})$ cusps, $K(\underset{\sim}{r})$ becomes infinite, and $G(\underset{\sim}{r})$ exhibits a discontinuity.

to 60°, the shape of the surface varies between the two extremes shown. As a general rule, the θ_2 boundary for a type 2 region was chosen such that there was fairly little variation in R_2^2 over the region. Type 3 boundaries are, of course, determined by the type 2 boundaries. A single type 4 region terminating at $R_2^4 = 10$ au was generally sufficient. Additional type 4 regions were generally included only when it was felt that there was too much variation in function values over a single region (i.e., if R_1^4 was < 3 au from a first-row nucleus). Of course, the choice of regions and their boundaries ultimately depends upon the number of points used in the quadrature over those regions. It is best if a novice experiment a little with a simple molecule to familiarize himself with the technique.

The stationary point in BH_3F^- was found 1.90790218 au from the F nucleus. The calculation of each gradient path was commenced 10^{-6} au from this point, in a direction perpendicular to the B-F axis. Seven paths were evaluated, with initial ϕ coordinates of 0, 2½, 7, 15, 30, 45, and 60°. Note that the 0° and 60° paths begin (and, of course, remain) in symmetry planes. Also note that the initial spacing between ϕ coordinates is not even. The variation of the ϕ coordinates is similar to that illustrated for the paths in Fig. AI-3. It is best to have a relatively even spacing of paths over the surface as a whole, and the initial ϕ coordinates should be chosen with this in mind. This generally means a few paths should be studied before attempting integration over any fragment.

D. The Integration Program

It is expected that copies of the integration program, and

all details regarding its use, will shortly be available from the Quantum Chemistry Program Exchange Centre, Chemistry Department, Indiana University, Bloomington, Indiana. Any additional information may be obtained by writing to the author, c/o Professor R. F. W. Bader, Department of Chemistry, McMaster University, Hamilton, Ontario L8S 4M1, Canada.

APPENDIX II

EXPANSION OF THE QUANTUM MECHANICAL VIRIAL THEOREM

The virial theorem, in its most general form, for a system of N interacting particles, may be written

$$-2\bar{T} = -\left\langle \sum_{k=1}^{3N} q_k \frac{\partial \hat{V}}{\partial q_k} \right\rangle \qquad [AII.1]$$

where $\bar{T}$ is the average kinetic energy of the system, $\hat{V}$ is the total interactive potential operator, and the q_k denote the 3N Cartesian coordinates of the particles. For electronic wavefunctions calculated within the Born-Oppenheimer approximation (i.e., solutions of [1.4]), the theorem becomes

$$-2\bar{T}_e = -\left\langle \sum_{i=1}^{3n} q_i \frac{\partial \hat{V}_e}{\partial q_i} \right\rangle \qquad [AII.2]$$

where $\bar{T}_e$ now denotes the average electronic potential energy, $\hat{V}_e$ denotes the electronic potential energy operator (the last two terms in [1.6]), and the summation on the right-hand side is carried out only over electronic coordinates.

Euler's theorem states that for homogeneous functions, $f(q_1, q_2, \ldots q_r)$, of degree p,

$$\sum_{k=1}^{r} q_k \frac{\partial f(q_1, q_2, \ldots, q_r)}{\partial q_k} = p f(q_1, q_2, \ldots, q_r) \qquad [AII.3]$$

The electronic potential energy operator, $\hat{V}_e$, when considered as a function of both the electronic and nuclear coordinates, q_i and q_α, respectively, is homogeneous of degree minus one. If a summation

over nuclear coordinates, $\langle -\sum_\alpha q_\alpha \frac{\partial \hat{V}_e}{\partial q_\alpha} + \sum_\alpha q_\alpha \frac{\partial \hat{V}_e}{\partial q_\alpha} \rangle$, is added to the right-hand side of [AII.2], Euler's theorem may be immediately applied to yield

$$-2\bar{T}_e = \bar{V}_e + \langle \sum_\alpha q_\alpha \frac{\partial \hat{V}_e}{\partial q_\alpha} \rangle \qquad [AII.4]$$

where $\bar{V}_e$ denotes the average electronic potential energy of the system.

For solutions of [1.4] we have, from the Hellmann-Feynman theorem,

$$-F^{el}_{q_\alpha} = \frac{\partial E_e}{\partial q_\alpha} = \langle \frac{\partial H_e}{\partial q_\alpha} \rangle = \langle \frac{\partial \hat{V}_e}{\partial q_\alpha} \rangle \qquad [AII.5]$$

where $F^{el}_{q_\alpha}$ is the component of the electronic force on nucleus α in the q_α direction. Multiplying [AII.5] by q_α, summing over α, and substituting into [AII.4] yields

$$-2\bar{T}_e = \bar{V}_e - \sum_\alpha q_\alpha F^{el}_{q_\alpha} \qquad [AII.6]$$

If $\vec{R}_\alpha$ denotes the position vector of the α^{th} nucleus and $\vec{F}^{el}_\alpha$ denotes the electronic force on that nucleus, [AII.6] may be rewritten as

$$-2\bar{T}_e = \bar{V}_e - \sum_\alpha \vec{R}_\alpha \cdot \vec{F}^{el}_\alpha \qquad [AII.7]$$

The right-hand side of Equation [AII.1] is called the <u>virial</u>, $\bar{V}$, of the system. In the expanded form given in [AII.7], $\bar{V}_e$ will be termed the electronic virial, $\bar{V}_e$, and $-\sum_\alpha \vec{R}_\alpha \cdot \vec{F}^{el}_\alpha$ will be known as the nuclear virial, $\bar{V}_n$. Since the electronic force exerted on the α^{th} nucleus, $\vec{F}^{el}_\alpha$, is equal to the total force on that nucleus, $\vec{F}_\alpha$, minus the nuclear repulsion force, $\vec{F}^{nuc}_\alpha$, the nuclear virial may be further expanded to

$$\bar{V}_n = \sum_\alpha \vec{R}_\alpha \cdot \vec{F}^{nuc}_\alpha - \sum_\alpha \vec{R}_\alpha \cdot \vec{F}_\alpha \qquad [AII.8]$$

Alternately, $\overline{V}_n$ may be written in terms of the external forces, $\vec{F}_\alpha^{ext} = -\vec{F}_\alpha$ which must be applied to the nuclei to hold them in any other than their equilibrium configuration. The nuclear virial may then be viewed as the virial of the nuclear repulsion forces plus the virial of the external forces. The virial of the nuclear repulsion forces, $\sum_\alpha \vec{R}_\alpha \cdot \vec{F}_\alpha^{nuc}$, reduces to the nuclear replusion energy, $\overline{V}_n$. $\overline{V}_n$ may then be written as

$$\overline{V}_n = \overline{V}_n + \sum_\alpha \vec{R}_\alpha \cdot \vec{F}_\alpha^{ext} \qquad [A11.9]$$

Substitution of [A11.9] into [A11.7] yields

$$-2\overline{T}_e = \overline{V} + \sum_\alpha \vec{R}_\alpha \cdot \vec{F}_\alpha^{ext} \qquad [A11.10]$$

where $\overline{V}$ is the average potential energy of the system (nuclear plus electronic). Alternately, Equations [A11.7] and [A11.10] may be written in terms of the electronic energy and total energy, $\overline{E}_e$ and $\overline{E}$, respectively, as

$$-\overline{T}_e = \overline{E}_e - \sum_\alpha \vec{R}_\alpha \cdot \vec{F}_\alpha^{el} \qquad [A11.11]$$

and

$$-\overline{T}_e = \overline{E} + \sum_\alpha \vec{R}_\alpha \cdot \vec{F}_\alpha^{ext} \qquad [A11.12]$$

From Equation [A11.12] it follows that when a system is in its equilibrium geometry (i.e., when all $\vec{F}_\alpha^{ext}$ are zero), $\overline{E} = -\overline{T}_e$. When a system is not at equilibrium geometry, $-\overline{T}_e$ will differ from $\overline{E}$ by an amount which depends upon both the direction and the magnitude of the external forces.

APPENDIX III

SYMMETRY ORBITALS FOR D_{3h} SYMMETRY GROUPS CONSTRUCTED FROM TERMINAL GAUSSIAN d-FUNCTIONS

The following symmetry orbitals were constructed using projection operator techniques. For the E' and E'' irreducible representations, the operators were constructed from corresponding elements of the 2 x 2 matrices which formed a representation in the (x,y) basis. This gave the projected symmetry orbitals the correct orthogonality properties with p_x and p_y functions on the central nucleus.

The molecule is assumed to be in the xy plane. The origin of the coordinate system is at the central nucleus. The y axis points towards terminal nucleus 1; the x axis points towards terminal nucleus 3. In what follows, xx_n, yy_n, zz_n, xy_n, xz_n, and yz_n denote <u>normalized</u> d-type Gaussian orbitals on terminal nucleus n. The symmetry orbitals are not normalized.

<u>A_1' symmetry</u>

$$xx_1 + 1/4(xx_2 + xx_3) + 3/4(yy_2 + yy_3) - 1/2(xy_2 - xy_3)$$

$$yy_1 + 1/4(yy_2 + yy_3) + 3/4(xx_2 + xx_3) + 1/2(xy_2 - xy_3)$$

$$zz_1 + zz_2 + zz_3$$

<u>A_2' symmetry</u>

$$xy_1 - 1/2(xy_2 + xy_3) + 3/4(xx_2 - xx_3) - 3/4(yy_2 - yy_3)$$

E'(x) symmetry

$1/4(xx_2 - xx_3) + 3/4(yy_2 - yy_3) - 1/2(xy_2 + xy_3)$

$1/4(yy_2 - yy_3) + 3/4(xx_2 - xx_3) + 1/2(xy_2 + xy_3)$

$2\ xy_1 + 1/2(xy_2 + xy_3) - 3/4(xx_2 - xx_3) + 3/4(yy_2 - yy_3)$

$-zz(2) + zz(3)$

E'(y) symmetry

$2\ xx_1 - 1/4(xx_2 + xx_3) - 3/4(yy_2 + yy_3) + 1/2(xy_2 - xy_3)$

$2\ yy_1 - 1/4(yy_2 + yy_3) - 3/4(xx_2 + xx_3) - 1/2(xy_2 - xy_3)$

$3/4(xx_2 + xx_3) - 3/4(yy_2 + yy_3) - 1/2(xy_2 - xy_3)$

$2\ zz(1) - (zz_2 + zz_3)$

A_1'' symmetry

$2\ xz - (xz_2 + xz_3) + \sqrt{3}\ (yz_2 - yz_3)$

A_2'' symmetry

$2\ yz - (yz_2 + yz_3) - \sqrt{3}\ (xz_2 - xz_3)$

E''(x) symmetry

$4\ xz_1 + (xz_2 + xz_3) - \sqrt{3}\ (yz_2 - yz_3)$

$\sqrt{3}\ (xz_2 + xz_3) + (yz_2 - yz_3)$

E''(y) symmetry

$4\ yz_1 + (yz_2 + yz_3) + \sqrt{3}\ (xz_2 - xz_3)$

$\sqrt{3}\ (yz_2 + yz_3) - (xz_2 - xz_3)$

It is worthwhile noting that when a projection operator is applied to

an unnormalized function, all components of the projected symmetry orbital must also be considered as unnormalized. A program such as POLYATOM[52] requires that the coefficients in a given symmetry orbital multiply normalized basis functions. This is not important when one is dealing with s- or p-type Gaussian basis functions. In this case, the components of any given symmetry orbital have identical normalization coefficients, and the coefficients obtained from the projection operators may be used in the program directly. However, for d-type Gaussian functions, the normalization factors for the xx, yy, and zz components are different than those for xy, xz, and yz components. For this reason, the coefficients obtained from a projection operator may have to be adjusted to take account of this difference before they can be used in a program such as POLYATOM. (This adjustment has already been made to the symmetry orbitals listed above.)

REFERENCES

1. A. Fröman, Rev. Mod. Phys., 32, 317 (1960).
2. M. Born and J. R. Oppenheimer, Ann. Phys., 84, 457 (1927).
3. J. C. Slater, Phys. Rev., 34, 1293 (1929).
4. D. R. Hartree, Proc. Cambridge Phil. Soc., 24, 89 (1927).
5. V. Fock, Z. Physik, 61, 126 (1930).
6. J. C. Slater, Phys. Rev., 35, 210 (1930).
7. C. E. Eckert, Phys. Rev., 36, 878 (1930).
8. E. A. Hylleraas and B. Undheim, Z. Physik, 65, 759 (1930).
9. J. K. L. MacDonald, Phys. Rev., 43, 830 (1933).
10. C. C. J. Roothaan, Rev. Mod. Phys., 23, 69 (1951).
11. S. F. Boys, Proc. Roy Soc., A200, 542 (1950); see also I. Shavitt in "Methods of Computational Physics", Vol. 2, Academic Press, New York, (1963), p. 1.
12. L. Brillouin, "Les Champs 'self-consistents' de Hartree-Fock", Hermann et Cie, Paris (1934), p. 19.
13. C. Moller and M. S. Plesset, Phys. Rev., 46, 618 (1934).
14. M. Cohen and A. Dalgarno, Proc. Phys. Soc. (London), 77, 748 (1961).
15. H. Hellmann, "Einführung in die Quantumchemie", F. Deuticke, Leipzig (1937), p. 285.
16. R. P. Feynman, Phys. Rev., 56, 340 (1939).
17. R. E. Stanton, J. Chem. Phys., 36, 1298 (1962).
18. V. A. Fock, Z. Physik, 63, 855 (1930).
19. P.-O. Löwdin, J. Mol. Spectry., 3, 46 (1959).
20. J. C. Slater, J. Chem. Phys., 1, 687 (1933).
21. J. O. Hirschfelder, J. Chem. Phys., 33, 1462 (1960).
22. J. H. Epstein and S. T. Epstein, Am. J. Phys., 30, 266 (1962).

23. J. O. Hirschfelder and C. A. Coulson, J. Chem. Phys., 36, 941 (1962).

24. P.-O. Löwdin, "Advances in Chemical Physics", Vol. II, Interscience, New York (1959), p. 207.

25. E. Clementi, J. Chem. Phys., 38, 2248 (1963).

26. E. Clementi, J. Chem. Phys., 39, 175 (1963).

27. H. Hartmann and E. Clementi, Phys. Rev., 133, A1295 (1964).

28. L. C. Snyder, J. Chem. Phys., 46, 3602 (1967).

29. C. W. Kern and M. Karplus, J. Chem. Phys., 40, 1374 (1964).

30. P. E. Cade, Trans. Amer. Crystallogr. Assn., 8, 1 (1972).

31. W. N. Lipscomb, Trans. Amer. Crystallogr. Assn., 8, 79 (1972).

32. A. J. Duke and R. F. W. Bader, Chem. Phys. Lett., 10, 631 (1971).

33. R. S. Mulliken, J. Chem. Phys., 23, 1833 (1955).

34. See P. Politzer and R. Harris (Ref. 39) for most of the references to this work.

35. R. S. Mulliken, J. Chem. Phys., 36, 3428 (1962).

36. C. Edmiston and K. Ruedenberg, Rev. Mod. Phys., 35, 457 (1963).

37. W. England, L. S. Salmon, and K. Ruedenberg in "Topics in Current Chemistry", Springer-Verlag, New York (1971), p. 31.

38. S. Rothenberg, (a) J. Chem. Phys., 51, 3389 (1969); (b) J. Am. Chem. Soc., 93, 68 (1971).

39. P. Politzer and R. R. Harris, J. Am. Chem. Soc., 92, 6451 (1970).

40. C. Aslangul, R. Constanciel, R. Daudel, and P. Kottis in "Advances in Quantum Chemistry", Vol. 6, Academic Press, New York (1973), p. 93.

41. P.-O. Löwdin, Phys. Rev., 97, 1474 (1955).

42. R. McWeeny, Rev. Mod. Phys., 32, 335 (1960).

43 R. F. W. Bader and P. M. Beddall, J. Chem. Phys., 56, 3320 (1972).

R. F. W. Bader, P. M. Beddall and J. Peslak, Jr., J. Chem. Phys., 58, 557 (1973).

45 R. F. W. Bader and P. M. Beddall, J. Am. Chem. Soc., 95, 305 (1973).

46 T. Kato, Commun. Pure Appl. Math., 10, 151 (1957).

47 E. Steiner, J. Chem. Phys., 39, 2365 (1963).

48. W. A. Bingel, Z. Naturforsch, 18a, 1249 (1963).

49. R. T. Pack and W. Byers-Brown, J. Chem. Phys., 45, 556 (1966).

50. R. F. W. Bader, W. H. Henneker, and P. E. Cade, J. Chem. Phys., 46, 3341 (1967).

51. H. Primas, Int. J. Quant. Chem., 1, 493 (1967).

52. D. B. Neumann, H. Basch, R. L. Kornegay, L. C. Snyder, J. W. Moskowitz, C. Hornback, S. P. Leibmann, "The POLYATOM (Version 2) Program System", Quantum Chemistry Program Exchange, Chemistry Department, Indiana University, Bloomington, Indiana 47401, U. S. A.

53. S. Huzinaga, J. Chem. Phys., 42, 1293 (1965).

54. T. H. Dunning, Jr., J. Chem. Phys., 55, 716 (1971).

55. S. H. Bauer, G. Hertzberg, and J. W. C. Johns, J. Mol. Spectr., 13, 256 (1964).

56. A. H. Nielson, J. Chem. Phys., 22, 659 (1954).

57. W. Gordy, H. Ring, A. B. Burg, Phys. Rev., 78, 512 (1950).

58. D. H. Rank, A. H. Guenther, G. D. Saksena, J. N. Shearer, and T. A. Wiggins, J. Opt. Soc. Am., 47, 686 (1957).

59. R. Onaka, J. Chem. Phys., 27, 374 (1957).

60. W. E. Palke and W. N. Lipscomb, J. Chem. Phys., 45, 3948 (1966).

61. B. D. Joshi, J. Chem. Phys., 46, 875 (1967).

S. D. Peyerimhoff, R. J. Buenker, L. C. Allen, J. Chem. Phys., 45, 734 (1966).

63 D. M. Bishop, Theor. Chim. Acta (Berlin), 1, 410 (1963).

64 E. L. Albasiny and J. R. A. Cooper, Proc. Phys. Soc., 82, 289 (1963).

65 P. T. Ford and R. E. Richards, Disc. Farad. Soc., 19, 230 (1955).

66 L. E. Sutton, Ed., "Tables of Interatomic Distances and Configurations in Molecules and Ions", The Chemical Society, London (1958), Special Publication No. 11, p. M117.

67. G. Hertzberg, "Molecular Spectra and Molecular Structure. I. Spectra of Diatomic Molecules", 2nd Ed., D. Van Nostrand Co. Inc., Toronto (1950).

68. S. R. Gunn and L. G. Green, J. Chem. Phys., 36, 1118 (1962).

69. T. P. Feldmann and W. S. Koski, J. Am. Chem. Soc., 87, 409 (1965).

70. A. G. Gaydon, "Dissociation Energies and Spectra of Diatomic Molecules", 2nd Ed. (revised), Chapmann and Hall, London (1953).

71. V. H. Diebler and S. K. Liston, Inorg. Chem., 7, 1742 (1968).

72. R. A. Hegstrom, W. E. Palke, and W. N. Lipscomb, J. Chem. Phys., 46, 920 (1967).

73. R. E. McCoy and S. H. Bauer, J. Am. Chem. Soc., 78, 2061 (1956).

74. D. R. Armstrong and P. G. Perkins, J. Chem. Soc. A1044 (1969).

75. I. G. Csizmadia, private communication.

76. A. D. McLean and M. Yoshimine, "Tables of Linear Molecule Wavefunctions", I.B.M. Corp., San Jose Research Laboratories, San Jose, California (1967).

77. P. N. Noble and R. N. Kortzeborn, J. Chem. Phys., 52, 5375 (1970).

78. P. A. Kollmann and L. C. Allen, J. Am. Chem. Soc., 92, 6101 (1970).

79. J. Almlöf, Chem. Phys. Lett., 17, 49 (1972).

80. H. L. Carrell and J. Donahue, Isr. J. Chem., 10, 195 (1972).

81. S. A. Harrell and D. H. McDaniel, J. Am. Chem. Soc., 86, 4497 (1964).

82. M. E. Schwartz and L. C. Allen, J. Am. Chem. Soc., 92, 1466 (1970).

83. D. R. Armstrong and P. G. Perkins, Theor. Chim. Acta (Berlin), 15, 413 (1969).

84. J. A. Pople and D. L. Beveridge, "Approximate Molecular Orbital Theory", McGraw-Hill, New York (1970), p. 119.

85. R. G. Pearson, J. Am. Chem. Soc., 85, 3533 (1963); Science, 151, 172 (1966).

86. P. Politzer and J. W. Timberlake, J. Org. Chem., 37, 3557 (1972).

87. W. A. G. Graham and F. G. A. Stone, J. Inorg. Nucl. Chem., 3, 164 (1956/57).

88. C. K. Ingold, "Structure and Mechanism in Organic Chemistry", 2nd Ed., Cornell University Press, Ithaca, New York (1969).

89. D. T. Clark, J. N. Murrell, and J. M. Tedder, J. Chem. Soc., 1250 (1963).

90. R. F. W. Bader, A. J. Duke, and R. R. Messer, J. Chem. Phys. (1973) (in press).

91. R. F. W. Bader and P. M. Beddall, Chem. Phys. Lett., 8, 29 (1971).

92. R. F. W. Bader and H. J. T. Preston, Int. J. Quant. Chem., 3, 327 (1969).

93. R. F. W. Bader, I. Keaveny, and P. Cade, J. Chem. Phys., 47, 3381 (1967).

94. R. G. Pearson, Chem. Brit., 3, 103 (1967).

95. N. H. March and J. C. Stoddart, Editor F. Herman, "Computational Solid State Physics", Plenum Press, New York, pp. 205-218.

96. P. Hohenberg and W. Kohn, Phys. Rev., 136B, 864 (1964).

97. See, for example: J. B. Scarborough, "Numerical Mathematical Analysis", 5th Edition, John Hopkins Press, Baltimore (1962): (a) p. 150, (b) p. 74.

98. See, for example: H. Goldstein, "Classical Mechanics", Addison-Wesley Publ. Co., Reading, Massachusetts (1965), p. 107.

99. C. H. Reinsch, Numer. Math., 10, 177 (1967); Numer. Math., 16, 451 (1971).

100. J.F. O'Shea, "A Molecular Orbital Theory of Polymers", Ph.D. Thesis, McMaster University (1973).